

NUCLEAR MAGNETIC RESONANCE INVESTIGATIONS:  
STRUCTURE, FUNCTION, AND DYNAMICS

Thesis by

Thomas Gardner Perkins

In Partial Fulfillment of the Requirements  
For The Degree of  
Doctor of Philosophy

California Institute of Technology  
Pasadena, California

1982

(submitted July 20, 1981)

-ii-

To Cathy,  
with love.



## ACKNOWLEDGEMENTS

I would like to thank Dr. John Richards for giving me the freedom to work on research projects which I found interesting. I would also like to thank the California Institute of Technology and the National Science Foundation for financial assistance during my graduate career.

Many people were involved in the production of the experiments that follow. From my research group, I thank Dr. George Adler, Betty Aalseth, Neal Handly, Dr. Brian Herndier, Rob Kaiser, Jim Neitzel, Dr. Jim Satterlee, and Dan Sand for many hours of help, hope, and frustration. Within the Caltech community, Dr. Amy Abe, Ken Block, Dr. Bill Croasmun, Tom Dunn, David Horowitz, Irv Moskowitz, Kevin Ott, and, posthumously, Dr. Robert Vaughan, provided support. And, from the outside world, special thanks are in order for Dr. Mike Albright from JEOL, Dr. Robert Horowitz from the USDA Fruit and Vegetable Laboratory, Dr. Steve Smallcombe from Varian, and last, but certainly not least, Dr. Jim Sudmeier, from U.C. Riverside.

This thesis was put together by Ms. Debbie Chester, whose ever present smile and pheonomenal typing skills will always make her worth more than she gets paid.

Finally, I would like to thank my parents, Stanley and Harriet Perkins, for their constant encouragement. (No, I have not found a cure for cancer.)

ABBREVIATIONS

CO	carbon monoxide
CSA	chemical shift anisotropy
D-D	dipole-dipole
DSS	sodium 2,2-dimethyl-2-silicopentane-5-sulfonate
FID	free induction decay
FT	Fourier transform
HbA	human hemoglobin
Hb-I	<u>Glycera dibranchiata</u> dimeric hemoglobin
Hb-II	<u>Glycera dibranchiata</u> monomeric hemoglobin
HbR	New Zealand white rabbit hemoglobin
ir	infrared
LADH	liver alcohol dehydrogenase
Mb	myoglobin
NAD <sup>+</sup>	nicotinamide adenine dinucleotide
NADH	reduced nicotinamide adenine dinucleotide
nmr	nuclear magnetic resonance
NOE	nuclear Overhauser effect
<u>1</u>	protoheme IX dimethyl ester
1-MeIm	1-methylimidazole
1-MeIm- <u>1</u>	1-methylimidazole-protoheme IX dimethyl ester

-v-

$r_{\text{eff}}$	effective proton-carbon distance
$T_1$	spin-lattice relaxation time
$T_2$	spin-spin relaxation time
TMS	tetramethyl silane
<u>2</u>	protoheme mono(3-(1-imidazolyl)- propyl)amide monomethyl ester
YADH	yeast alcohol dehydrogenase

TABLE OF CONTENTS

INTRODUCTION . . . . .	1
PART I - Nuclear Magnetic Resonance Investigation of $^{13}\text{CO}$ Binding to Heme Systems: Carbon- $^{13}$ Chemical Shifts and Spin-Lattice Relaxation Times	
INTRODUCTION . . . . .	5
EXPERIMENTAL . . . . .	7
Chemicals . . . . .	7
Sample Preparation . . . . .	7
Instrumental . . . . .	8
$T_1$ Measurements . . . . .	8
Viscosities and Densities . . . . .	8
THEORY . . . . .	9
RESULTS AND DISCUSSION . . . . .	13
Chemical Shifts . . . . .	13
Relaxation . . . . .	18
REFERENCES . . . . .	27
PART II - Nuclear Magnetic Resonance Investigation to $^{13}\text{CO}$ Binding to Heme Proteins: Relaxation Mechanisms	
INTRODUCTION . . . . .	32
EXPERIMENTAL . . . . .	34
Sample Preparation . . . . .	34
Instrumental . . . . .	35
$T_1$ Measurements . . . . .	35
Viscosities and Densities . . . . .	36
THEORY . . . . .	37
RESULTS AND DISCUSSION . . . . .	43
REFERENCES . . . . .	55

PART III - Nuclear Magnetic Resonance Investigation  
of  $^{13}\text{CO}$  Binding to Heme Proteins:  
Structure and Function

INTRODUCTION. . . . .	58
EXPERIMENTAL. . . . .	60
Sample Preparation. . . . .	60
Instrumental. . . . .	61
$T_1$ Measurements . . . . .	62
Viscosities and Densities . . . . .	62
THEORY. . . . .	63
Dioxygen Binding Curves . . . . .	63
$T_1$ Relaxation with Internal Motion . . . . .	67
RESULTS AND DISCUSSION. . . . .	77
CONCLUSION. . . . .	91
REFERENCES. . . . .	92

PART IV - Carbon Nuclear Magnetic Resonance Studies  
of the Histidine Residue  $\alpha$ -lytic Protease.  
A Reexamination at Higher Magnetic Field

INTRODUCTION. . . . .	97
EXPERIMENTAL. . . . .	99
Materials . . . . .	99
NMR Samples . . . . .	101
NMR Spectra . . . . .	102
RESULTS . . . . .	103
DISCUSSION . . . . .	112
CONCLUSION . . . . .	116
REFERENCES . . . . .	117

PART V - A General Method for Performing  
Magnetization Transfer Experiments

INTRODUCTION. . . . .	121
EXPERIMENTAL. . . . .	123
NMR Measurements. . . . .	123
Calculations. . . . .	123
THEORY. . . . .	124
Exchange. . . . .	124
Selective Pulse . . . . .	126
RESULTS AND DISCUSSION. . . . .	134
REFERENCES. . . . .	139

PART VI - 500.13 MHz  $^1\text{H}$  Nuclear Magnetic Resonance  
Investigation of Substrate Binding to  
Horse Liver Alcohol Dehydrogenase

INTRODUCTION. . . . .	141
EXPERIMENTAL. . . . .	143
Chemicals . . . . .	143
CD <sub>3</sub> CHDOD Synthesis. . . . .	143
NMR Measurements. . . . .	144
Calculations. . . . .	144
THEORY . . . . .	146
RESULTS AND DISCUSSION. . . . .	147
REFERENCES. . . . .	158

PART VII - Elucidation of the Structure of Crosslinked  
Verapamil using 500.13 MHz  $^1\text{H}$  Nuclear  
Magnetic Resonance Spectroscopy

INTRODUCTION. . . . .	161
EXPERIMENTAL. . . . .	162
Chemicals . . . . .	163
NMR Measurements. . . . .	163

RESULTS AND DISCUSSION. . . . .	164
Verapamil . . . . .	164
Crosslinked Verapamil . . . . .	168
REFERENCES. . . . .	180
APPENDIX. . . . .	181

TABLE OF FIGURES

Chapter	Number	Description	Page
1	1	Calculated log-log plots of (A) spin-lattice and (B) spin-spin relaxation for $^{13}\text{CO}$ at 25.14 and 90.5 MHz.	10
	2	$^{13}\text{CO}$ chemical shifts of protoheme IX dimethyl ester- $^{13}\text{CO}$ and protoheme-mono(3-(1-imidazolyl)propyl)-amide monomethyl ester- $^{13}\text{CO}$ in $\text{DMSO-d}_6$ -DMSO (4:1).	14
	3	Solvent dependence of the $^{13}\text{C}\equiv\text{O}$ chemical shift of 0.01 M ferrous.	16
	4	$^{13}\text{CO}$ progressive saturation $T_1$ measurements of 0.015 M 1-methylimidazole-protoheme IX dimethyl ester- $^{13}\text{CO}$ taken at $29.0 \pm 1.5^\circ\text{C}$ .	22
2	1	Calculated log-log plots of spin-lattice relaxation ( $T_1$ ) and linewidth for $^{13}\text{CO}$ .	40
	2	Dependence of $^{13}\text{CO}$ $T_1$ 's on hemoglobin concentration.	44
	3	Plot of the data from Figure 2 <sup>14</sup> along with theoretical curves generated using eq. 3 with $\Delta\sigma = 194 \pm 37$ ppm and $r_{\text{eff}} = 1.81 \pm 0.02 \text{ \AA}$ .	46



2	4	Field dependence of the $^{13}\text{CO}$ resonances of carbonmonoxy rabbit hemoglobin in 0.15 M NaCl.	49
	5	Postulated Lewis base interaction between the distal histidine (E7) and heme bound CO.	51
3	1	Theoretical $\text{O}_2$ saturation curves for Hb obtained using eq. 2.	65
	2	Schematic representation of $^{13}\text{CO}$ bound to hemoglobin.	70
	3	Calculated log-log plots of spin-lattice relaxation ( $T_1$ ) for $^{13}\text{CO}$ using eq. 6.	73
	4	Calculated log-log plot of the total spin-lattice relaxation ( $T_1$ ) for $^{13}\text{CO}$ using eq. 6.	75
	5	Plot of the $T_1$ relaxation data for $^{13}\text{CO}$ bound to the $\alpha$ -chain of New Zealand white rabbit hemoglobin.	78
	6	Plot of the $T_1$ relaxation data for $^{13}\text{CO}$ bound to the $\beta$ -chain of New Zealand white rabbit hemoglobin.	80
	7	Plot of the $T_1$ relaxation data for $^{13}\text{CO}$ bound to the monomeric hemoglobin from the marine annelid <u>Glycera dibranchiata</u> .	82
	8	Schematic representation of $^{13}\text{CO}$ bound to New Zealand white rabbit hemoglobin.	88

4	1	25.14 MHz proton-decoupled $^{13}\text{C}$ nmr spectrum of $\alpha$ -lytic protease in 10% $\text{D}_2\text{O}$ .	104
	2	125.76 MHz proton-coupled $^{13}\text{C}$ nmr spectrum of $\alpha$ -lytic protease in 10% $\text{D}_2\text{O}$ .	106
	3	125.76 MHz proton-coupled $^{13}\text{C}$ nmr spectra of $\alpha$ -lytic protease in 10% $\text{D}_2\text{O}$ at $25^\circ$ .	109
5	1	Plot of $M_y$ and $M_z$ vs frequency offset for a selective $90^\circ$ pulse.	128
	2	Plot of $M_y$ and $M_z$ vs frequency offset for a selective $180^\circ$ pulse.	130
	3	Plot of $M_y$ and $M_z$ vs frequency offset for a selective $180^\circ$ pulse.	132
	4	$^{31}\text{P}$ magnetization transfer spectra of triphenylphosphine and tris(triphenylphosphine)-tetramethylene-nickel at $-90^\circ\text{C}$ .	135
6	1	500.13 MHz proton nmr spectra.	148
	2	500.13 MHz proton nmr spectrum of $\text{CD}_3\text{CHDOD}$ with $\text{CD}_3\text{CH}_2\text{OD}$ produced catalytically by LADH.	151
	3	Proposed orientation of ethanol when bound to LADH in the presence of NADH.	155

7	1	500.13 MHz proton magnetic resonance spectrum and peak assignments of verapamil in D <sub>2</sub> O.	165
	2	500.13 MHz proton magnetic resonance spectrum and peak assignments of crosslinked verapamil in D <sub>2</sub> O.	169
	3	Expansion of the inversion recovery proton nmr spectrum of crosslinked verapamil.	172
	4	Expansion of the isopropyl methyl region of the proton nmr spectrum of crosslinked verapamil.	175
	5	Expansion of the downfield region of the proton nmr spectrum of crosslinked verapamil in d <sub>6</sub> -DMSO.	177

TABLE OF TABLES

Chapter	Number	Description	Page
1	I	$^{13}\text{CO}$ chemical shifts of various heme complexes.	20
	II	Spin-lattice relaxation times of $^{13}\text{CO}$ bound to 0.015 M 1-methylimidazole-protoheme IX dimethyl ester in $\text{DMSO-d}_6$ -DMSO (4:1).	24
	III	$^{13}\text{CO}$ chemical shifts and shielding tensors.	25
2	I	Spin-lattice relaxation times and linewidth measurements of $^{13}\text{CO}$ bound to sperm whale myoglobin and rabbit (New Zealand white) hemoglobin.	53
3	I	Summary of relaxation parameters for $^{13}\text{CO}$ hemoglobins	84
	II	$^{13}\text{CO}$ shielding tensors and anisotropies	86
	III	Summary of information for CO binding to hemoglobins	90
4	I	NMR parameters for C-2 carbon in histidine residue of $\alpha$ -lytic protease.	111
5	I	Summary of exchange data for tris(triphenylphosphine)tetramethylene-nickel (II)	137
6	I	Summary of ethanol-LADH-NADH nmr parameters	153
7	I	NMR data for verapamil	167
	II	NMR data for crosslinked verapamil.	171

## ABSTRACTS

### PART I

Carbon-13 nuclear magnetic resonance (nmr) spectroscopy has been used to investigate the chemical shifts and spin-lattice relaxation times ( $T_1$ ) of  $^{13}\text{CO}$  bound to two derivatives of protoheme IX. The chemical shift is a function of the nature of the ligand trans to the  $^{13}\text{CO}$  and of the solvent.  $T_1$  measurements of the complex 1-methylimidazole-protoheme IX dimethyl ester- $^{13}\text{CO}$  reveal that Chemical Shift Anisotropy (CSA) is the dominant relaxation mechanism for the heme bound  $^{13}\text{CO}$ . The anisotropy of the chemical shift tensor,  $\Delta\sigma$ , for the  $^{13}\text{CO}$  was found to be  $584 \pm 132$  ppm. The chemical shifts are compared with those obtained for  $^{13}\text{CO}$  bound to the monomeric hemoglobin from the marine annelid Glycera dibranchiata.

### Part II

Carbon-13 nuclear magnetic resonance (nmr) spectroscopy has been used to reinvestigate the spin-lattice relaxation times ( $T_1$ ) of  $^{13}\text{CO}$  bound to human hemoglobin (HbA) and sperm whale myoglobin. It has been found that the Chemical Shift Anisotropy (CSA) and Dipole-Dipole (D-D) relaxation mechanisms contribute to the observed  $T_1$  for the protein-bound  $^{13}\text{CO}$ . This observation can explain the lack of an observable nuclear Overhauser effect (NOE) for

$^{13}\text{CO}$  bound to HbA. A reanalysis of the previously determined relaxation times indicates that  $\Delta\sigma = 194 \pm 37$  ppm and  $r_{\text{eff}} = 1.81 \pm 0.02$  Å for  $^{13}\text{CO}$  bound to HbA. The significance of these results in relation to the postulated nucleophilic base interaction between the distal residue His-E7 and the protein bound CO is also discussed.

### PART III

The spin-lattice relaxation ( $T_1$ ) times for  $^{13}\text{CO}$  bound to New Zealand white rabbit hemoglobin (HbR) and the monomeric hemoglobin from the marine annelid Glycera dibranchiata (Hb-II) have been investigated. It has been found that the anisotropies of the chemical shift tensor,  $\Delta\sigma$ , in each protein are vastly different. These results support the existence of a nucleophilic interaction between His-E7 and the heme-bound  $^{13}\text{CO}$  in HbR. In addition, the geometry and rate of internal motion for  $^{13}\text{CO}$  bound to HbR have also been obtained.

### PART IV

The pH dependence of the carbon-13 nuclear magnetic resonance (nmr) chemical shift for the C-2 carbon of selectively carbon-13 enriched histidine biosynthetically incorporated into the catalytic triad of the serine protease,  $\alpha$ -lytic protease, has been reinvestigated at three magnetic fields. The spectra acquired at all fields yield a value

for  $^1J_{^{13}\text{C-H}}$  at pH  $\sim 5$  which is consistent with full protonation of the active site imidazole ring of His<sup>57</sup> at this pH. Hence, the catalytically important ionization of pKa  $\sim 6.7$  can be assigned to His<sup>57</sup>. At 125.76 MHz and pH  $\lesssim 5$ , the carbon-13 spectrum of the enriched enzyme reveals two other structural forms of the histidine side chain within the protein which are not observed at lower fields. The presence of these species can explain previous carbon-13 nmr results which yielded an abnormally low pKa value for the catalytic histidine.

#### PART V

A general method is presented for obtaining the exchange rates for chemical systems undergoing slow exchange on the nuclear magnetic resonance (nmr) timescale. As an example of the generality of the method,  $^{31}\text{P}$  nmr spectroscopy has been used to measure the rate of exchange for the system  $(\text{PPh})_3\text{Ni} \square + \text{PPh}_3^* \rightleftharpoons \text{PPh}_3^* (\text{PPh}_3)_2\text{Ni} \square + \text{PPh}_3$ . The exchange rates obtained with this method are compared to those measured using lineshape analysis.

## PART VI

The binding of (R,S) d<sub>5</sub>-ethanol (CD<sub>3</sub>CHDOD) to horse liver alcohol dehydrogenase (LADH) has been studied using 500.13 MHz <sup>1</sup>H nuclear magnetic resonance (nmr) spectroscopy. In the presence of reduced nicotinamide adenine dinucleotide (NADH) the C-1 proton resonance moves such that the extrapolated chemical shift for the C-1 proton of the ethanol bound to the enzyme-coenzyme complex is shifted  $0.82 \pm 0.08$  ppm upfield from the free ethanol resonance. The chemical shifts for the (R) and (S) hydrogens of the bound ethanol do not differ by more than 0.16 ppm.

## PART VII

The structure of a formaldehyde-crosslinked dimer of verapamil, a Ca<sup>+2</sup> channel blocker, has been determined using 500.3 MHz <sup>1</sup>H nuclear magnetic resonance (nmr) spectra. The structure has been found to be asymmetric and, as with monomeric verapamil, possess a rigid conformation.



INTRODUCTION

Nuclear magnetic resonance (nmr) spectroscopy has proven to be a valuable, non-destructive tool for studying chemical systems. The variety of parameters that may be obtained from the nmr spectrum, such as the chemical shift, spin-lattice ( $T_1$ ) and spin-spin ( $T_2$ ) relaxation times, and exchange rates,<sup>1</sup> have yielded information about numerous chemical species in solution. This thesis examines four different systems with a variety of nmr techniques.

Parts I through III look at the relaxation behavior of carbon-13 carbon monoxide (CO) when bound to protoheme systems, primarily hemoglobins. Previous  $T_1$  and nuclear Overhauser effect (NOE) studies<sup>2</sup> of  $^{13}\text{CO}$  bound to human hemoglobin gave inconsistent results about the nature of the protein interactions with the heme-bound ligand. These inconsistencies are shown to be due to an incomplete understanding of the  $T_1$  relaxation behavior of  $^{13}\text{CO}$ . Using this knowledge, new information has been obtained about the protein-ligand interaction.

Part IV is a reexamination of the carbon-13 nmr spectrum of histidine enriched with carbon-13 and bio-synthetically incorporated into the catalytic triad of the serine protease,  $\alpha$ -lytic protease. Earlier workers<sup>3</sup> found that this histidine possessed an abnormally low pKa value; this was interpreted as supporting a "charge-relay" mechanism

as the mode of catalysis for serine proteases. The present investigation reveals that this previous interpretation was incorrect, primarily because of the magnetic field used. The results presented in Part IV show how advanced nmr technology helps in the understanding of complex biochemical problems.

A new method for measuring the exchange rate of a two site chemical system undergoing slow exchange is described in Part V. The advantages of this method are that it may be applied to any nmr-active nucleus, and that the relative populations of each site do not have to be the same.

Part VI discusses an attempt to observe the chirality of the active site of liver alcohol dehydrogenase using the racemic modification of the ethanol substrate,  $\text{CD}_3\text{CHDOD}$ . An estimate of the chemical shift difference due to environmental factors for each proton when the substrate is bound to the protein has been made using 500.13 MHz proton nmr data.

Lastly, Part VII demonstrates the use of a very high field nmr spectrometer to elucidate the structure of a dimer synthesized by crosslinking the drug verapamil using formaldehyde. It is shown that, at 500.13 MHz,  $^1\text{H}$  resonance assignments and the interpretation of spectra for large molecules become relatively straightforward when compared with lower field nmr data.

REFERENCES

1. James, T. L. "Nuclear Magnetic Resonance in Biochemistry: Principles and Applications," Academic Press, NY (1975).
2. Moon, R. B., Ph.D. Thesis, California Institute of Technology (1975).
3. Hunkapiller, M. W., Smallcombe, S. H., Whitaker, D. R. & Richards, J. H. Biochemistry 1973, 12, 4732-4743.

## PART I

Nuclear Magnetic Resonance Investigation of  
<sup>13</sup>CO Binding to Heme Systems: Carbon-13  
Chemical Shifts and Spin-Lattice  
Relaxation Times.

## INTRODUCTION

Heme prosthetic groups are found in the active sites of a variety of proteins including oxygen transport proteins (hemoglobin), oxygen storage proteins (myoglobin), and redox proteins, such as the cytochromes. Many of these proteins are able to bind carbon monoxide which has been used as a probe to study the heme environment via carbon-13 nuclear magnetic resonance (nmr) and infrared (ir) spectroscopies.<sup>1-11</sup>

The interpretation of ir spectra of carbonmonoxy hemoglobins<sup>4,6,8-10</sup> has been aided by data obtained on various carbonyl heme models which have demonstrated how cis<sup>2,11</sup> and trans<sup>1,2</sup> effects can perturb the vibrational modes of the CO ligand. These results have greatly helped in the understanding of ligand-protein interactions in the heme pocket.

The molecular effects which influence the carbon-13 chemical shifts of <sup>13</sup>CO bound to heme proteins are much less understood, however, although the chemical shifts in carbonmonoxy myoglobins and hemoglobins reconstituted with modified hemes have been shown to be sensitive to changes around the periphery of the heme.<sup>14a</sup> In order to help in the interpretation of the carbon-13 nmr spectroscopic parameters of <sup>13</sup>CO bound to heme proteins, two compounds, protoheme IX dimethyl ester (1) and protoheme mono(3-(1-imidazolyl)propyl)amide monomethyl ester (2), were studied using carbon-13 nmr.

The chemical shift experiments are directed towards understanding to what degree the protein influences the environment of the heme bound  $^{13}\text{CO}$  in a spectroscopically detectable manner. Several views<sup>3,6,11,15,16</sup> have been presented with regard to the functional specificity of the heme ligand-protein interactions, and in this chapter additional evidence is shown in support of some<sup>3,6,15,16</sup> of these arguments.

Another important nmr parameter which is examined is the spin-lattice relaxation time ( $T_1$ ) of  $^{13}\text{CO}$  coordinated to the heme. Understanding the contributions of the various  $T_1$  relaxation mechanisms can yield valuable information on the nature of the ligand's environment in the protein. Accordingly, a  $T_1$  study of  $^{13}\text{CO}$  bound to 1-methylimidazole-protoheme IX dimethyl ester (1-MeIm-1) has been carried out at three magnetic field strengths (2.35, 4.22, and 8.44 Tesla).

## EXPERIMENTAL

Chemicals: Protoheme IX mono-(3-(1-imidazolyl)propyl)-amide monomethyl ester was provided by Professor Taylor's group.<sup>17</sup> Protoheme IX dimethyl ester was prepared by the method of Fuhrop and Smith.<sup>18</sup> All buffers and solvents were reagent grade.

Sample Preparation: A heme sample was weighed and degassed in a 10 cc syringe with nitrogen. Approximately 5 ml of a 4:1 mixture of nitrogen-degassed DMSO:d<sub>6</sub>-DMSO was then added to the syringe. After the heme was dissolved, the solution was injected into a 10 or 12 mm nmr tube equipped with a 2 mm access port which had been degassed with nitrogen and sealed with a rubber sleeve. Approximately 3 ml of 90%-enriched <sup>13</sup>CO was then injected into the tube, after which the iron was reduced by injection of 15 µl of a 0.4 M phosphate buffer solution (pH ≈ 7) which was saturated with sodium dithionite. For the protoheme IX dimethyl ester samples, aliquots of 1-methylimidazole (1-MeIm) were injected into the nmr tubes using a 10 µl syringe. For the study of the solvent dependence the volume of the sample was 3 ml. An internal capillary was used for the deuterium lock.

Instrumental: Carbon-13 nmr spectra were obtained with three different spectrometers. Low field measurements were made on a Varian XL-100-15 spectrometer operating at 25.14 MHz in the pulse Fourier transform (FT) mode. Spectra at 45.28 MHz were obtained with a Bruker WH-180 spectrometer. High field FT spectra were acquired with the Stanford Magnetic Resonance Laboratory's HSX-360 spectrometer which has a carbon-13 resonant frequency of 90.5 MHz. For each spectrum the line broadening used was equal to the digital resolution of the transformed spectrum. Sample tubes (10 mm) were used on both the WH-180 and the HXS-360, while 12 mm tubes were used on the XL-100-15.

T<sub>1</sub> Measurements: Spin-lattice (T<sub>1</sub>) relaxation measurements were made using the techniques of inversion recovery<sup>19</sup> and progressive saturation.<sup>20</sup> In all cases the limitation for the use of progressive saturation that T<sub>2</sub>\* << T<sub>1</sub> was satisfied as determined by line-width measurements. The delay times (τ) were varied randomly so as to eliminate systematic errors. T<sub>1</sub> values were calculated using a non-linear least squares program<sup>21</sup> to fit the equation  $A_{\tau} = A_{\infty} + (A_0 - A_{\infty})\exp(-\tau/T_1)$ .

Viscosities and Densities: Viscosities of solutions were determined by the method described by Shoemaker et al.<sup>22</sup> Densities were measured with a 1 ml Weld type pycnometer.



## THEORY

Rotational Brownian motion in a magnetic field of a molecule containing an nmr active nucleus ( $I \geq 1/2$ ) will cause fluctuations in the local magnetic field of that nucleus if it possesses an anisotropic chemical shift tensor ( $\sigma_{xx} \neq \sigma_{yy} \neq \sigma_{zz}$ ). These local fluctuations provide a mechanism (Chemical Shift Anisotropy, CSA) for spin-lattice ( $T_1$ ) and spin-spin ( $T_2$ ) relaxation. If one assumes axial symmetry, i.e.,  $\sigma_{xx} = \sigma_{yy}$ , the CSA relaxation rates can be described by eqs. 1 and 2.<sup>23</sup> Both of these equations assumes

$$\frac{1}{T_{1\text{CSA}}} = \frac{2}{15} \times \omega^2 (\Delta\sigma)^2 \times \frac{\tau_r}{1 + \omega^2 \tau_r^2} \quad (1)$$

$$\frac{1}{T_{2\text{CSA}}} = \frac{2}{45} \times \omega^2 (\Delta\sigma)^2 \times \left\{ \frac{3}{1 + \omega^2 \tau_r^2} + 4 \right\} \tau_r \quad (2)$$

where

$\omega$  = Larmor frequency

$\Delta\sigma$  =  $|\sigma_{||} - \sigma_{\perp}|$

$\sigma_{||}$  =  $\sigma_{zz}$

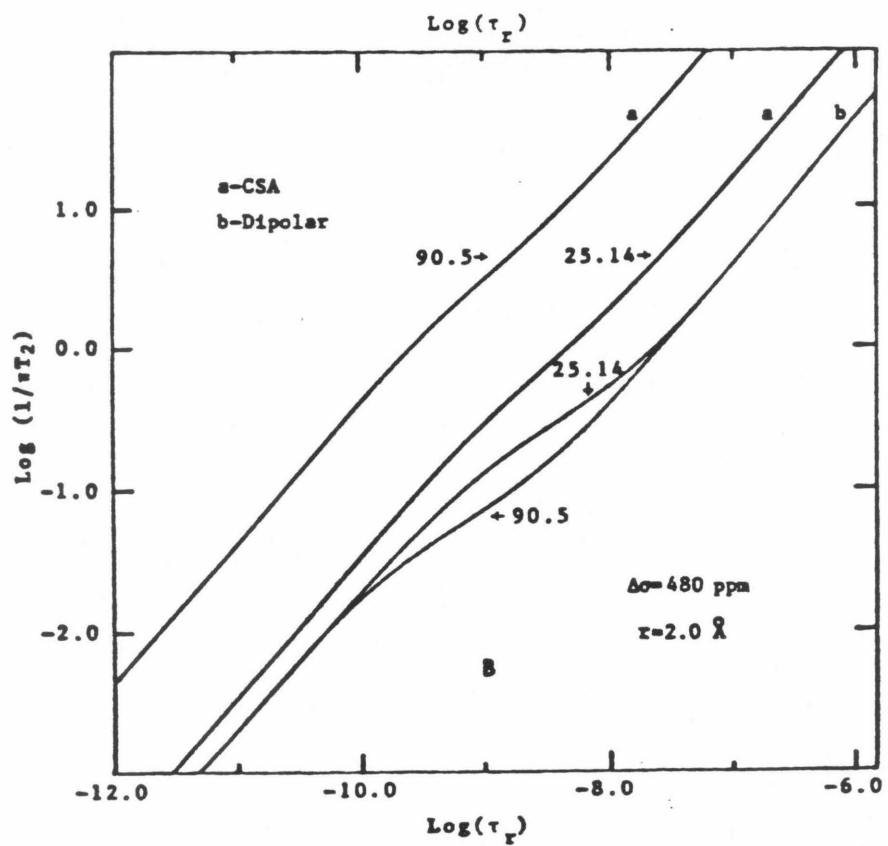
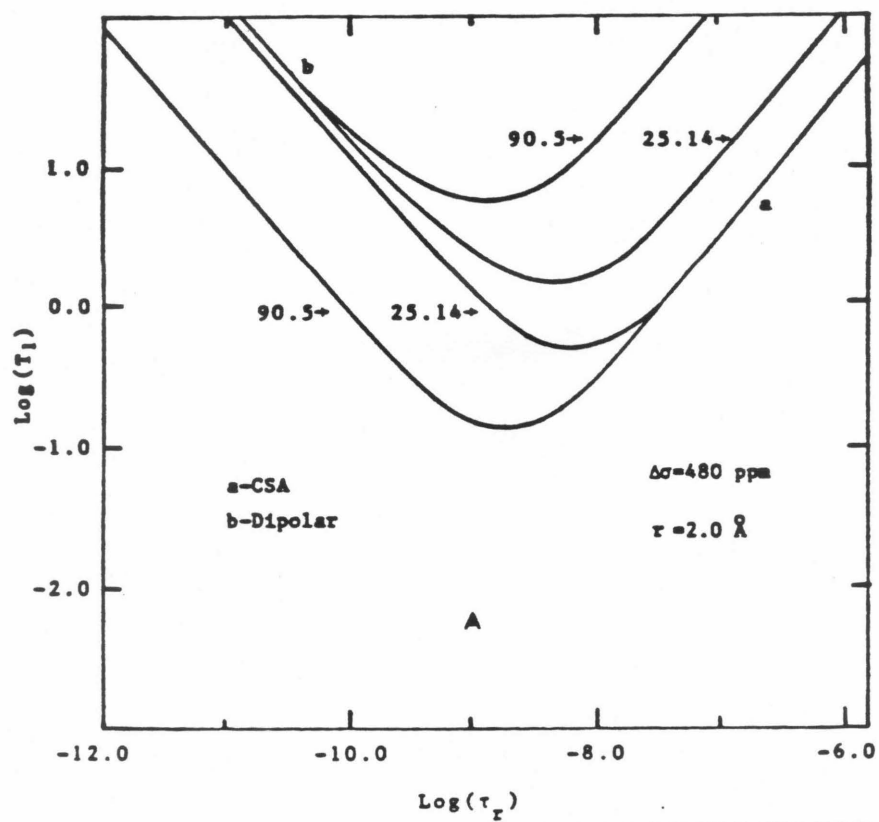
$\sigma_{\perp}$  =  $\sigma_{xx} = \sigma_{yy}$

$\tau_r$  = rotational correlation time in solution

isotropic rotation in solution. Figure 1 shows log-log plots for  $T_1$  and  $T_2$  relaxation via CSA at two different frequencies with  $\Delta\sigma = 480$  ppm. For the case of an ellipsoid (principle axes  $a \neq b \neq c$ ) undergoing anisotropic reorientation in

Figure 1

Calculated log-log plots of (A) spin-lattice and (B) spin-spin relaxation for  $^{13}\text{CO}$  at  $\omega = 25.14$  and 90.5 MHz using eqs. 1 and 2, with  $\Delta\sigma = 480$  ppm. Dipole-dipole relaxation times, assuming a  $^{13}\text{C}-^{1}\text{H}$  distance of  $2.0 \overset{\text{O}}{\text{\AA}}$ , have been included for comparison.



solution, eq. 1 becomes:<sup>24,25</sup>

$$\frac{1}{T_{1\text{CSA}}} = \frac{A}{T_{1A}} + \frac{B}{T_{1B}} + \frac{C}{T_{1C}} \quad (3)$$

where

$$\frac{1}{T_{1A,B,C}} = \frac{2}{15} \times \omega^2 (\Delta\sigma)^2 \times \frac{\tau_{A,B,C}}{1 + \omega^2 \tau_{A,B,C}^2} \quad (4)$$

$$A = \frac{1}{4} \times (3 \cos^2\theta - 1)^2 \quad (5)$$

$$B = 3 \sin^2\theta \cos^2\theta \quad (6)$$

$$C = \frac{3}{4} \sin^4\theta \quad (7)$$

$$\tau_A = \tau_{\perp} \quad (8)$$

$$\tau_B = 6 \tau_{\perp} \tau_{\parallel} (\tau_{\perp} + 5\tau_{\parallel})^{-1} \quad (9)$$

$$\tau_C = 3 \tau_{\perp} \tau_{\parallel} (2\tau_{\perp} + \tau_{\parallel})^{-1} \quad (10)$$

and where  $\tau_{\perp}$  and  $\tau_{\parallel}$  are the rotational correlation times perpendicular and parallel to the symmetry axis, respectively. If the approximation is made that the heme is an axially symmetric ellipsoid ( $a \neq b = c$ ),  $\theta$  equals zero for  $^{13}\text{CO}$  bound to the iron and eq. 3 reduces to eq. 1.

## RESULTS AND DISCUSSION

### Chemical Shifts

The carbon-13 nmr spectra of the  $^{13}\text{CO}$ -heme complexes show a single peak in the region near 200 ppm downfield from TMS. Equilibration of 1 with  $^{13}\text{CO}$  in  $\text{DMSO-d}_6$ -DMSO (4:1) leads to a single peak 207.7 ppm downfield from TMS (Figure 2a). Addition of aliquots of 1-MeIm causes a second peak to appear at 205.8 ppm (Figures 2b-2c); addition of more 1-MeIm causes the relative intensity of the upfield peak to increase until, at a 1-MeIm:heme ratio of 2:1, only the resonance at 205.8 ppm is observed (Figure 2d). The peak at 207.7 ppm has thus been assigned to the complex  $\text{DMSO-}\underline{1}\text{-}^{13}\text{CO}$  in which DMSO is bound to the heme trans to the  $^{13}\text{CO}$ . (Previous observations<sup>28,29</sup> have shown that DMSO coordinates to hemes through the oxygen.) Displacement of the axial DMSO by 1-MeIm yields the complex  $1\text{-MeIm-}\underline{1}\text{-}^{13}\text{CO}$  which is responsible for the resonance at 205.8 ppm. In support of this assignment, an analogous complex, 2, in which the imidazole ring is covalently attached to the heme and is known to be the axial ligand trans to  $^{13}\text{CO}$ , has a similar chemical shift at 205.8 ppm (Figure 2e).

Figure 3 shows the result of adding 1-MeIm to  $1\text{-MeIm-}\underline{1}\text{-}^{13}\text{CO}$  in DMSO. The 1.1 ppm change in the chemical shift is similar to the decrease of the C-O stretching frequency observed in going from a DMSO to 1-MeIm solution.<sup>29</sup>

Figure 2

$^{13}\text{CO}$  chemical shifts of protoheme IX dimethyl ester- $^{13}\text{CO}$  and protoheme mono(3-(1-imidazolyl)propyl)amide monomethyl ester- $^{13}\text{CO}$  in  $\text{DMSO:d}_6\text{-DMSO}$  (4:1): (a) 0.015 M 1- $^{13}\text{CO}$ ; (b) Sample (a) plus 2.3  $\mu\text{l}$  1-methylimidazole; (c) Sample (a) plus 4.6  $\mu\text{l}$  1-methylimidazole; (d) Sample (a) plus 13.1  $\mu\text{l}$  of 1-methylimidazole; (e) 0.014 M 2- $^{13}\text{CO}$ . All spectra were taken at room temperature.

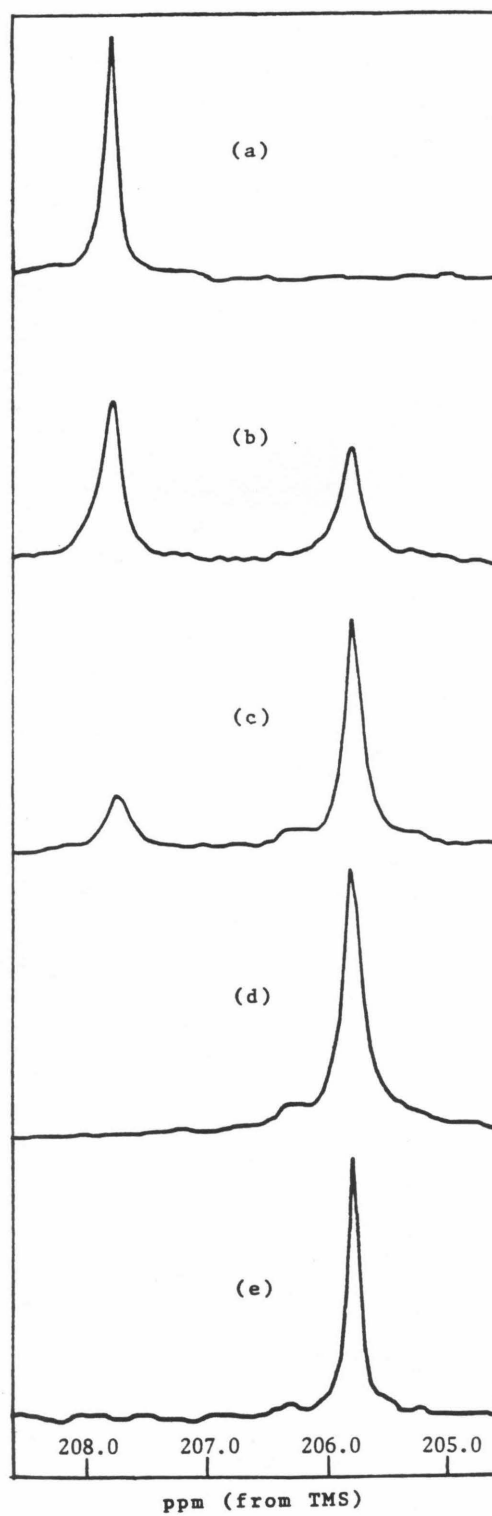
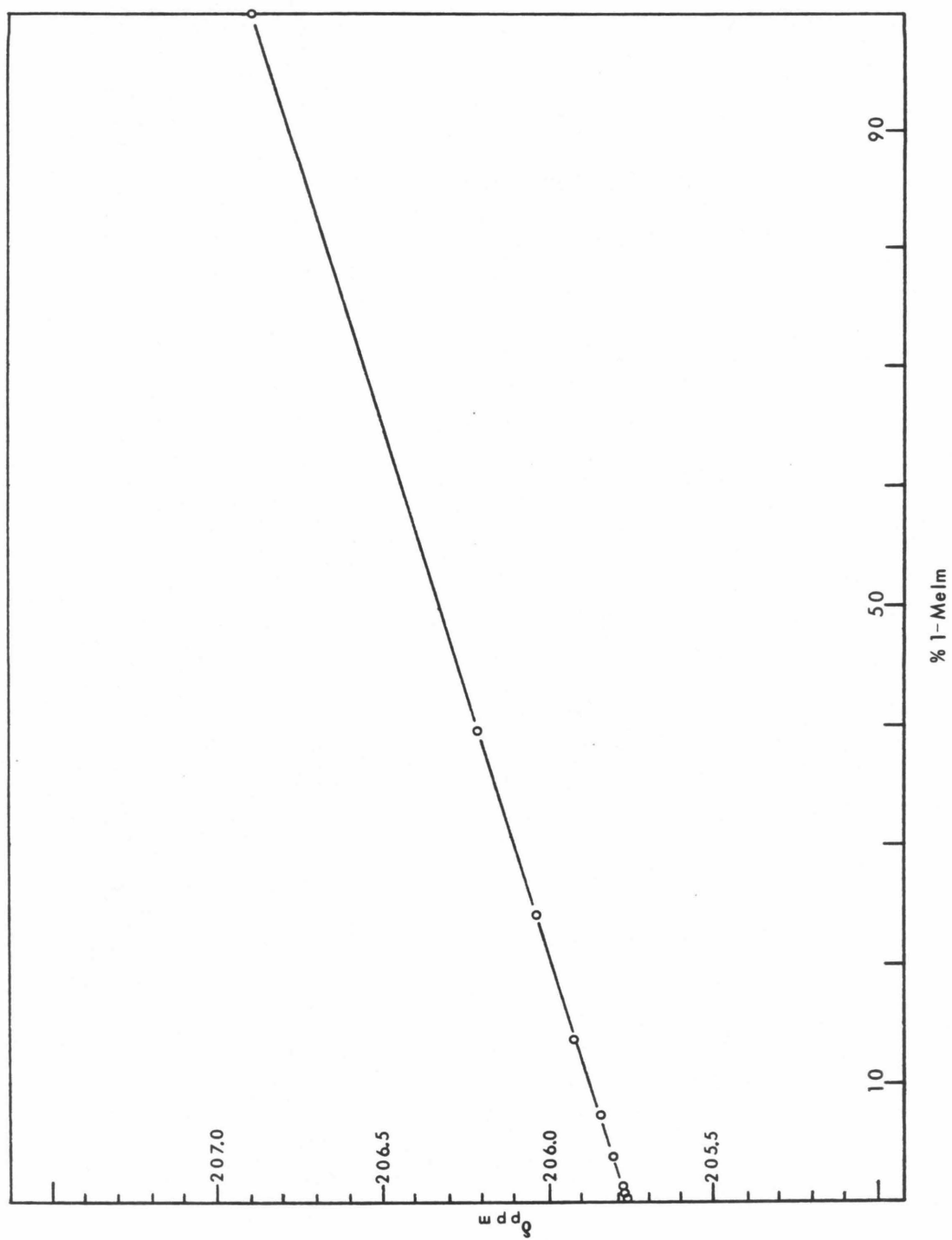


Figure 3

Solvent dependence of the  $^{13}\text{C}\equiv\text{O}$  chemical shift of 0.01 M ferrous protoporphyrin IX dimethyl ester- $^{13}\text{C}\equiv\text{O}$ . The chemical shifts were measured relative to internal TMS. The line drawn through the points is the least squares fit of the data. All spectra were collected at room temperature.





The resonances for these model systems are shifted upfield relative to those for heme coordinated  $^{13}\text{CO}$  in mammalian hemoglobins and myoglobins. The data in Table I show that the  $^{13}\text{C}$  nmr spectrum of the 1-MeIm-1- $^{13}\text{CO}$  complex in DMSO more closely resembles the spectrum obtained from the monomeric hemoglobin (HbII) of the marine annelid Glycera dibranchiata,<sup>28</sup> whereas in 1-MeIm the  $^{13}\text{CO}$  chemical shift is similar to that of HbA. Satterlee et al.<sup>6</sup> have previously suggested that this downfield shift is caused by a nucleophilic interaction between the heme bound ligand and the imidazole nitrogen of histidine E-7. Thus, in  $^{13}\text{CO}$ -HbII, which lacks His E-7 (His E-7  $\rightarrow$  Leu), the  $^{13}\text{CO}$  resonance appears at 206.2 ppm, which is very close to the  $^{13}\text{CO}$  resonances found for the model systems. In support of this argument is the fact that the  $^{13}\text{CO}$  resonance of 1-MeIm-1- $^{13}\text{CO}$  in 1-MeIm shifts downfield towards the chemical shifts observed for hemoglobins with a histidine at position E-7.

### Relaxation

The overall rate of spin-lattice relaxation can be described by eq. 11.

$$\frac{1}{T_{1\text{TOT}}} = \frac{1}{T_{1\text{D-D}}} + \frac{1}{T_{1\text{SC}}} + \frac{1}{T_{1\text{CSA}}} + \frac{1}{T_{1\text{P}}} + \frac{1}{T_{1\text{Q}}} + \frac{1}{T_{1\text{SR}}} \quad (11)$$

where

D-D	=	nuclear dipole-dipole relaxation
SC	=	scalar relaxation
CSA	=	chemical shift anisotropy
P	=	paramagnetic relaxation
Q	=	quadrupolar relaxation
SR	=	spin-rotation relaxation

If the relaxation measurements are made at two different field strengths, the difference between the two rates is given by eq. 12. For this system the dipole-dipole, scalar, para-

$$\Delta \frac{1}{T_{1TOT}} = \Delta \frac{1}{T_{1D-D}} + \Delta \frac{1}{T_{1SC}} + \Delta \frac{1}{T_{1CSA}} + \Delta \frac{1}{T_{1P}} + \Delta \frac{1}{T_{1Q}} + \Delta \frac{1}{T_{1SR}} \quad (12)$$

magnetic, and quadrupolar contributions to the total rate should be small compared to the CSA and spin-rotational relaxation rates. For a molecule of the size of 1,  $1/T_{1SR}$  should be negligible at all field strengths used in this study,<sup>33</sup> hence  $\Delta 1/T_{1SR}$  should be much less than  $\Delta 1/T_{1CSA}$ . Thus, eq. 12 reduces to

$$\Delta \frac{1}{T_{1TOT}} = \Delta \frac{1}{T_{1CSA}} \quad (13)$$

Combining eqs. 1 and 13 and solving for  $\Delta\sigma$  yields:

Table I

 $^{13}\text{CO}$  Chemical Shifts of Various Heme Complexes

<u>Complex</u>	<u>Chemical Shift (ppm)<sup>a</sup></u>	<u>Ref.</u>
DMSO- <u>1</u> - $^{13}\text{CO}$	207.7	this work
1-MeIm- <u>1</u> - $^{13}\text{CO}$ (DMSO solvent)	205.8	this work
1-MeIm- <u>1</u> - $^{13}\text{CO}$ (1-MeIm solvent)	206.9	this work
<u>2</u> - $^{13}\text{CO}$	205.8	this work
Human Hemoglobin		
$\alpha$ -chains	207.5	14b, 28
$\beta$ -chains	207.1	14b, 28
Sperm Whale Myoglobin	208.7	14b, 28
<u>G. dibranchiata</u>	206.2	28

a) shifts are downfield from TMS, error limits are  $\pm 0.1$  ppm.

$$|\Delta\sigma| = \left[ \frac{\Delta 1/T_{\text{tot}}}{\frac{2}{15} \left\{ \omega_A^2 / (1 + \omega_A^2 \tau_r^2) - \omega_B^2 / (1 + \omega_B^2 \tau_r^2) \right\} \tau_r} \right]^{1/2} \quad (14)$$

where  $\omega_A > \omega_B$ . From eq. 14 one can determine  $|\Delta\sigma|$  directly from relaxation measurements obtained at two different frequencies. It should be noted that if there is any contribution to  $1/T_{1\text{tot}}$  from the other mechanisms,

$$\Delta \frac{1}{T_{1\text{TOT}}} < \Delta \frac{1}{T_{1\text{CSA}}} \quad (15)$$

Thus, the value for  $|\Delta\sigma|$  obtained with eq. 14 will be a lower bound.

Figure 4 shows a set of typical progressive saturation  $T_1$  stack plots obtained at 25.14 and 90.5 MHz. Table II summarizes the relaxation data collected at three frequencies. Table III contains the chemical shift information for solid  $^{13}\text{CO}$  and three carbonyl complexes.

A significant decrease is observed in  $\sigma_{\perp}$  (from -123 ppm for solid  $^{13}\text{CO}$  to -207 ppm for 1-MeIm-1- $^{13}\text{CO}$ ) which reflects the change in the electronic environment of the carbon nuclide.<sup>31</sup> The increase in  $\sigma_{\parallel}$  for 1-MeIm-1- $^{13}\text{CO}$  is probably caused by a ring current shift due to the  $\pi$  network of the heme.<sup>35</sup> Such an effect of the heme ring current can also explain the significant difference between  $\Delta\sigma$  for 1-MeIm-1- $^{13}\text{CO}$  and  $\text{Fe}(^{13}\text{CO})_5$ .

Figure 4

$^{13}\text{CO}$  progressive saturation  $T_1$  measurements of 0.015 M 1-methylimidazole- $\alpha$ -protoheme IX dimethyl ester- $^{13}\text{CO}$  taken at  $29.0 \pm 1.5^\circ\text{C}$ : (a) 25.14 MHz; (b) 90.5 MHz. Note the increase in linewidth in going from (a) to (b).

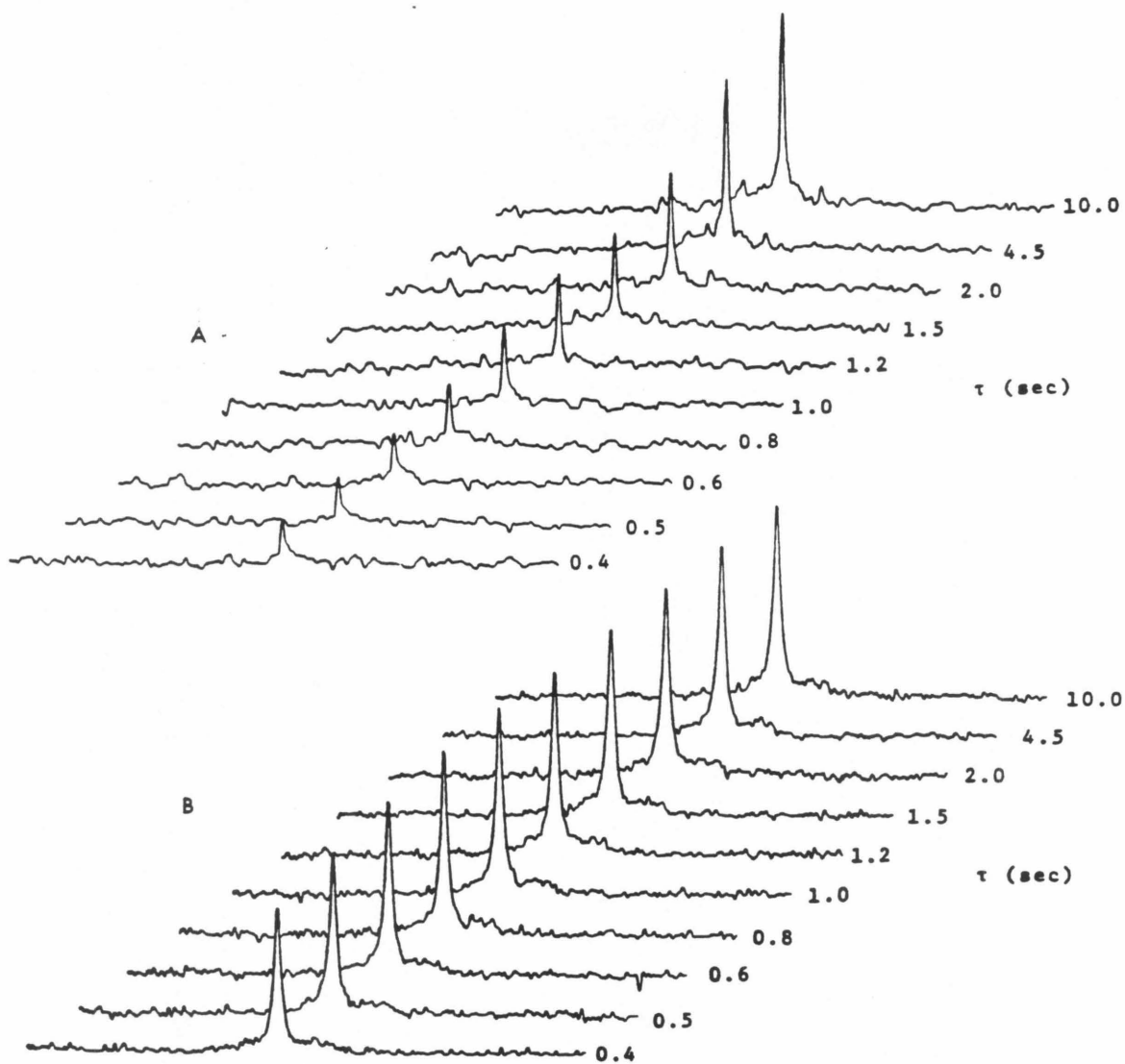


Table II

Spin-Lattice Relaxation Times of  $^{13}\text{CO}$  Bound to 0.015 M  
 1-Methylimidazole-Protoheme IX Dimethyl Ester in  $\text{DMSO-d}_6$ -DMSO (4:1)

<u>T(+1.5°C)</u>	<u><math>\nu</math>(MHz)</u>	<u><math>T_1</math>(sec)<sup>a</sup></u>	<u><math>\tau_r(\times 10^{10}\text{sec})^b</math></u>	<u><math> \Delta\sigma </math> (ppm)<sup>c</sup></u>
	25.14	2.3 $\pm$ 0.2		
21.0	45.28	0.63 $\pm$ 0.23	4.1 $\pm$ 0.8	574 $\pm$ 122
	90.5	0.19 $\pm$ 0.02		
	25.14	2.6 $\pm$ 0.2		
29.0	90.5	0.20 $\pm$ 0.02	3.2 $\pm$ 0.6	614 $\pm$ 63

a) Errors are standard deviation obtained from a non-linear curve fit; b)  $\tau_r$  calculated using a solvent radius of  $2.1 \pm 0.1 \text{ \AA}$  and a heme radius of  $7.2 \pm 0.2 \text{ \AA}$  as estimated from the crystal structure of  $\alpha$ -chlorohemin. The error limits reflect the uncertainty in the viscosity measurements and radius estimates; c) Obtained with eq. 14. Error limits obtained using a propagation of errors analysis.



Table III

<sup>13</sup>CO Chemical Shifts and Shielding Tensors<sup>a</sup>

Compound	$\sigma_{\parallel}^b$	$\sigma_{\perp}^b$	$\sigma_{AV}^c(\pm 10)$	$\Delta\sigma^d$	Ref.
<sup>13</sup> CO	283	-123	+12	406 $\pm$ 30	33
Ni( <sup>13</sup> CO) <sub>4</sub>	294	-146	+ 1	440 $\pm$ 44	34
Fe( <sup>13</sup> CO) <sub>5</sub>	253	-155	-19	408 $\pm$ 41	34
1-MeIm-1- <sup>13</sup> CO	377	-207	-12	584 $\pm$ 132	this work

a) units are in ppm; b) calculated given the two equations  $\Delta\sigma = |\sigma_{\parallel} - \sigma_{\perp}|$  and  $\sigma_{AV} = (\sigma_{\parallel} + 2\sigma_{\perp})/3$ ; c) equation for  $\sigma_{AV}$  given in (b). Chemical shifts are based on an absolute scale, with  $\sigma_{AV} = 12 \pm 10$  for <sup>13</sup>CO.<sup>31</sup> Positive  $\sigma_{AV}$  denotes up-field shift; d) sign of  $\Delta\sigma$  is positive.<sup>34</sup>

Understanding the influence ligands trans to  $^{13}\text{CO}$  have on the carbon chemical shift and of the mechanism of spin-lattice relaxation in the protoheme derivatives studied provides a basis for the interpretation of these nmr parameters in carbonmonoxy hemoglobins and myoglobins. Extension of this work to the heme-containing proteins, specifically the spin-lattice relaxation of  $^{13}\text{CO}$  bound to hemoglobin and myoglobin, will be presented in Part II.

REFERENCES

1. Alben, J. O. & Caughey, W. S. Biochemistry 1968, 7, 175-183.
2. Caughey, W. S. Ann. N. Y. Acad. Sci. 1970, 174, 148-153.
3. Caughey, W. S., Bayne, R. A. & McCoy, S. J. C. S. Chem. Comm. 1970, 950-951.
4. Maxwell, J. C., Barlow, C. H., Spellholz, J. & Caughey, W. S. Biochem. Biophys. Res. Commun. 1974, 61, 230-236.
5. Volpe, J. H., O'Toole, M. C. & Caughey, W. S. Biochem. Biophys. Res. Commun. 1975, 69, 48-53.
6. Satterlee, J. D., Teintze, M. & Richards, J. H. Biochemistry 1978, 17, 1456-1462.
7. Matwiyoff, N. A., Vergamini, P. J., Needham, T. E., Gregg, G. T., Volpe, J. A. & Caughey, W. S. J. Am. Chem. Soc. 1973, 95, 4429-4431.
8. Caughey, W. S., Alben, J. O., McCoy, S., Boyer, S. H., Charache, S. & Hathway, P. Biochemistry 1969, 8, 59-62.
9. McKoy, S. & Caughey, W. S., in "Probes of Structure and Function of Macromolecules and Membranes," Chance, B., Yonetani, T. & Mildvan, A. S., editors, Academic Press, New York, pp. 289-295 (1971).

10. Barlow, C. H., Ohlsson, P. I. & Paul, K. G. Biochemistry 1976, 15, 2225-2229.
11. Collman, J. P., Baumann, J. I., Halbert, T. R. & Suslick, K. S. Proc. Natl. Acad. Sci. USA 1976, 73, 3333-3337.
12. Conner, W. M. & Straub, D. K. Inorg. Chem. 1976, 2289-2291.
13. Alben, J. O. & Caughey, W. S. Biochemistry 1968, 7, 175.
14. a) Moon, R. B., Dill, K. & Richards, J. H. Biochemistry 1977, 16, 221. b) Moon, R. B. & Richards, J. H. Biochemistry 1974, 13, 3437-3443. c) Moon, R. B. & Richards, J. H. J. Am. Chem. Soc. 1972, 94, 5093-5095.
15. Satterlee, J. D. & Richards, J. H. submitted for publication.
16. Caughey, W. S., Eberspaecher, H., Fuchsman, W. H., McCoy, S. & Alben, J. O. Ann. N. Y. Acad. Sci. 1969, 722-737.
17. Geibel, J. Cannon, J., Campbell, D. & Traylor, T. G. J. Am. Chem. Soc. 1978, 100, 35-75.

18. Fuhrop, J. H. & Smith, K. M. "Laboratory Methods in Porphyrin and Metalloporphyrin Research," Elsevier Scientific Publishing Co., Amsterdam, pp. 79-80 (1975).
19. Farrar, T. C. & Becker, E. D. "Pulse and Fourier Transform NMR," Academic Press, Inc., N.Y., p. 21 (1971).
20. Freeman, R. & Hill, H. D. W. J. Chem. Phys. 1971, 54, 3367.
21. Hull, W. E. Ph.D. Thesis, Harvard University (1975).
22. Shoemaker, D. P., Garland, C. W. & Steinfeld, J. I., "Experiments in Physical Chemistry," McGraw-Hill, Inc., N.Y., pp. 392-400 (1974).
23. Farrar, T. C. & Becker, E. D. "Pulse and Fourier Transform NMR," Academic Press, Inc., N.Y., p. 59, (1971).
24. Woessner, D. E. J. Chem. Phys. 1962, 37N, 647.
25. Wilber, D. J., Norton, R. S., Clouse, A. O., Addleman, R. & Allerhand, A., J. Am. Chem. Soc., 1976, 98, 8250.
26. Reed, C. A. 1977, private communication.
27. LaMar, G. N. 1978, private communication.
28. Satterlee, J. D., Teintze, M. & Richards, J. H. submitted for publication.
29. Maxwell, J. C. & Caughey, W. S. Biochemistry 1976, 15, 388.

30. Koenig, D. F. Acta, Cryst. 1965, 18, 663.
31. Appleman, B. R. & Dailey, B. P. "Advances in Magnetic Resonance," Waugh, J. S., editor, Vol. 7, Academic Press, N.Y., p. 231 (1974).
32. Gibson, A. A., Scott, T. A. & Fukushima, E. J. Magn. Res. 1977, 27:1, 29.
33. Spiess, H. V. W. & Mahnke, H. Berichte der Bunsen-Gesellschaft 1972, 76:10, 990.
34. Spiess, H. V. W., Schwitzer, D., Haeberlen, U. & Hausser, K. H. J. Magn. Res. 1971, 5, 101.
35. Emsley, J. W., Fenney, J. & Sutcliffe, L. H., "High Resolution Nuclear Magnetic Resonance Spectroscopy," Pergamon Press, Oxford, p. 147 (1965).

PART II

Nuclear Magnetic Resonance Investigation  
to  $^{13}\text{C}$  CO Binding to Heme Proteins:  
Relaxation Mechanisms.

## INTRODUCTION

Examination of the interaction between  $^{13}\text{C}$ -enriched carbon monoxide and the heme environment of myoglobins and hemoglobins has been investigated in recent years through the use of carbon-13 nuclear magnetic resonance (nmr) spectroscopy.<sup>1-5</sup> The information obtained with these experiments has been relatively limited, as the parameters measured (chemical shift and spin-lattice relaxation times,  $T_1$ ) has not been fully understood. Recently, Satterlee et al<sup>4,5</sup> have been able to explain the chemical shifts of  $^{13}\text{CO}$  bound to the monomeric hemoglobin of the marine annelid Glycera dibranchiata and to rabbit (New Zealand white) hemoglobin as a function of the distal residue E7 (histidine in rabbit, leucine in Glycera) and its interaction (or lack of one) with the bound ligand.

Moon,<sup>1</sup> in an attempt to understand the nature of the interaction between the heme bound  $^{13}\text{CO}$  and the distal residues in human hemoglobin and sperm whale myoglobin, carried out  $T_1$  and nuclear Overhauser effect (NOE) measurements. His  $T_1$  results indicated that the  $^{13}\text{CO}$  was being relaxed by a  $^{13}\text{C}$ - $^1\text{H}$  dipolar mechanism, the hydrogen atoms being associated with the heme pocket residues. However, this interpretation was not supported by the NOE data which, within experimental error,<sup>6</sup> gave an NOE of 1.0 ( $\eta = 0$ ).



With Moon's contradictory results in mind, the concepts discussed previously<sup>19</sup> have been applied to his data, namely, that Chemical Shift Anisotropy (CSA), in addition to dipole-dipole (D-D) interactions, contributes to the observed spin-lattice relaxation rates. With this analysis, it is possible to explain all of his observations, including the lack of a measurable  $\eta$ . In order to solidify this interpretation,  $T_1$  measurements of  $^{13}\text{CO}$  bound to sperm whale myoglobin have been made at 2.35 and 8.44 Tesla. The linewidth field dependence of  $^{13}\text{CO}$ -coordinated rabbit hemoglobin was also carried out. It is believed that such nmr measurements have been used to obtain information about the role of His-E7 in the binding of carbon monoxide to hemoglobins and myoglobins.

## EXPERIMENTAL

Sample Preparation: Approximately 400 mg of sperm whale myoglobin (Sigma) were dissolved in 15 ml of 0.1 M Tris buffer, pH 7.1. After the removal of solid impurities by centrifugation at 15,000 rpm for 30 min, the sample was concentrated by pressure ultrafiltration (Amacon UM-10). The concentrated myoglobin was purified by chromatography on a Sephadex G-75 column, equilibrated with 0.1 M Tris buffer, pH 8.0, and concentrated again. The sample was then taken up in a 50 cc syringe, degassed with nitrogen, and injected into another syringe (degassed) with approximately 10 mg of sodium dithionite. 5 ml of  $^{13}\text{CO}$  were added to the sample which was then concentrated to 6 ml, diluted to 9 ml with  $\text{D}_2\text{O}$ , and concentrated to 6.8 ml. The sample was again degassed with nitrogen, after which 3 ml of  $^{13}\text{CO}$  were added to the sample. The resulting solution was then injected into two degassed nmr tubes (10 and 12 mm o.d.) like those previously described.<sup>19</sup>

Rabbit (New Zealand white) hemoglobin was prepared from 50 cc of freshly drawn, citrated blood. The red cells were separated from the plasma by centrifugation at 2000 rpm for 30 min and washed three times with 0.15 M NaCl. The cells were then lysed with distilled water at 4°C. The cell debris was removed by centrifugation

at 15,000 rpm for one hour. The resulting hemoglobin was purified with 0.15 M NaCl using continuous flow high pressure ultrafiltration (Amacon UM-10) for 24 hrs at 4°C. The sample was then concentrated to approximately 12 ml and deoxygenated in a 30 cc syringe with nitrogen. 2 ml of degassed D<sub>2</sub>O were added to the protein solution, after which the sample was injected into two nmr tubes (10 mm and 12 mm), each containing approximately 3 mg of sodium dithionite. Nine ml of <sup>13</sup>CO were then injected into each of the degassed sample tubes.

The concentration of the carbonmonoxy myoglobin sample was determined spectrophotometrically at 423 nm using an extinction coefficient of  $\epsilon = 187 \text{ mM}$ . The rabbit carbonmonoxy hemoglobin concentration was approximated using  $\epsilon = 764 \text{ mM}$  for its absorption at 419 nm.

Instrumental: The nmr spectrometers which were used were described in Part I. 10 mm sample tubes were used on all spectrometers except the XL-100-15, which requires 12 mm nmr tubes. For the high field measurements, the digital line broadening used was greater than the digital resolution of the spectrum in order to improve the signal-to-noise ratio of the myoglobin spectra at 90.5 MHz, and the rabbit hemoglobin spectrum at 45.28.

T<sub>1</sub> Measurements: Spin-lattice (T<sub>1</sub>) relaxation measurements were made using progressive saturation.<sup>7</sup> In all

cases the limitation that  $T_2^* \ll T_1$  was satisfied. The delay times ( $\tau$ ) were varied randomly so as to eliminate systematic errors.  $T_1$  values were calculated using a non-linear least squares program<sup>8</sup> to fit the equation  $A_\tau = A_\infty + (A_0 - A_\infty)\exp(-\tau/T_1)$ .

Viscosities and Densities: Viscosities of solutions were determined by the method described by Shoemaker et al.<sup>9</sup> Densities were measured with a 1 ml Weld type pycnometer.

THEORY

As described previously,<sup>19</sup> the overall rate of spin-lattice relaxation is given by eq. 1:

$$\frac{1}{T_{1\text{TOT}}} = \frac{1}{T_{1\text{D-D}}} + \frac{1}{T_{1\text{CSA}}} + \frac{1}{T_{1\text{SC}}} + \frac{1}{T_{1\text{SR}}} + \frac{1}{T_{1\text{Q}}} + \frac{1}{T_{1\text{P}}} \quad (1)$$

where the subscripts are defined in Part I. For most macromolecular systems (including myoglobins and hemoglobins),  $\tau_r$ , the rotational correlation time in solution, is on the order of  $10^{-8}$  sec. In this region, the dominant mechanism for carbon-13 relaxation is, in most cases, the  $^1\text{H}$ - $^{13}\text{C}$  dipole-dipole (D-D) interaction.<sup>10</sup> For isotropic rotation in solution (a valid assumption for most proteins),<sup>11</sup> the dipolar relaxation rate is given by eq. 2:<sup>12</sup>

$$\begin{aligned} \frac{1}{T_{1\text{D-D}}} &= \gamma_x^2 \gamma_s^2 \hbar^2 s(s+1) \\ &\times \sum_{i=1}^n \left\{ \frac{1}{12} J_0(\omega_x - \omega_s) + \frac{3}{2} J_1(\omega_x) + \frac{3}{4} J_2(\omega_x + \omega_s) \right\} \end{aligned} \quad (2)$$

where

$\gamma_x$  = magnetogyric ratio of the observed nucleus  
( $^{13}\text{C}$ )

$\gamma_s$  = magnetogyric ratio of the relaxing nucleus  
( $^1\text{H}$ )

$\hbar$  = Planck's constant/ $2\pi$

$s$  = spin of the relaxing nucleus ( $s = \frac{1}{2}$  for  $^1\text{H}$ )

$$J_0(\omega_x - \omega_s) = (24/15)(r_i^{-6})(\omega_r/(1 + (\omega_x - \omega_s)^2\tau_r^2)^2$$

$$J_1(\omega_x) = (4/15)(r_i^{-6})(\omega_r/(1 + \omega_x^2\tau_r^2)^2$$

$$J_2(\omega_x + \omega_s) = (16/15)(r_i^{-6})(\omega_r/(1 + (\omega_x + \omega_s)^2\tau_r^2)^2$$

$r_i$  = distance between nucleus x ( $^{13}\text{C}$ )  
and nucleus  $s_i$  ( $^1\text{H}$ )

$\omega_x$  = Larmor frequency of the observed  
nucleus ( $^{13}\text{C}$ )

$\omega_s$  = Larmor frequency of the relaxing  
nucleus ( $^1\text{H}$ )

$\tau_r$  = rotational correlation time

A similar expression describes spin-spin ( $T_2$ ) relaxation.<sup>12</sup>  
Log-log relaxation plots for the dipolar mechanism are  
given in Figures 1a and 1b.

Because of the results obtained on model heme systems,<sup>19</sup>  
Chemical Shift Anisotropy (CSA) must be included when describ-  
ing the overall rate of relaxation for  $^{13}\text{CO}$  bound to hemo-  
globins and myoglobins. So, for  $^{13}\text{CO}$  coordinated to these  
proteins, eq. 1 becomes<sup>13</sup>

$$\frac{1}{T_{1\text{TOT}}} = \frac{1}{T_{1\text{D-D}}} + \frac{1}{T_{1\text{CSA}}} \quad (3)$$

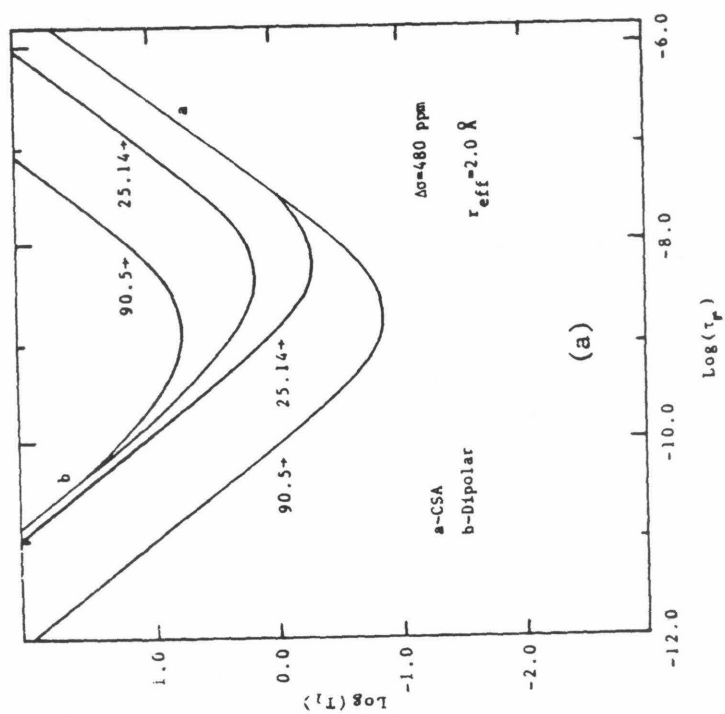
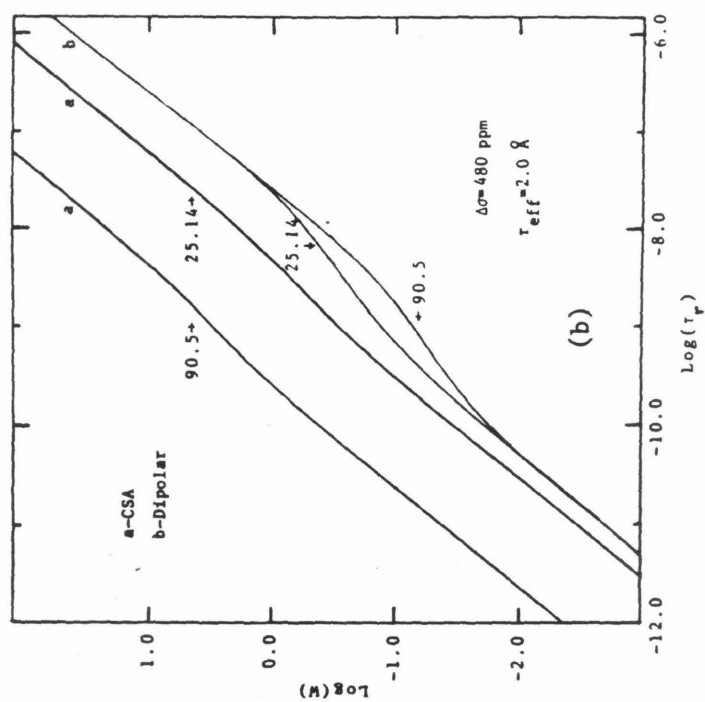
Figure 1c is a log-log plot generated from eq. 3. An inter-  
esting phenomenon is revealed in this figure. For  $\tau_r < 10^{-8}$   
sec, the observed field dependence is like that for the

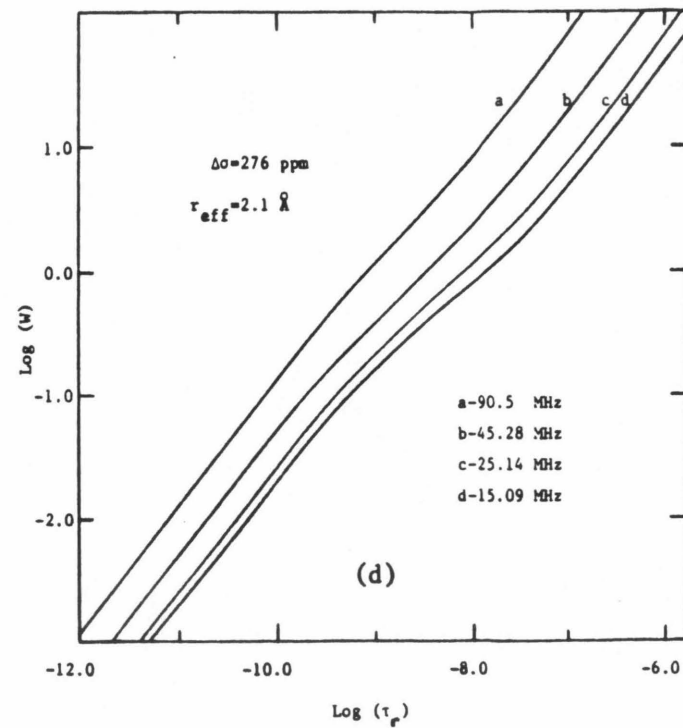
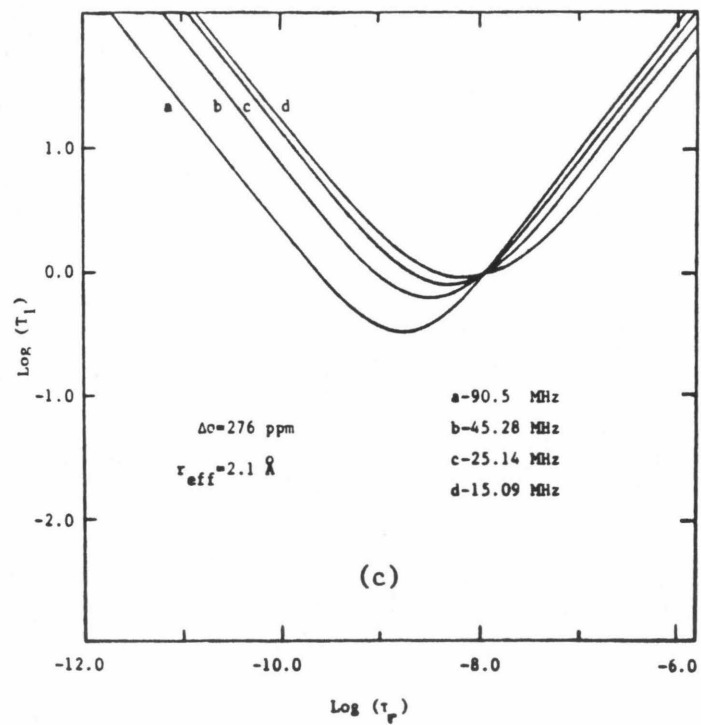
dipolar mechanism. Thus, for  $^{13}\text{CO}$  bound to hemoglobins, the measured  $T_1$  will appear to be dominated by the dipolar mechanism, even if CSA is the dominant relaxation mechanism. For  $^{13}\text{CO}$  coordinated to myoglobins,  $\tau_r$  is on the order of  $5 \times 10^{-9}$  sec, so the  $T_1$  that is observed should show a CSA-like field dependence. However, in all cases the linewidth will have a frequency dependence characteristic of the CSA mechanism (see Figure 1d).

Figure 1

Calculated log-log plots of spin-lattice relaxation ( $T_1$ ) and linewidth for  $^{13}\text{CO}$ : (a)  $T_1$  calculated using eq. 2 and  $r_{\text{eff}} = 2.0 \text{ \AA}$ ; (b) linewidth calculated using an equation similar to eq. 2 and  $r_{\text{eff}} = 2.0 \text{ \AA}$ ; <sup>12</sup> (c)  $T_1$  calculated using eq. 3 with  $r_{\text{eff}} = 2.1 \text{ \AA}$  and  $\Delta\sigma = 276 \text{ ppm}$ ; (d) linewidth calculated using an expression similar to eq. 3 and  $r_{\text{eff}} = 2.1 \text{ \AA}$  and  $\Delta\sigma = 276 \text{ ppm}$ .







## RESULTS AND DISCUSSION

Figure 2 is a copy of the  $T_1$  data obtained by Moon<sup>1</sup> of  $^{13}\text{CO}$  bound to human hemoglobin. As can be seen by this figure, the  $T_1$ 's exhibit a dipolar field dependence. Moon fit these data using eq. 2 and obtained an effective proton-carbon distance ( $r_{\text{eff}}$ ) of  $1.77 \pm 0.05 \text{ \AA}$  at 2.35 Tesla and  $1.77 \pm 0.07 \text{ \AA}$  at 1.41 Tesla. However, this observation was not supported by the NOE data, as the expected signal enhancement of 1.17 was not observed. This left many doubts concerning the analysis of the  $T_1$  data. However, if one assumes that there are two mechanisms contributing to the observed  $T_1$ , then these data can be explained, i.e., if the  $^{13}\text{CO}$  is not being relaxed totally by the dipolar mechanism, then the NOE which is observed will only be a fraction of the expected signal enhancement.

Equation 3 can be rewritten as

$$\frac{1}{T_{1\text{TOT}}} = f(H_0, \tau_r, r_{\text{eff}}, \Delta\sigma) \quad (4)$$

where  $H_0$ , the magnetic field strength, is now included as a second variable. This can now be looked upon as a non-linear function with parameters  $r_{\text{eff}}^{-6} (= \sum_{i=1}^n r_i^{-6})$  and  $\Delta\sigma^2$ . Thus, both sets of  $T_1$  data (2.35 and 1.4 Tesla) can be fit to this equation using a non-linear least squares approach.

Figure 3 shows the weighted non-linear least squares fit of the HbA- $^{13}\text{CO}$   $T_1$  data shown in Figure 2.<sup>14</sup> The  $r_{\text{eff}}$

## Figure 2

Dependence of  $^{13}\text{CO}$   $T_1$ 's on hemoglobin concentration.  
The values were obtained for carbonmonoxy hemoglobin  
in 0.15 M NaCl, pH 6.9-7.0. The figure is from  
ref. 1 (reproduced without permission).

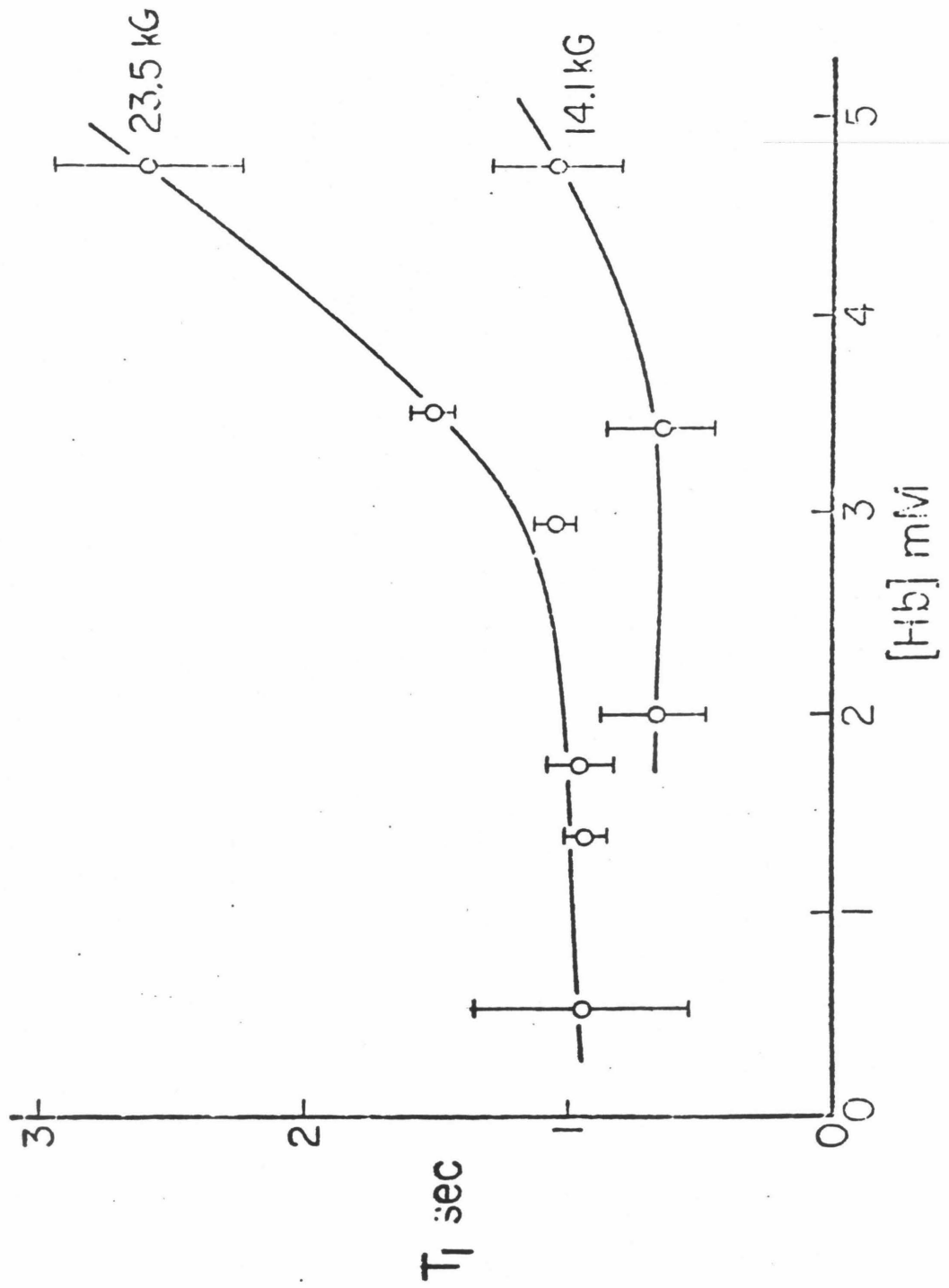
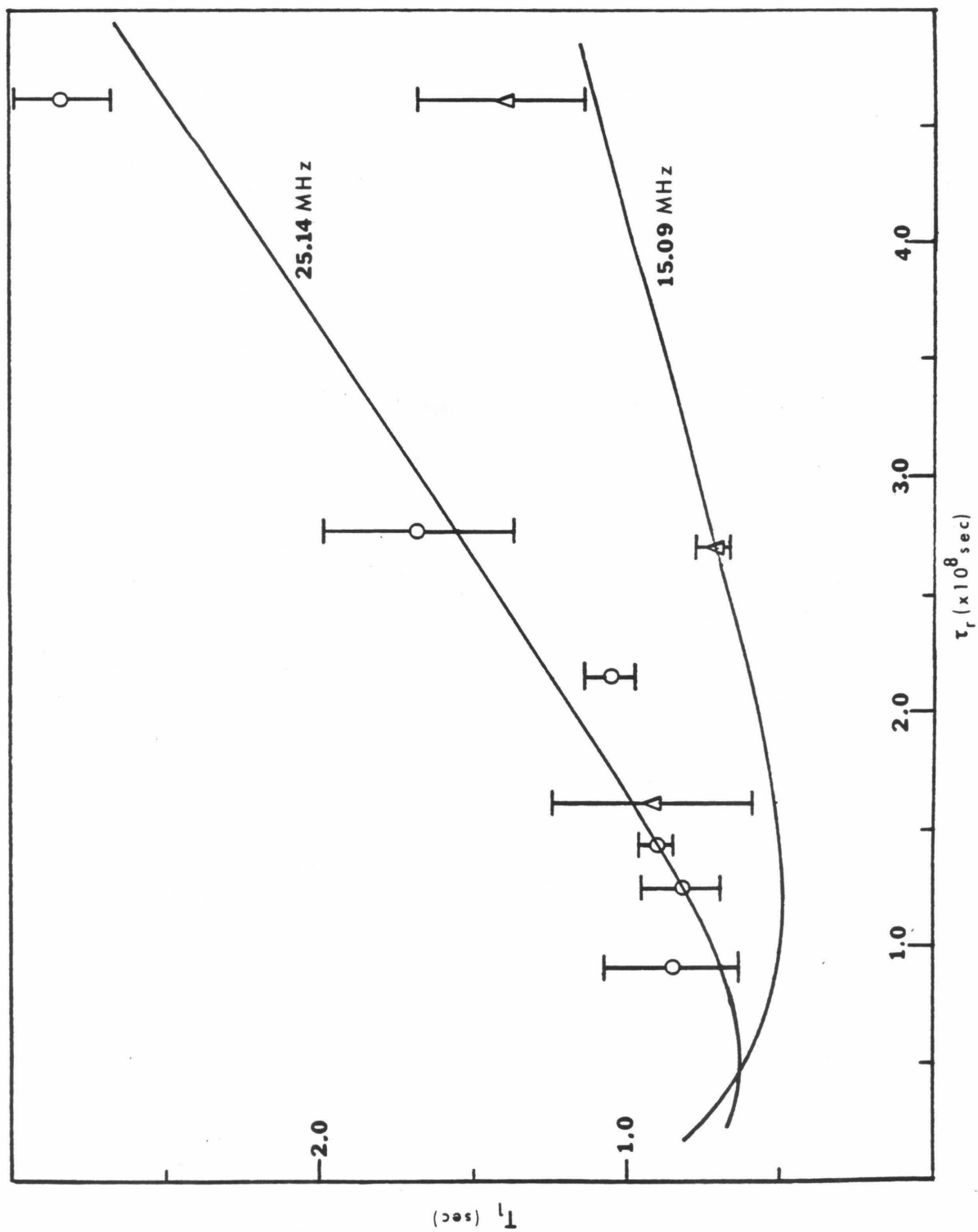


## Figure 3

Plot of the data from Figure 2<sup>14</sup> along with theoretical curves generated using eq. 3 with  $\Delta\sigma = 194 \pm 37$  ppm and  $r_{\text{eff}} = 1.81 \pm 0.02 \text{ \AA}^{\text{O}}$ .

The correlation times were obtained from ref. 1.



obtained with this analysis ( $r_{\text{eff}} = 1.81 \pm 0.02 \text{ \AA}$ ) is consistent with that estimated from the crystal structure of carbonmonoxy myoglobin.<sup>15</sup> The significance of the anisotropy which was obtained ( $\Delta\sigma = 194 \pm 37 \text{ ppm}$ ) will be discussed later.

Confirmation of this interpretation was needed, however, as there still was no direct evidence that CSA was contributing to the relaxation of the  $^{13}\text{CO}$ . Table I summarizes the  $T_1$  and linewidth measurements of  $^{13}\text{CO}$  bound to myoglobin and the linewidth data for rabbit hemoglobin. Figure 4 shows the frequency dependence of the linewidths of  $^{13}\text{CO}$  bound to rabbit hemoglobin. The linewidth data for both proteins clearly show that CSA is contributing to the observed relaxation rates. Also, the myoglobin- $^{13}\text{CO}$   $T_1$  exhibits the postulated field dependence.

The question now becomes -- what can  $T_1$  data reveal about the environment of  $^{13}\text{CO}$  bound to these proteins? Both Satterlee et al<sup>4,5</sup> and Tucker et al<sup>16</sup> have implicated an interaction between His-E7 and CO when it is bound to hemoglobin. Satterlee et al<sup>4</sup> believe that there is a nucleophilic interaction between the unprotonated nitrogen of the histidine's imidazole ring and the carbon atom of the CO ligand (see Figure 5). Evidence for this has been inferred from the difference in the CO stretching frequency and absorption intensity of the ligand bound to the  $\alpha$  and  $\beta$  subunits of rabbit hemoglobin.



Figure 4

Field dependence of the  $^{13}\text{CO}$  resonances of carbon-monooxy rabbit hemoglobin in 0.15 M NaCl: (a) 25.14 MHz; (b) 45.28 MHz. Note the increase in line-width in going from (a) to (b).

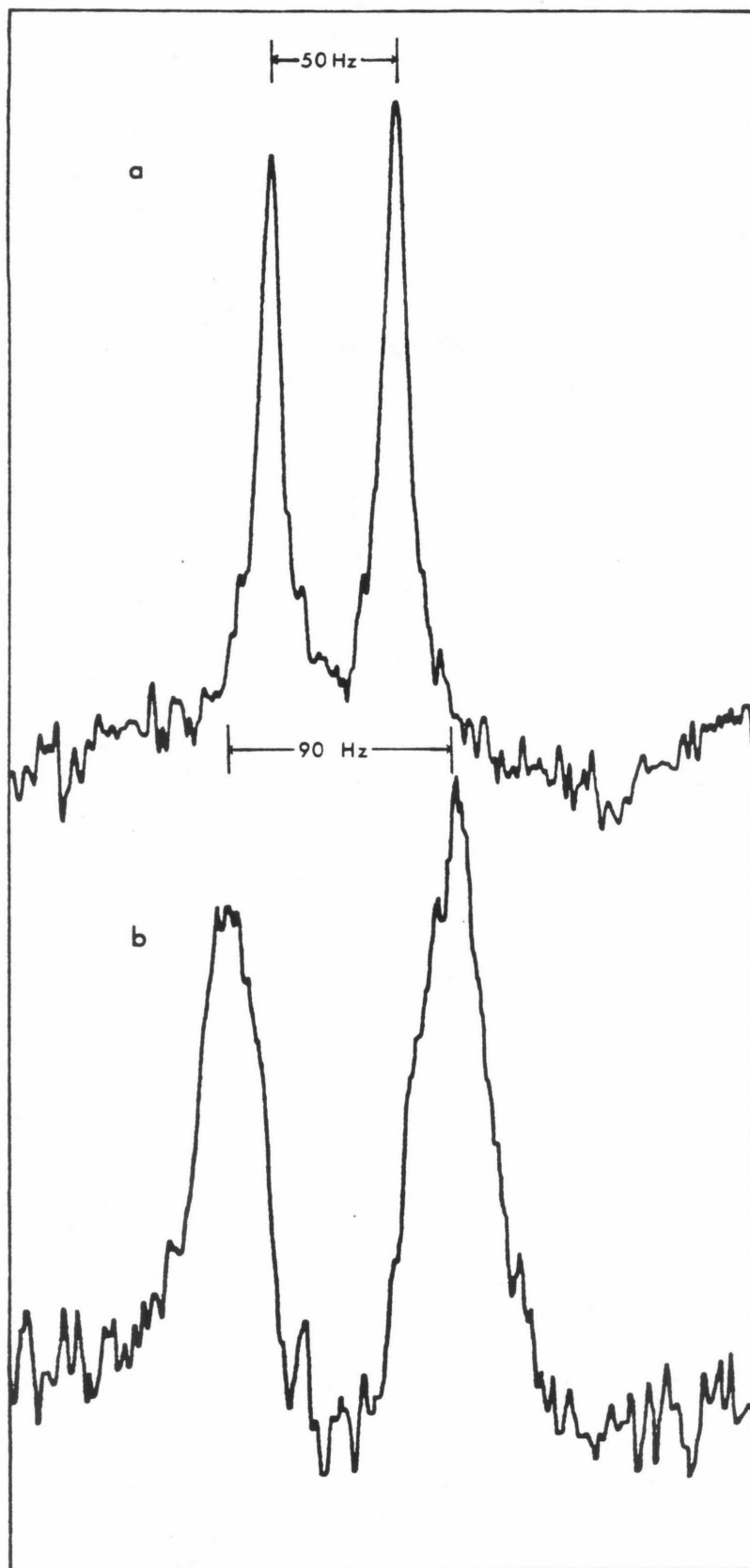


## Figure 5

Postulated Lewis base interaction between the distal histidine (E7) and heme bound CO. The figure is from ref. 4 (reproduced without permission).

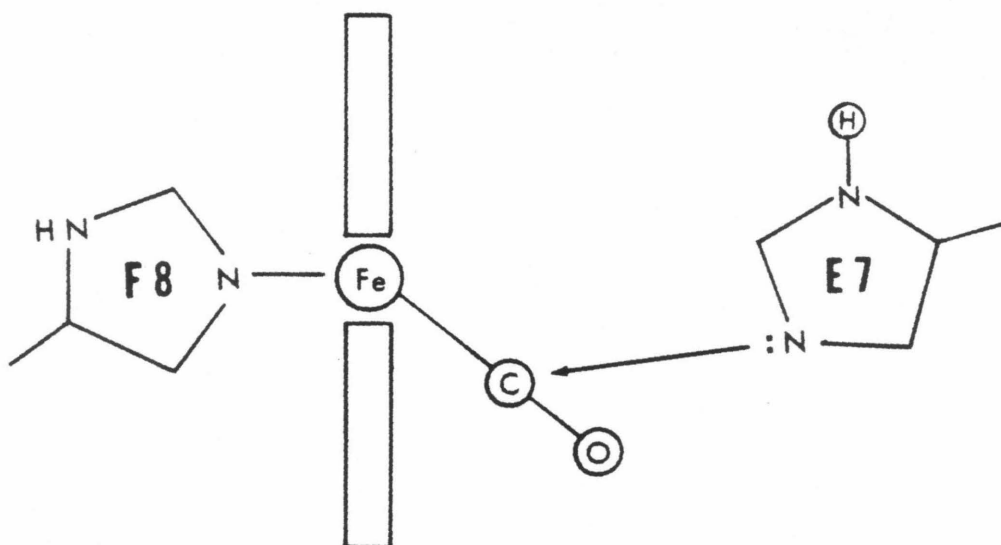


Table I

Spin-Lattice Relaxation Times and Linewidth Measurements of  $^{13}\text{CO}$ 

Bound to Sperm Whale Myoglobin and Rabbit (New Zealand White) Hemoglobin

Sample <sup>a</sup>	Temp( $^{\circ}\text{C}$ )	$\nu$ (MHz)	$T_1$ (sec) <sup>b</sup>	$\nu_{1/2}$ (Hz) <sup>c</sup>	
Mb- $^{13}\text{CO}$	21 $\pm$ 1	25.14	0.52 $\pm$ 0.17	$\sim$ 7	
		90.5	< 0.20 <sup>d</sup>	$\sim$ 50	
Hb- $^{13}\text{CO}$	28 $\pm$ 3	25.14		$\frac{\alpha}{10}$	$\frac{\beta}{11}$
	29 $\pm$ 2	45.28	$\sim$ 30	$\sim$ 32	

a) [Mb- $^{13}\text{CO}$ ] = 1.1 mM,  $\tau_r = 4.1 \times 10^{-9}$  sec, [Hb- $^{13}\text{CO}$ ]  $\approx$  2.4 mM,  $\tau_r = 2.3 \times 10^{-8}$  sec at 31 $^{\circ}\text{C}$ . Radii used for calculation of  $\tau_r$ :  $R_{\text{Mb}} = 16.2 \text{ \AA}$ ,<sup>1</sup>  $R_{\text{Hb}} = 24.2 \text{ \AA}$ ,<sup>18</sup>  $R_{\text{H}_2\text{O}} = 1.5 \text{ \AA}$ ;<sup>1</sup>

b) errors are standard deviation obtained from non-linear curve fit;

c) linewidths at 45.28, 50.3, and 90.5 MHz contain digital line broadening on the order of 6-10 Hz;

d) because of the width of the  $^{13}\text{CO}$  resonance, a more accurate determination of  $T_1$  was not possible. Using the available data, the non-linear curve fit gave  $T_1 = 0.11 \pm 0.04$  sec, although this value and its precision should not be taken very seriously.

$\Delta\sigma$  should be a very sensitive indicator of the presence, absence, or extent of such a nucleophilic interaction.

It gives a direct measure of the electronic environment and local symmetry of the carbon-13 nucleus in  $^{13}\text{C}\equiv\text{O}$ .<sup>17</sup>

As local symmetry decreases (as would be the case for the type of interaction shown in Figure 5),  $\Delta\sigma$  decreases.<sup>17</sup>

Such an effect is seen with the human hemoglobin data which indicates that the symmetry of  $^{13}\text{CO}$  coordinated to the protein ( $\Delta\sigma = 194 \pm 37$  ppm) is vastly different than that for  $^{13}\text{CO}$  bound to 1-methylimidazole-*protoheme IX* dimethyl ester ( $\Delta\sigma = 584 \pm 132$ )

In order to further examine this nucleophilic interaction,  $T_1$  studies have been carried out to measure  $\Delta\sigma$  and  $r_{\text{eff}}$  for  $^{13}\text{CO}$  bound to rabbit hemoglobin and to the monomeric hemoglobin from the marine annelid Glycera dibranchiata. The results of these studies shall be discussed in Part III.

REFERENCES

1. Moon, R. B. Ph.D. Thesis, California Institute of Technology (1975)
2. a) Moon, R. B. & Richards, J. H. J. Am. Chem. Soc. 1972, 94, 5093-5095; b) Moon, R. B. & Richards, J. H. Biochemistry 1974, 13, 3437-3443; c) Moon, R. B., Dill, K. & Richards, J. H. Biochemistry 1977, 16, 221-228.
3. Vergamini, P. J., Matwiyoff, N. A., Wohl, R. C. & Bradley, T. Biochem. Biophys. Res. Commun. 1973, 55, 453.
4. Satterlee, J. D., Teintze, M. & Richards, J. H. Biochemistry 1978, 17, 1456-1465.
5. Satterlee, J. D., Teintze, M. & Richards, J. H. submitted for publication.
6. Satterlee, J. D. 1978, private communication.
7. Freeman, R. & Hill, H. D. W. J. Chem. Phys. 1971, 54, 3367. 3367.
8. Hull, W. D. Ph.D. Thesis, Harvard University (1975).
9. Shoemaker, D. P., Garland, C. W. & Steinfeld, J. I. "Experiments in Physical Chemistry," McGraw Hill, Inc., N.Y., pp. 392-400 (1974).
10. Oldfield, E., Norton, R. S. & Allerhand, A. J. Biol. Chem. 1975, 250, 6368.
11. Allerhand, A., Doddrell, D., Glosko, V., Cochran, D. W., Wenkert, E., Lawson, P. J. & Gurd, F. R. N. J. Am. Chem. Soc. 1971, 93, 544.

12. Farrar, T. C. & Becker, E. D. "Pulse and Fourier Transform NMR," Academic Press, Inc., N.Y., pp. 55-56 (1971).
13. The contribution to the total rate should be dominated by  $1/T_{1\text{CSA}}$  and  $1/T_{1\text{D-D}}$ , so the other rates can be neglected. See Norton, R. S., Clouse, A. O., Addleman, R. & Allerhand, A. J. Am. Chem. Soc. 1977, 99, 79.
14. The  $T_1$  data in Figure 2 were recalculated with the non-linear least squares method discussed in the experimental section before fitting the data to eq. 4.
15. Antonini, E. & Brunori, M. "Hemoglobin and Myoglobin in Their Reactions with Ligands," North-Holland Publishing Company, Amsterdam, Chapter 4 (1971).
16. Tucker, P. W., Phillips, S. E. V., Perutz, M. F., Houtchens, R. & Caughey, W. S. Proc. Natl. Acad. Sci. USA 1978, 1076-1080.
17. Appleman, B. R. & Dailey, B. P. "Advances in Magnetic Resonance," J. S. Waugh, ed., Vol. 7, Academic Press, N.Y., p. 231 (1974).
18. Schneider, R., Mayer, A., Schmatz, W., Kaiser, B. & Scherm, R. J. Mol. Biol. 1969, 41, 231.
19. Perkins, T. G. Ph.D. Thesis, California Institute of Technology, Part I (1981).



PART III

Nuclear Magnetic Resonance Investigation of  
 $^{13}\text{CO}$  Binding to Heme Proteins:  
Structure and Function.

## INTRODUCTION

Much work has been presented in the literature<sup>1-15</sup> regarding the interaction of the distal residues of hemoglobins and myoglobins with heme-bound carbon monoxide. It is generally agreed that the distal residue E7 influences the CO affinity of these proteins, although the exact nature of the distal interaction with the heme-coordinated ligand has been subject to debate.<sup>1-12</sup> Recent work with model systems<sup>6,12</sup> has yielded conflicting results: One group<sup>6</sup> has found that with a sterically constrained model heme, the CO affinity was lower than that for the same model without any steric hindrance, thus supporting a distal steric interaction with the heme pocket; Traylor and Berzini<sup>12</sup> were able to mimic the reduced CO affinity with a model heme which was not sterically hindered. In neither case has a model system been constructed which would allow for the study of the proposed nucleophilic interaction between His-E7 and the heme-coordinated CO.<sup>3,4,10,11</sup> Because of this and the conflicting results from the model studies, it becomes necessary to reexamine the protein-CO complex in such a way that one of the proposed distal interactions, the nucleophilic interaction, may be confirmed or rejected.

As described previously,<sup>16</sup> the anisotropy of the chemical shift tensor,  $\Delta\sigma$ , can be obtained for heme-coordinated  $^{13}\text{CO}$  through the measurement of spin-lattice relaxation times ( $T_1$ ) from the nuclear magnetic resonance (nmr) spectrum of  $^{13}\text{CO}$ .  $\Delta\sigma$  can be used to elucidate the nature of the interaction between the distal residue His-E7 and the heme-bound CO, as  $\Delta\sigma$  is very sensitive to changes in the local electronic environment of the carbon nucleus.<sup>17</sup> Thus, if the nucleophilic interaction exists, then there should be a dramatic difference in  $\Delta\sigma$  for the heme-bound  $^{13}\text{CO}$  relative to  $^{13}\text{CO}$  coordinated in a protein which lacks His-E7. In this regard, the  $T_1$  relaxation behavior of  $^{13}\text{CO}$  bound to New Zealand white rabbit hemoglobin (HbR), which, unlike human hemoglobin (HbA), has resolved resonances for  $^{13}\text{CO}$  bound to the  $\alpha$  and  $\beta$  chains, and to the monomeric hemoglobin from the marine annelid, Glycera dibranchiata (His-E7  $\rightarrow$  Leu, Hb-II), has been examined at three different magnetic field strengths (1.41, 2.35, and 4.7 Tesla). These experiments have yielded not only values for  $\Delta\sigma$  that confirm the existence of the nucleophilic interaction within the heme pocket, but also, in the case of HbR, the geometry and motional behavior of the  $^{13}\text{CO}$  when bound to the heme.

## EXPERIMENTAL

Sample Preparation: Rabbit (New Zealand white) hemoglobin samples were prepared from 50 cc of freshly drawn, citrated blood. The red cells were separated from the plasma by centrifugation at 2000 rpm for 30 minutes and washed three times with 0.15 M NaCl. The cells were then lysed with distilled water at 4°C, and the cell debris was removed by centrifugation at 15,000 rpm for one hour. The resulting hemoglobin was purified first with 0.1 M Tris (pH=8.1) using continuous flow high pressure ultrafiltration (Amacon UM-10) for 24 hours at 4°C and then chromatographed on a Sephadex G-75 column equilibrated with 0.1 M Tris (pH=8.1). The sample was then concentrated by ultrafiltration to the appropriate volume, usually 10 ml, and degassed with nitrogen in a 30 cc syringe. Approximately 10 ml of  $^{13}\text{CO}$  were then added to the syringe, after which the sample was injected into a sealed, degassed 10, 12, or 18 mm nmr tube; each tube contained a  $\text{D}_2\text{O}$  locking capillary.

G. dibranchiata hemoglobin samples were prepared by allowing the coelomic fluid from freshly sacrificed worms to drain into a flask containing 0.5 M NaCl and 0.5 M sodium citrate. The cells were separated from the plasma by centrifugation at 2000 rpm for 30 minutes and

washed three times with 0.5 M NaCl. The cells were then lysed with distilled water at 4°C and centrifuged at 7000 rpm for 90 minutes and 13,000 rpm for 15 minutes. The dimer hemoglobin (Hb-I) was precipitated from the centrifuged solution by first adding ammonium sulfate to create a solution concentration of 1.2 M and letting the solution remain at 4°C for 16 hours. The solution was then centrifuged and more ammonium sulfate added, this time to a concentration of 3.2 M, for 24 hours. After centrifugation, the sample was dialyzed against 0.03 M  $\text{NaH}_2\text{PO}_4$  (pH ~ 7) for 24 hours and then concentrated to about 10 ml by ultrafiltration (Amacon UM-10) under  $^{13}\text{CO}$ . The resulting solution was then chromatographed on a Sephadex G-75 column (0.1 M Tris, pH=8.1). Only one band, the monomer eluted off the column. The remaining sample preparation was the same as that for the rabbit hemoglobin samples.

The concentration of the carbonmonoxy rabbit hemoglobin samples was estimated spectrophotometrically using the absorption at 419 nm and an extinction coefficient at  $\epsilon = 764 \text{ mM}$ . The G. dibranchiata carbonmonoxy hemoglobin concentrations were determined using  $\epsilon = 232 \text{ mM}$  for the absorption at 422 nm.

Instrumental: Carbon-13 nmr spectra were obtained with three different spectrometers. Low field measurements were made on a JEOL FX-60 spectrometer operating at 15.04 MHz.

Spectra at 25.14 MHz were obtained on a Varian XL-100-15 spectrometer. The high field spectra were acquired with a Varian XL-200 spectrometer which has a carbon-13 resonant frequency of 50.3 MHz. Ten mm sample tubes were used on the FX-60, 12 mm tubes on the XL-100-15 and 18 mm tubes on the XL-200. The probe temperatures were in the range of  $28 \pm 3^{\circ}\text{C}$ .

$T_1$  Measurements: Spin-lattice ( $T_1$ ) relaxation measurements were made using progressive saturation.<sup>18</sup> In all cases the limitation that  $T_2^* \ll T_1$  was satisfied. The delay times ( $\tau$ ) were varied randomly so as to eliminate systematic errors.  $T_1$  values were calculated using a non-linear least squares program<sup>19</sup> to fit the equation  $A_{\tau} = A_{\infty} + (A_0 - A_{\infty})\exp(-\tau/T_1)$ .

Viscosities and Densities: Viscosities of solutions were determined by the method of Shoemaker et al.<sup>20</sup> Densities were measured with a 5 ml Weld pycnometer. These measurements were used in the determination by microviscosity theory<sup>21</sup> of  $\tau_r$  for each solution.

## THEORY

Dioxygen Binding Curves: For all known oxygen carriers which contain heme prosthetic groups, the relative affinity for CO versus O<sub>2</sub> is given by the partition coefficient M, which is defined by eq. 1:<sup>22</sup>

$$M = \frac{[\text{HbCO}]}{[\text{HbO}_2]} \times \frac{p\text{O}_2}{p\text{CO}} \quad (1)$$

where

$p\text{O}_2$  = pressure of O<sub>2</sub>

$p\text{CO}$  = pressure of CO

In most cases, M is greater than 1, as the formation of an Fe-CO bond is a very favorable process.<sup>23</sup> For human hemoglobin (HbA),  $M = 250$ .<sup>14</sup> This is a very reasonable number, if one takes into consideration both the amount of CO produced catabolically in the body,<sup>5,24,25</sup> and what would happen if M were larger. In order to examine this, the following calculations were performed.

Roughton and Darling<sup>26</sup> studied the binding of CO to HbA and its effect on the HbO<sub>2</sub> binding curve. They obtained the following expression to describe their results:

$$p\text{O}_{2\text{CO}} = p\text{O}_2 / (1 + (\bar{Y}_{\text{CO}} / \bar{Y}_{\text{O}_2})) \quad (2)$$

where

$pO_{2CO}$  = pressure of  $O_2$  with HbCO present

$pO_2$  = pressure of  $O_2$  with no HbCO present

$\bar{Y}_{CO}$  = fractional saturation of Hb with carbon  
monoxide

$\bar{Y}_{O_2}$  = fractional saturation of Hb with dioxygen

If one assumes that<sup>27</sup>

$$M = \frac{L_1}{K_1} = \frac{L_2}{K_2} = \frac{L_3}{K_3} = \frac{L_4}{K_4} \quad (3)$$

where

$L_i$  = Adair constant for carbon monoxide  
( $i = 1, 2, 3, 4$ )

$K_i$  = Adair constant for dioxygen ( $i = 1, 2, 3, 4$ )

then

$$L_i = M \cdot K_i \quad (4)$$

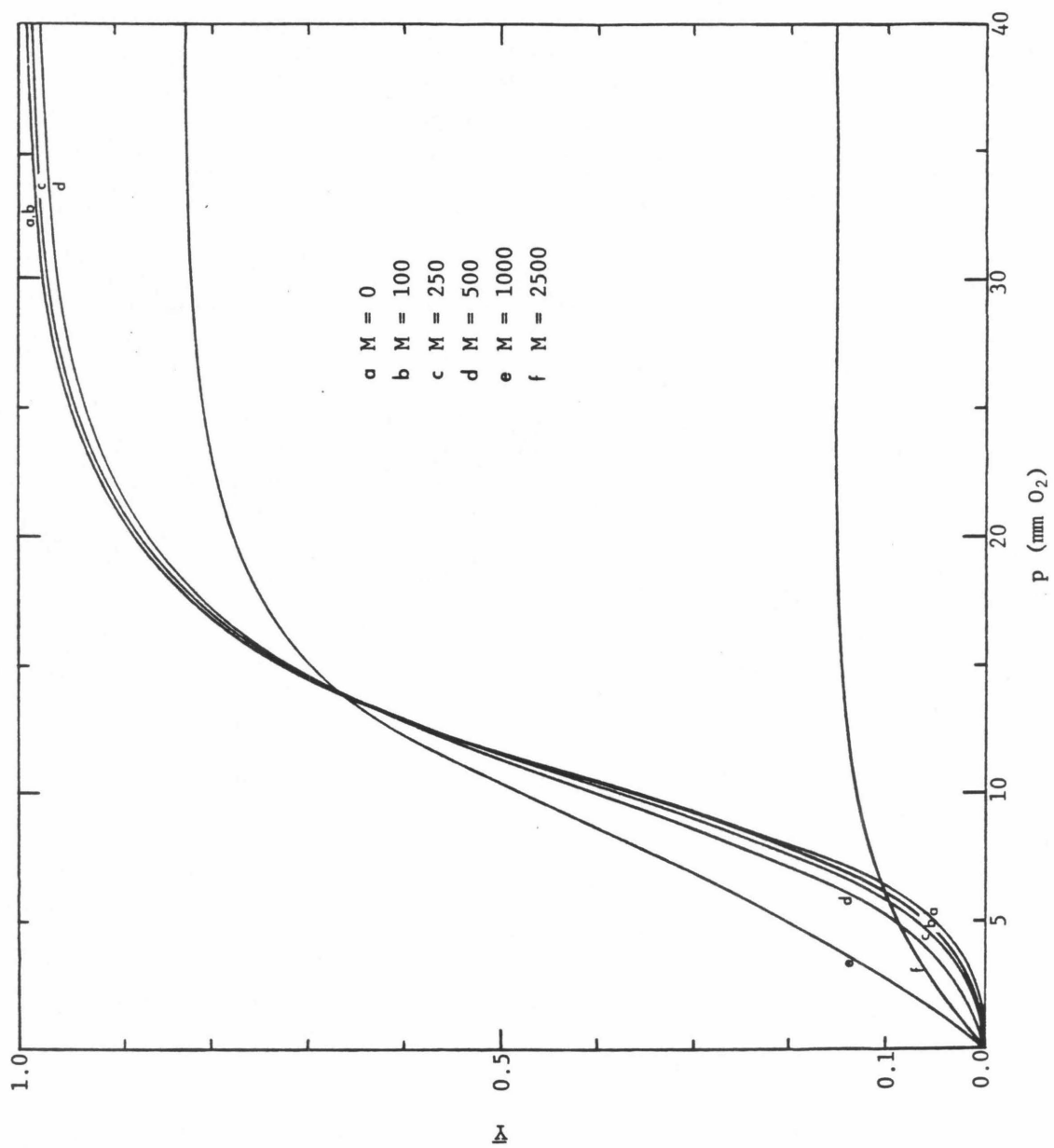
Thus, given values for  $K_1$ ,  $K_2$ ,  $K_3$ ,  $K_4$ , and  $M$ , eq. 2 can be used to generate dioxygen fractional saturation curves.

A collection of these curves is shown in Figure 1. One observation which is noteworthy is that as  $M$  becomes larger than 500, both the cooperativity of the hemoglobin and the amount of available dioxygen binding sites decreases dramatically with increasing  $M$ . Therefore,  $M$  must remain low ( $\leq 500$ ) or else CO poisoning would be very common among humans.



Figure 1

Theoretical  $O_2$  saturation curves for Hb obtained using eq. 2. Adair constants used are  $K_1 = 0.00949$ ,  $K_2 = 0.031$ ,  $K_3 = 0.019$ ,  $K_4 = 9.78$  (pH = 7.4 2 mM DPG,  $25^\circ\text{C}$ ), and  $L_1 = M \times 0.0238$ ,  $L_2 = M \times 0.1$ ,  $L_3 = M \times 0.13$ ,  $L_4 = M \times 6.86$  (pH = 7.4,  $25^\circ\text{C}$ ).<sup>28</sup> Units of Adair constants are mm Hg.  $p_{\text{CO}} = 3 \times 10^{-3}$  mm Hg.<sup>24</sup>  $[\text{Hb}] = 0.24 \text{ mM}$ .



T<sub>1</sub> Relaxation with Internal Motion: As described previously,<sup>16</sup> the relaxation behavior of <sup>13</sup>CO bound to hemoglobin may be represented as a sum of the dipolar (D-D) and chemical shift anisotropy (CSA) relaxation rates:

$$\frac{1}{T_{1\text{TOT}}} = \frac{1}{T_{1\text{D-D}}} + \frac{1}{T_{1\text{CSA}}} \quad (5)$$

If the <sup>13</sup>CO is undergoing internal rotation when bound to the protein, than eq. 5 may be expanded as follows:<sup>28,29</sup>

$$\begin{aligned} \frac{1}{T_{1\text{TOT}}} = & \frac{1}{15} \times \gamma_x^2 \gamma_s^2 \hbar^2 s(s+1) r_{\text{eff}}^{-6} F_1 \\ & + \frac{1}{15} \times \omega_x^2 (\Delta\sigma)^2 F_2 \end{aligned} \quad (6)$$

where

$\gamma_x$  = magnetogyric ratio of the observed nucleus (<sup>13</sup>C)

$\gamma_s$  = magnetogyric ratio of the relaxing nucleus (<sup>1</sup>H)

$\hbar$  = Planck's constant/2 $\pi$

$s$  = spin of the relaxing nucleus ( $s = \frac{1}{2}$  for <sup>1</sup>H)

$r_{\text{eff}}^{-6} = \frac{1}{N} \sum_{i=1}^N r_i^{-6}$

$r_i$  = distance between nucleus x (<sup>13</sup>C) and nucleus  $s_i$  (<sup>1</sup>H)

$F_1 = J(\omega_x - \omega_s) + 3J(\omega_x) + 6J(\omega_x + \omega_s)$

$$J(\omega) = A\tau_r/(1+\omega^2\tau_r^2) + B\tau_1/(1+\omega^2\tau_1^2) \\ + C\tau_2/(1+\omega^2\tau_2^2)$$

$$A = \frac{1}{2}(3\cos^2\theta - 1)^2$$

$$B = 6\cos^2\theta\sin^2\theta$$

$$C = \frac{3}{2}\sin^4\theta$$

$\tau_r$  = rotational correlation time of the protein

$$\tau_1 = 1/(1/\tau_r + 1/\tau_i)$$

$$\tau_2 = 1/(1/\tau_r + 4/\tau_i)$$

$\tau_i$  = internal correlation time about an axis which  
reorients with  $\tau_r$

$\theta$  = angle between  $\hat{r}_{\text{eff}}$  and the axis of internal  
rotation

$\omega_x$  = Larmor frequency of the observed nucleus ( $^{13}\text{C}$ )

$\omega_s$  = Larmor frequency of the relaxing nucleus ( $^1\text{H}$ )

$\Delta\sigma$  = anisotropy of the chemical shift tensor

$$F_2 = C_0\tau_r/(1+\omega_x^2\tau_r^2) + C_1\tau_1/(1+\omega_x^2\tau_1^2) \\ + C_2\tau_2/(1+\omega_x^2\tau_2^2)$$

$$C_0 = \frac{1}{2}(3\cos^2\beta - 1)^2$$

$$C_1 = 6\cos^2\beta\sin^2\beta$$

$$C_2 = \frac{3}{2}\sin^4\beta$$

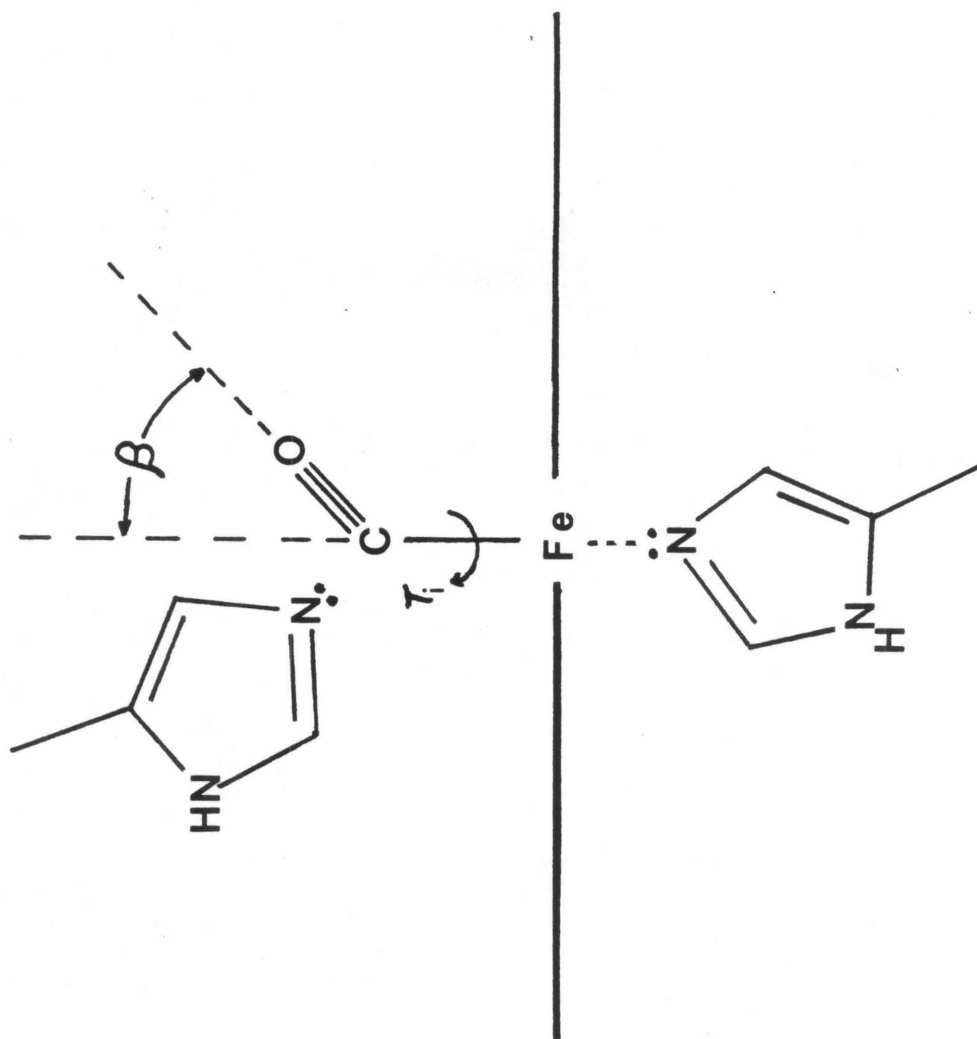
$\beta$  = angle between the internal rotation axis and  
and the principle chemical shift axis

For the heme-bound  $^{13}\text{CO}$ ,  $\beta$  represents the angle between the  $^{13}\text{CO}$  axis and the Fe-C bond, the only possible axis of rotation (Figure 2).

Log-log relaxation plots calculated using eq. 6 are shown in Figures 3 and 4. It can be seen that for  $\tau_r \gg \tau_i$  and non-zero values of  $\beta$  and  $\theta$ ,  $T_1$  is independent of  $\tau_r$ . If these angles are equal to zero, then internal motion cannot be detected, even though it may exist.

## Figure 2

Schematic representation of  $^{13}\text{CO}$  bound to hemoglobin. The angle  $\beta$  and correlation time  $\tau_i$  are discussed in the text.



(THIS PAGE IS BLANK, DUE TO ERROR IN PAGINATION)



Figure 3

Calculated log-log plots of spin lattice relaxation ( $T_1$ ) for  $^{13}\text{CO}$  using eq. 6: (A) Dipolar contribution; (B) Chemical shift anisotropy contribution. The angles  $\theta$  and  $\beta$  are discussed in the text.

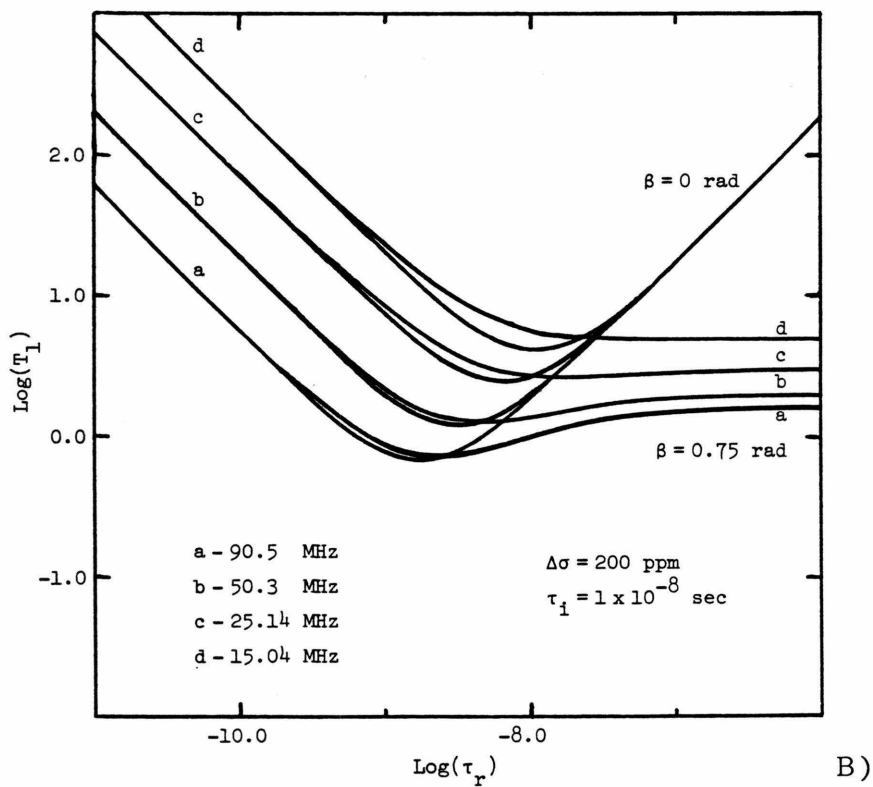
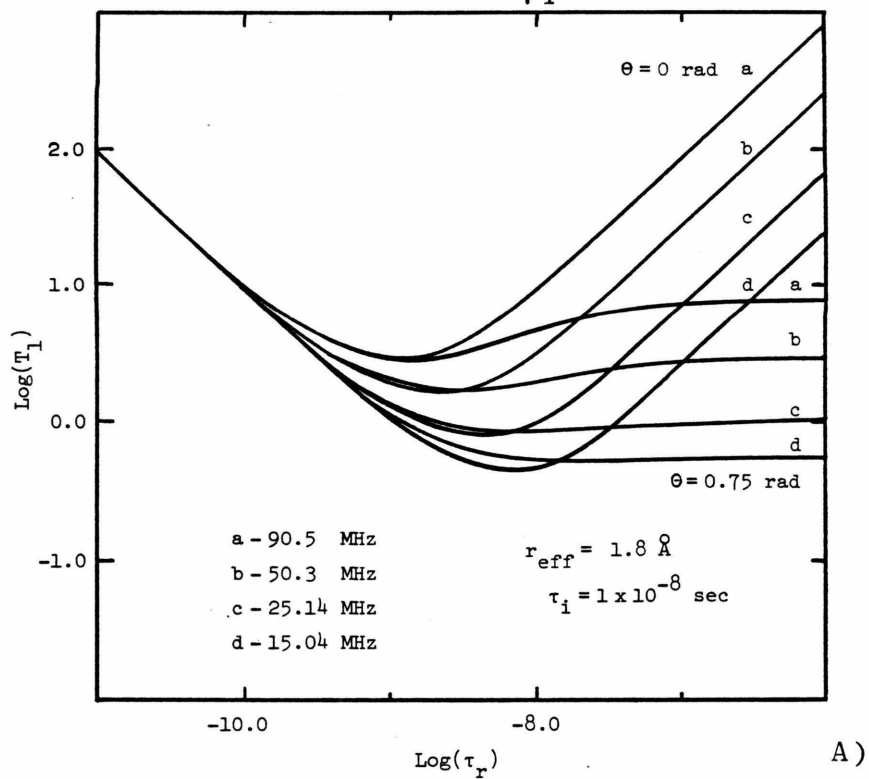
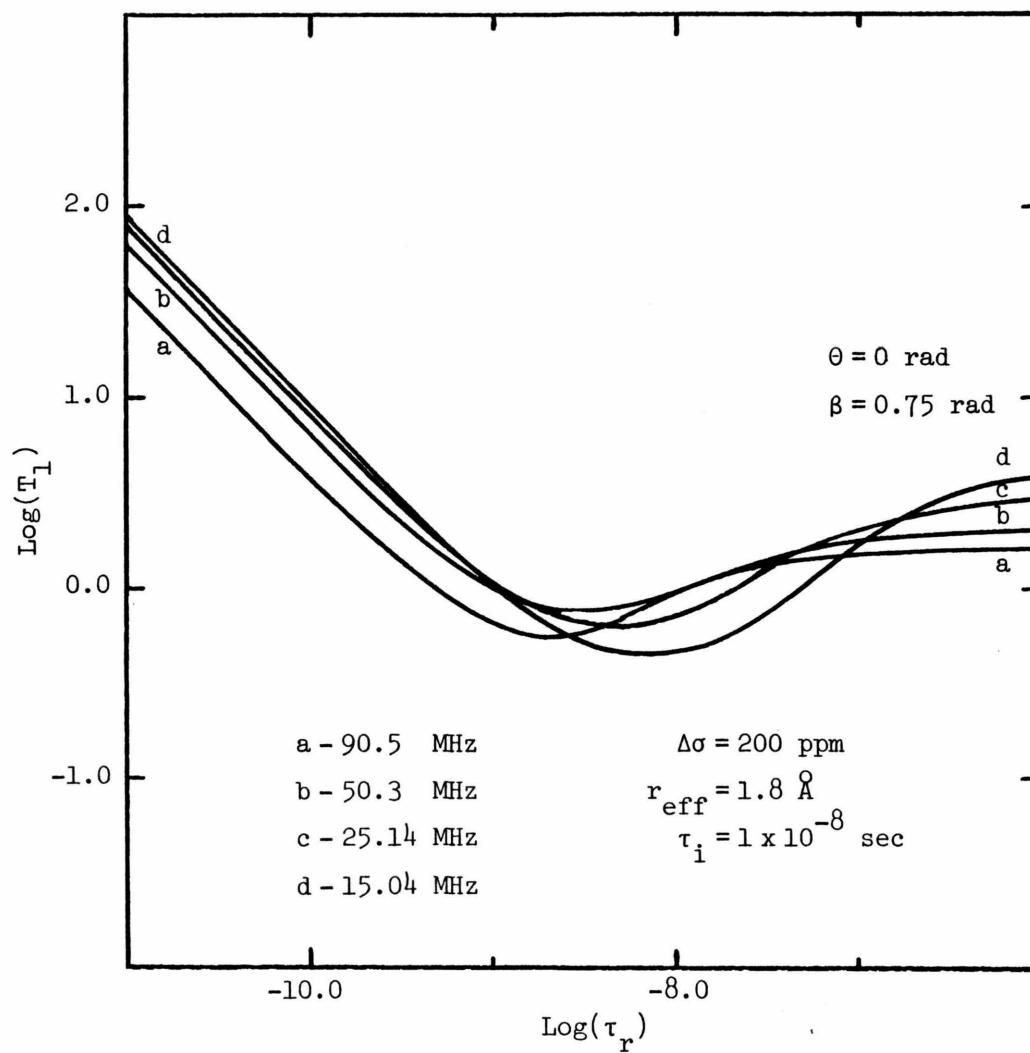


Figure 4

Calculated log-log plot of the total spin-lattice relaxation ( $T_1$ ) for  $^{13}\text{CO}$  using eq. 6.



## RESULTS AND DISCUSSION

Figures 5 through 7 show the  $T_1$  data for  $^{13}\text{CO}$  bound to HbR and Hb-II. In the case of both the  $\alpha$  and  $\beta$  chains of HbR, it is clear that as  $\tau_r$  increases,  $T_1$  becomes constant. This indicates the presence of internal motion for the  $^{13}\text{CO}$  bound to HbR. For Hb-II, the correlation time region is such that, with or without internal motion,  $T_1$  should not vary significantly with  $\tau_r$ . In order to extract the various nmr parameters ( $\Delta\sigma$ ,  $r_{\text{eff}}$ ,  $\tau_i$ ,  $\beta$ , and  $\Theta$ ), multi-variable non-linear least squares methods have been used to analyze the data. Eq. 6 may be rewritten as

$$\frac{1}{T_{1\text{TOT}}} = f(H_O, \tau_r, \Delta\sigma, r_{\text{eff}}, \tau_i, \beta, \Theta) \quad (7)$$

where  $H_O$ , the magnetic field strength, and  $\tau_r$  are the two variables, and  $\Delta\sigma$ ,  $r_{\text{eff}}$ ,  $\tau_i$ ,  $\beta$ , and  $\Theta$  are the parameters to be obtained from the data. Because of the periodic nature of  $\beta$  and  $\Theta$ , a three-dimensional surface with dimensions  $\beta$ ,  $\Theta$ , and the weighted root mean square (rms) deviation for the least squares fit of the data was created.  $\beta$  and  $\Theta$  were varied manually while the values for  $\Delta\sigma$ ,  $r_{\text{eff}}$ , and  $\tau_i$  were obtained from the least squares analysis; this process continued until values for  $\beta$  and  $\Theta$  were found which yielded a minimum rms deviation. The results of this data analysis are summarized in Table I.

Figure 5

Plot of the  $T_1$  relaxation data for  $^{13}\text{CO}$  bound to the  $\alpha$ -chain of New Zealand white rabbit hemoglobin. The theoretical curves were generated using eq. 6 with  $\Delta\sigma = 162 \pm 19$ ,  $r_{\text{eff}} = 1.82 \pm 0.05 \text{ \AA}$ ,  $\tau_i = 7.9 \pm 5.0 \text{ nsec}$ ,  $\beta = 45^\circ$ , and  $\theta = 0^\circ$ .

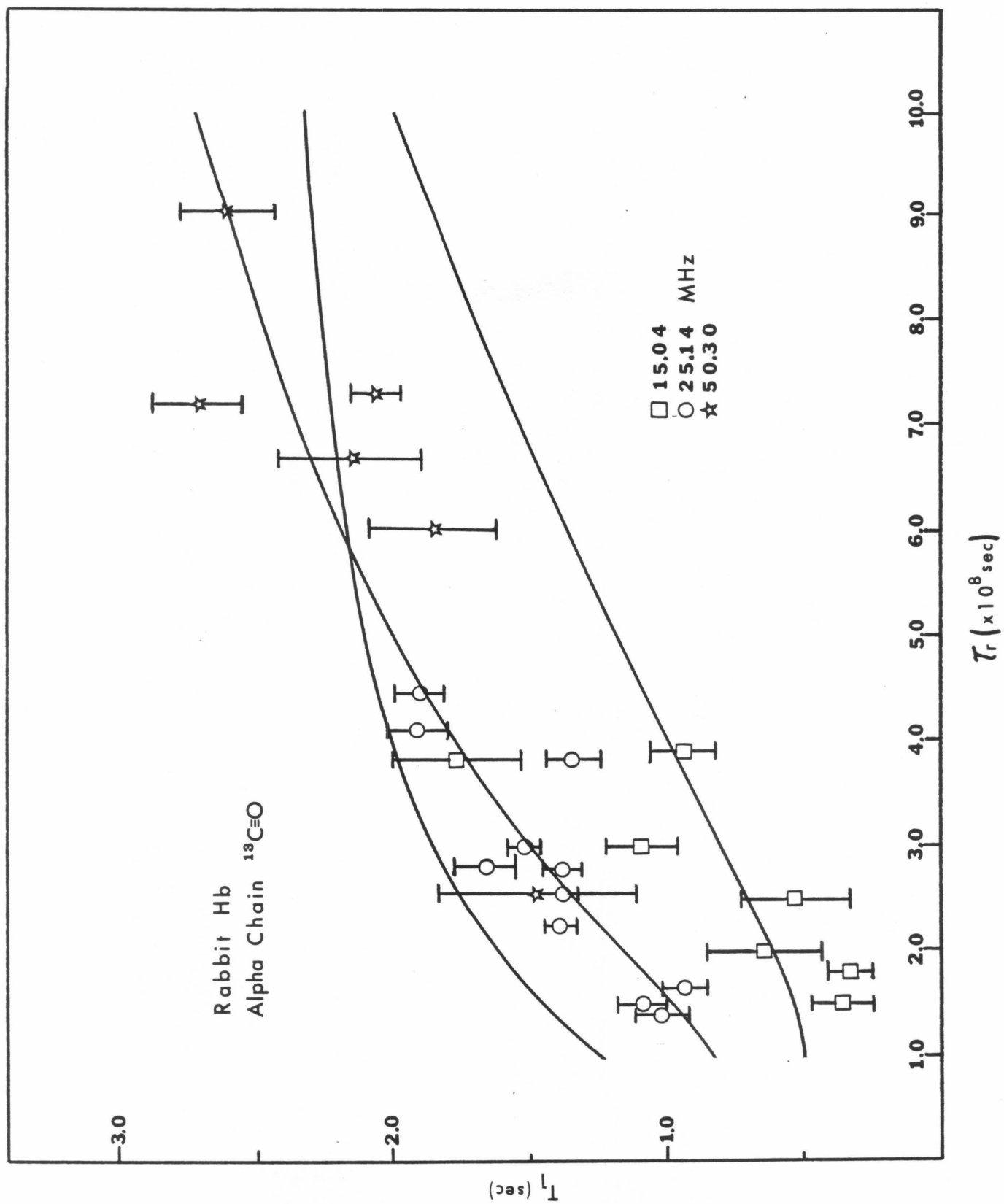


Figure 6

Plot of the  $T_1$  relaxation data for  $^{13}\text{CO}$  bound to the  $\beta$ -chain of New Zealand white rabbit hemoglobin. The theoretical curves were generated using eq. 6 with  $\Delta\sigma = 168 \pm 18$ ,  $r_{\text{eff}} = 1.81 \pm 0.04 \text{ \AA}$ ,  $\tau_1 = 8.4 \pm 4.4 \text{ nsec}$ ,  $\beta = 43^\circ$ , and  $\theta = 0^\circ$ .



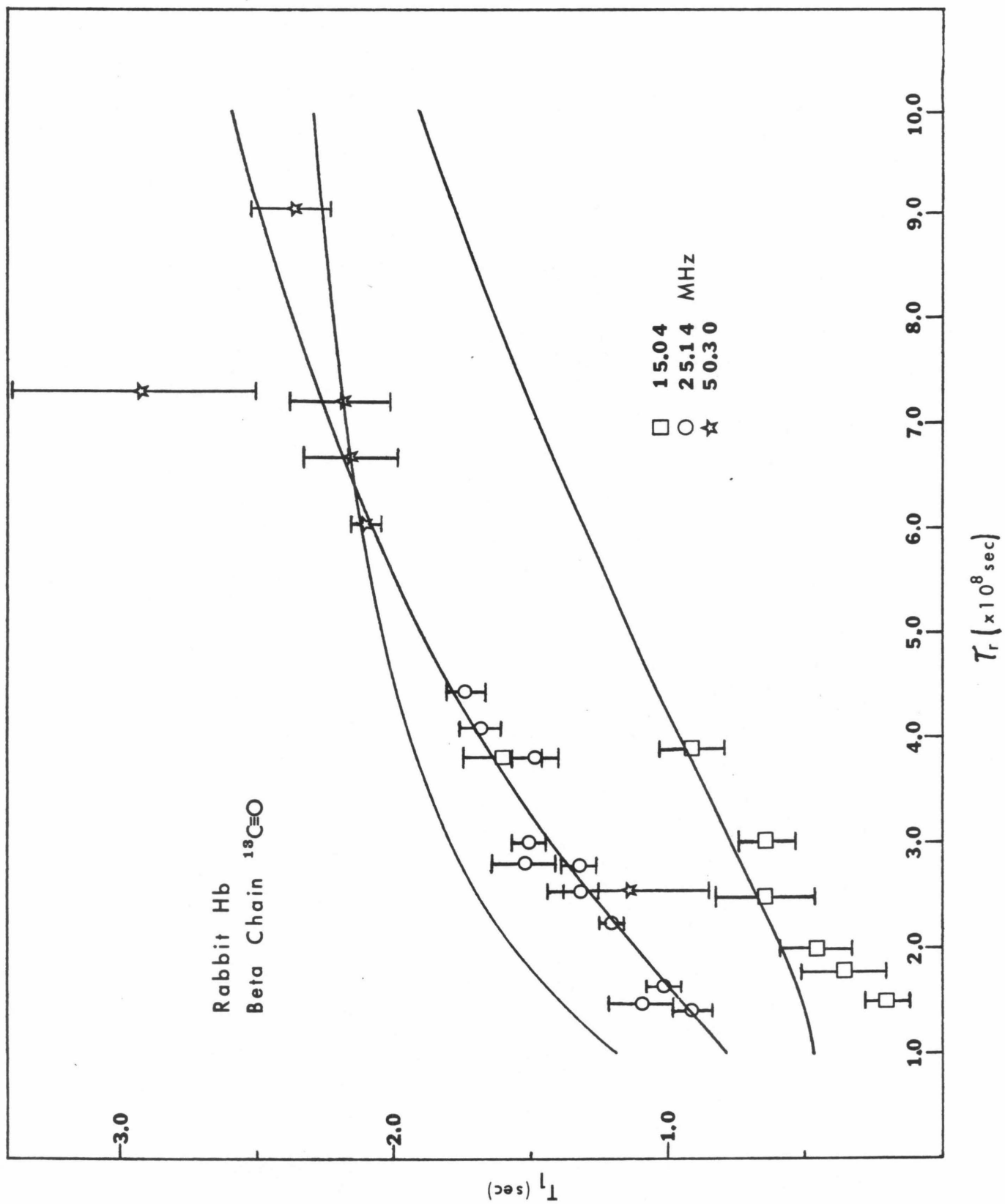


Figure 7

Plot of the  $T_1$  relaxation data for  $^{13}\text{CO}$  bound to the monomeric hemoglobin from the marine annelid Glycera dibranchiata. The theoretical curves were generated using eq. 6 with  $\Delta\sigma = 419 \pm 56$ ,  $r_{\text{eff}} = 1.83 \pm 0.11 \overset{\text{O}}{\text{\AA}}$ , and  $\beta$  and  $\Theta = 0$ .

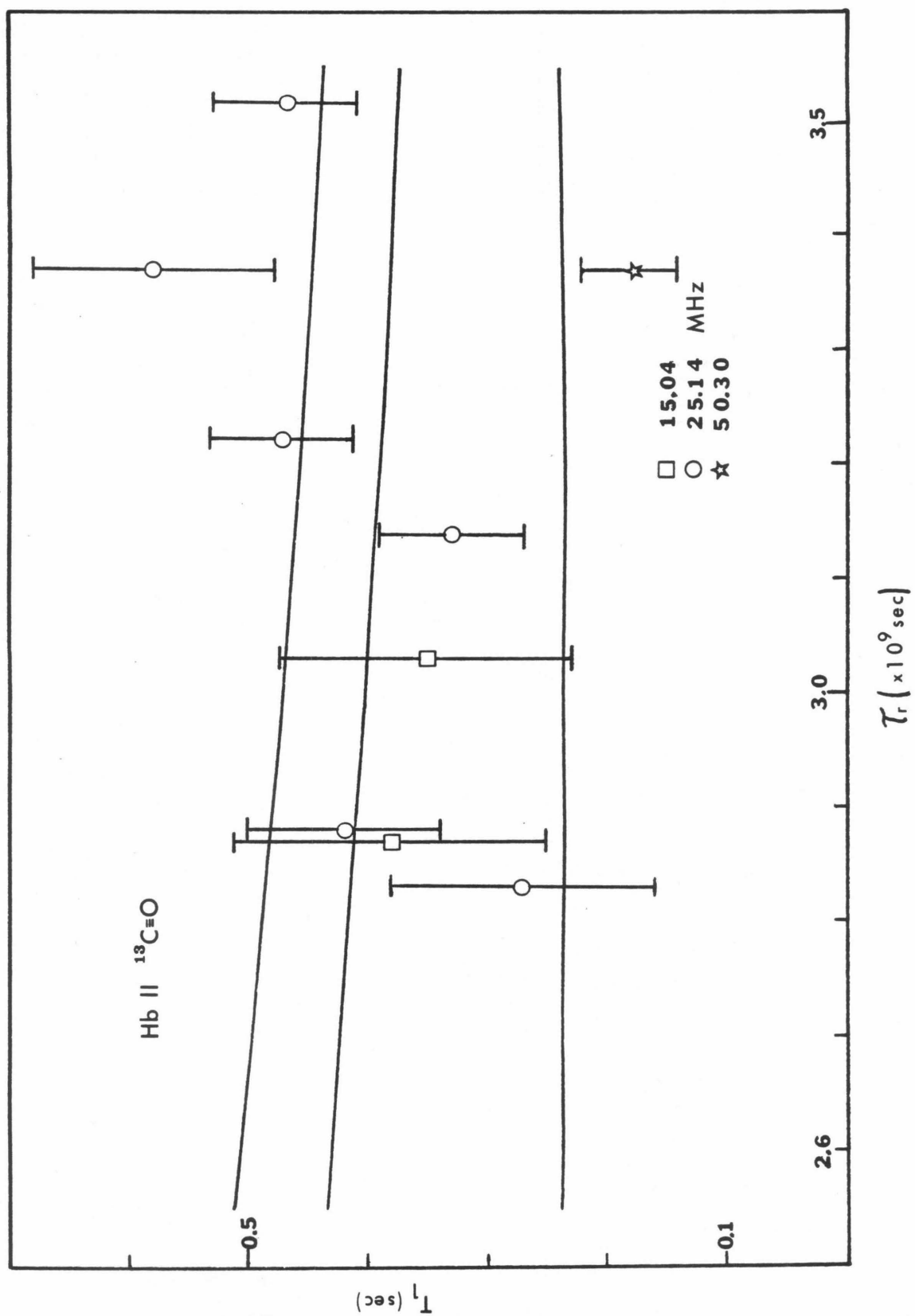


Table I

Summary of Relaxation Parameters for  $^{13}\text{CO}$  Hemoglobins

<u>Parameter</u>	<u>HbR</u>		<u>Hb-II</u>	<u>HbA</u> <sup>a</sup>
	<u><math>\alpha</math>-chain</u>	<u><math>\beta</math>-chain</u>		
$ \Delta\sigma $ (ppm)	162 $\pm$ 19	168 $\pm$ 18	419 $\pm$ 56	194 $\pm$ 37
$r_{\text{eff}}$ ( $\text{\AA}$ )	1.82 $\pm$ 0.05	1.81 $\pm$ 0.04	1.83 $\pm$ 0.1	1.81 $\pm$ 0.02
$\tau_i$ (nsec)	7.9 $\pm$ 5.0	8.4 $\pm$ 4.4	---	---
$\beta$	45°	43°	0°	---
$\theta$	0°	0°	0°	---

a) Calculated using average  $T_1$  values for  $\alpha$ - and  $\beta$ -bound  $^{13}\text{CO}$ . From reference 16.

As in the case of HbA, the values obtained for  $r_{\text{eff}}$  and  $\theta$  in both proteins are consistent with a "reservoir" effect, i.e., the dipolar relaxation is due to all of the protons in the heme pocket, not just a select few. This does not support the proposed hydrogen bond interaction between the NH proton of His-E7 and the  $^{13}\text{CO}$ .<sup>35</sup>

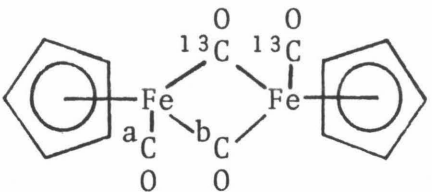
The values obtained for  $\Delta\sigma$  clearly show that, when histidine is the E7 residue, there is a large perturbation in the local electronic environment of the heme-coordinated  $^{13}\text{CO}$ . This is not true in the case of the Hb-II, which has a leucine residue in the E7 position.

Listed in Table II are values of  $\Delta\sigma$  for a variety of  $^{13}\text{CO}$  complexes. The only complex that has a  $\Delta\sigma$  value which approaches those of  $^{13}\text{CO}$  bound to HbA and HbR is one with a bridging  $^{13}\text{CO}$ . This is the same kind of geometry expected in the protein when His-E7 interacts with the  $^{13}\text{CO}$  via a nucleophilic effect. On the other hand,  $\Delta\sigma$  for Hb-II- $^{13}\text{CO}$  is the same as  $\Delta\sigma$  for  $\text{Fe}(^{13}\text{CO})_5$  and the model complex 1-methylimidazole-protoheme-IX-dimethyl ester- $^{13}\text{CO}$  (1-MeIm-PHDME- $^{13}\text{CO}$ ). Thus these observations support the existence of a nucleophilic interaction between the histidine nitrogen and the heme-coordinated  $^{13}\text{CO}$ .

The internal motion parameters  $\tau_i$  and  $\beta$  give further insight into the geometry of  $^{13}\text{CO}$  when bound to HbR. The magnitude of  $\tau_i$  ( $8 \pm 5$  nsec) indicates that the  $^{13}\text{CO}$

Table II

 $^{13}\text{CO}$  Shielding Tensors and Anisotropies

Compound	$\sigma_{\parallel}$	$\sigma_{\perp}$	$\sigma_{\text{AV}}^{\text{a}}$	$ \Delta\sigma $	Reference
HbR- $^{13}\text{CO}$ $\alpha$ -chain	93	- 69	- 15	$162 \pm 19$	This work
$\beta$ -chain	99	- 69	- 13	$168 \pm 18$	
Hb-II- $^{13}\text{CO}$	267	-152	- 12	$419 \pm 56$	This work
HbA- $^{13}\text{CO}$	116	- 78	- 13	$194 \pm 37$	16
1-MeIm-PHDME- $^{13}\text{CO}$	377	-207	- 12	$584 \pm 132$	16
$^{13}\text{CO}$	283	-123	+ 12	$406 \pm 30$	32
$\text{Fe}(^{13}\text{CO})_5$	253	-155	- 19	$408 \pm 41$	33
	a 277	-167	- 19	(444)	34
	b 11	-127	- 81	(138)	

a) Chemical shifts are based on absolute scale, with  $\sigma_{\text{AV}} = 12 \pm 10$  ppm for  $^{13}\text{CO}$ .<sup>17</sup>  
 Positive  $\sigma_{\text{AV}}$  denotes upfield shift.

is essentially immobilized within the heme pocket. This compares with a  $\tau_i$  value of 0.4 nsec for the C-1 carbon of ethyl isocyanide when bound to HbA.<sup>36</sup> Clearly, it is not steric hindrance alone that causes the restriction of the  $^{13}\text{CO}$  motion within the heme pocket. Figure 8 illustrates the orientation along with one of the contributing resonance structures, of  $^{13}\text{CO}$  bound to HbR. The values obtained for  $\beta$  are in excellent agreement with those derived from the x-ray structure of carbonmonoxy-HbA.<sup>15</sup> It should be noted that the present study cannot reveal whether or not the Fe-C bond is perpendicular to the heme plane.

Table III summarizes some of the CO binding data from various studies. The correlation between M and  $\Delta\sigma$  is what would be expected if the nucleophilic interaction were contributing to the reduced CO affinity in hemoglobins.

Figure 8

Schematic representation of  $^{13}\text{CO}$  bound to New Zealand white rabbit hemoglobin.  $\beta_{\alpha\text{-chain}} = 45^\circ$ ,  $\beta_{\beta\text{-chain}} = 43^\circ$ . Also shown is the most probable  $^{13}$  resonance form for the nucleophilic interaction.



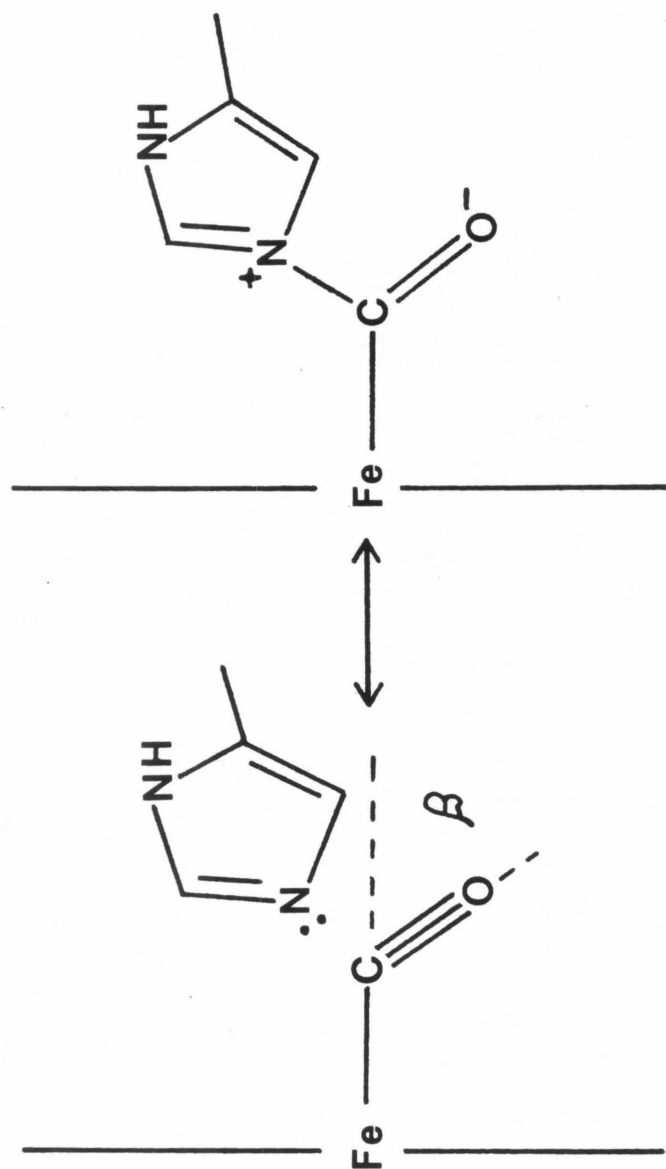


Table III

Summary of Information for CO Binding to Hemoglobins

		<u>HbA(ref.)</u>	<u>HbR(ref.)</u>	<u>Hb-II(ref.)</u>	<u>HbZurich(ref.)</u>	
Distal	$\alpha$	His	His		His	
		(14)	(14)	Leu (37)	(1)	
E7	$\beta$	His	His		Arg	
M		250 (14)	102 (14)	20,000 (37)	> 500 (1)	
C-O stretch	$\alpha$	1951	1928		1952	96
( $\text{cm}^{-1}$ )	$\beta$	(3) 1951	(3) 1951	1970 (4)	(1) 1958	
$^{13}\text{CO}$ chemical	$\alpha$	207.5	209.1		207.5	
shifts (ppm)	$\beta$	(16) 207.1	(4) 207.1	206.2 (4)	(8) < 207.1	
$\Delta\sigma$ (ppm)	$\alpha$		162 $\pm$ 19		---	
	$\beta$	194 $\pm$ 37 (16)	(this work) 168 $\pm$ 18	419 $\pm$ 56 (this work)	---	

CONCLUSION

The present investigation demonstrates how chemical shift anisotropy may be used to obtain structural information about a particular chemical system. The applicability of this method to other problems should be fairly straightforward. It is hoped that these methods will prove useful in the future study of protein confirmation.

REFERENCES

1. Tucker, P. W., Phillips, S. E. V., Perutz, M. F., Houtchens, R. & Caughey, W. S. Proc. Natl. Acad. Sci. USA 1978, 76, 1076-1080.
2. Tucker, P. W., Phillips, S. E. V., Perutz, M. F., Houtchens, R. A. & Caughey, W. S. "Biochemical and Clinical Aspects of Hemoglobin Abnormalities," Caughey, W. S., ed., Academic Press, N.Y. p. 1-15, (1978).
3. Satterlee, J. D., Teintze, M. & Richards, J. H. Biochemistry 1978, 17, 1456-1462.
4. Satterlee, J. D., Teintze, M. & Richards, J. H. submitted for publication.
5. Collman, J. P., Brauman, J. I., Halbert, T. R. & Suslick, K. S. Proc. Natl. Acad. Sci. USA 1976, 73, 3333-3337.
6. Collman, J. P., Brauman, J. I., Collins, T. J., Iverson, B. & Sessler, J. L. J. Am. Chem. Soc. 1981, 103, 2450-2452.
7. Case, D. A. & Karplus, M. J. Mol. Biol. 1978, 123, 697-701.
8. Giacometti, G. M., Antonini, E., Brunori, M., DiIorio, E. E. & Winterhalter, K. H. Colloq. Inst. Natl. Santa Rech. Med. 1977, 70, 245-254.

9. Brunori, M., Antonini, E., Giacometti, G., DiIorio, E. & Winterhalter, K. H. "Biochemical and Clinical Aspects of Hemoglobin Abnormalities," Caughey, W. S., ed., Academic Press, p. 17-28 (1978).
10. Maxwell, J. C. & Caughey, W. S. Biochemistry 1976, 15, 383-396.
11. Caughey, W. S., Houtchens, R. A., Lanir, A., Maxwell, J. C. & Charache, S. "Biochemical and Clinical Aspects of Hemoglobin Abnormalities," Caughey, W. S., ed., Academic Press, p. 29-56 (1978).
12. Traylor, T. G. & Berzini, A. P. Proc. Natl. Acad. Sci. USA 1980, 77, 3171-3175.
13. Fuchsman, W. H. & Appleby, C. A. Biochemistry 1979, 18, 1308-1321.
14. Holland, R. A. B. & Ross, J. A. Comp. Biochem. Physiol. 1978, 59A, 343-346.
15. Heidner, E. J., Ladner, R. C. & Perutz, M. F. J. Mol. Biol. 1976, 104, 707-722.
16. Perkins, T. G., Ph.D. Thesis, California Institute of Technology, Parts I and II (1981).
17. Appleman, B. R. & Dailey, B. P. "Advances in Magnetic Resonance," Waugh, J. S., ed., Vol. 7, Academic Press, N.Y., p. 231 (1974).

18. Freeman, R. & Hill, H. D. W. J. Chem. Phys. 1971, 54, 3367.
19. Hull, W. D., Ph.D. Thesis, Harvard University (1975).
20. Shoemaker, D. P., Garland, C. W. & Steinfeld, J. I. "Experiments in Physical Chemistry," McGraw-Hill, Inc., N.Y. pp. 392-400 (1974).
21. Emsley, J. W., Feeney, J. & Sutcliffe, L. H. "High Resolution Nuclear Magnetic Resonance Spectroscopy," Pergamon Press, Oxford, Chap. 2 (1965).  $r_{\text{HbR}} = 25.0 \text{ \AA}$ ,  $r_{\text{Hb-II}} = 15.6 \text{ \AA}$ , and  $r_{\text{H}_2\text{O}} = 1.5 \text{ \AA}$ .
22. Antonini, E. & Brunori, M. "Hemoglobin and Myoglobin in Their Reaction with Ligands," American Elsevier Publishing Co., N.Y. p. 224-225 (1971).
23. Huheey, J. E. "Inorganic Chemistry: Principles of Structure and Reactivity," Harper and Row, Inc. N.Y. p. 307 (1972).
24. Suslick, K. S. private communication, 1978.
25. Metz, G. & Sjostrand, T. Acta Physiol. Scand. 1954, 31, 343-384.
26. Roughton, F. J. W. & Darling, R. C. Am. J. Physiol. 1944, 141, 17-31.
27. Although not a very good assumption, this will still yield ballpark values for the  $L_i$ 's.
28. Imai, K. & Yonetani, T. J. Biol. Chem. 1975, 250, 7093.

29. Hull, W. E. & Sykes, B. D. Biochemistry 1974, 13, 3431-3437.
30. Hull, W. E. & Sykes, B. D. J. Mol. Biol. 1975, 98, 121-153.
31. This is a good assumption for the proteins under study. See reference 29.
32. Gibson, A. A., Scott, T. A. & Fukushima, E. J. Magn. Reson. 1977, 27, 29.
33. Spiess, H. V. W. & Mahnke, H. Berichte der Bunsen-Gesellschaft 1972, 76, 990.
34. Gleeson, J. W., private communication, 1981.
35. Moon, R. B., Ph.D. Thesis, California Institute of Technology (1975).
36. Gilman, J. G. Biochemistry 1979, 18, 2273-2279. The value for  $\tau_i$  was scaled to conform to the definition of  $\tau_i$  in references 29 and 30.
37. Seamonds, B., McCray, J. A., Parkhurst, L. J. & Smith, P. D. J. Biol. Chem. 1976, 251, 2579-2583.

PART IV

Carbon Nuclear Magnetic Resonance Studies of  
the Histidine Residue  $\alpha$ -lytic Protease.  
A Reexamination at Higher Magnetic Field.

---



## INTRODUCTION

In catalysis by serine proteases, three residues, Asp<sup>102</sup>, His<sup>57</sup>, and Ser<sup>195</sup>, form a catalytic triad in which the hydroxyl group of the serine acts as a nucleophile to attack the carbonyl carbon of the scissile amide bond while the Asp-His diad stores the proton thus released.<sup>1-3</sup> The question of the microscopic ionization behavior of the Asp and His residues has received attention, the primary focus being the degree to which the proton on N<sup>δ1</sup> of His<sup>57</sup> may be transferred to the carboxylate anion of Asp<sup>102</sup>. A <sup>13</sup>C study<sup>4</sup> of the enzyme, α-lytic protease, suggested that this transfer was complete, resulting in a neutral imidazole ring and a neutral carboxylic acid group; its observations<sup>5</sup> and theoretical calculations<sup>6-9</sup> supported this suggestion. In contrast, <sup>15</sup>N and <sup>1</sup>H studies<sup>10-16</sup> and a structural determination by neutron diffraction<sup>17</sup> show that the proton never leaves N<sup>δ1</sup> of His<sup>57</sup>; accordingly, the diad exists as a carboxylate anion and imidazolium cation in the range pH 4-6.5. This suggests by analogy that, during catalysis, a proton likewise remains bonded to N<sup>δ1</sup> of His<sup>57</sup> and that the role of Asp<sup>102</sup> is to stabilize this adjacent cationic center and also to maintain the imidazole ring in the proper orientation<sup>10</sup> to act as an efficient acceptor of the proton of the hydroxyl group of Ser<sup>195</sup> as its oxygen adds across the carbonyl group of the amide to form the tetrahedral oxyanion.<sup>3</sup> In this regard,

proton inventory studies showing that two protons are concertedly involved during catalysis of appropriate substrates<sup>18-21</sup> can be understood as representing transfer of one proton to N<sup>ε2</sup> of His<sup>57</sup> and the formation of an exceptionally strong hydrogen bond between the carboxylate anion of Asp<sup>102</sup> and N<sup>δ1</sup> of the imidazolium cation of His<sup>57</sup>.<sup>20</sup>

To understand the apparent discrepancy between the <sup>13</sup>C results and others, we have reexamined the nmr behavior of α-lytic protease enriched with <sup>13</sup>C at C-2 of the imidazole ring of its single histidine residue (His<sup>57</sup>). The suggestion that this ring remains neutral at acid pH rested on the behavior of the coupling between the <sup>13</sup>C nucleus and its attached hydrogen (<sup>1</sup>J<sub>CH</sub>). Examination of the nmr spectra at 25, 50 and 125 MHz reveals the presence of three forms of the enzyme at acid pH which are in slow exchange at 125 MHz but in intermediate to fast exchange at 25 MHz; for all forms, the observed coupling constants suggest the presence of the protonated imidazolium cation form of His<sup>57</sup>.

## EXPERIMENTAL

Materials: L-[2- $^{13}\text{C}$ ]-histidine was synthesized by the method of Hunkapiller et al.,<sup>4</sup> starting with L-2,5-diamino-4-ketovaleric acid dihydrochloride and  $\text{K}^{13}\text{CN}$  (purchased from Prochem, 90.6%  $^{13}\text{C}$ , lot 43 X 80). Yield from 5.0g of  $\text{K}^{13}\text{CN}$  was 4.2g of L-[2- $^{13}\text{C}$ ]-histidine. The  $^1\text{H}$  and  $^{13}\text{C}$  nmr spectra in  $\text{D}_2\text{O}$  were consistent with L-histidine enriched 90.6% with  $^{13}\text{C}$  at C-2.

New Myxobacter 495 cultures were procured from Dr. E. A. Peterson of Agriculture Canada, Research Branch. The basic growth procedure was that of Hunkapiller et al.,<sup>4</sup> with a modified culture medium designed to reduce incorporation of unlabeled histidine into the protein and also dilution of the  $^{13}\text{C}$  label into nonspecific protein sites.

The bacteria were grown initially on slopes (1% agar, 0.2% Difco tryptone) for 36-48 hours prior to transfer to shake cultures. The shake cultures (first 100 ml in 300 ml flasks, then 1ℓ in 2.8ℓ flasks) consisted of the following synthetic medium: L-amino acids (mg/ℓ): Ala-120; Asp-200; Arg-120; Asn-120; Gln-200; Gly-100; Ile-150; Lys-200; Leu-250; Met-100; Phe-75; Pro-250; Ser-150; Thr-100; Tyr-50; Val-130; Inorganic Salts (mg/ℓ):  $\text{K}_2\text{HPO}_4 \cdot 3\text{H}_2\text{O}$ -2000;  $\text{NaCl}$ -2000;  $\text{MgSO}_4 \cdot 7\text{H}_2\text{O}$ -1000;  $\text{KNO}_3$ -500;  $\text{Fe}_2(\text{SO}_4)_3$ -15;  $\text{ZnSO}_4 \cdot 7\text{H}_2\text{O}$ -15;  $\text{MnSO}_4 \cdot \text{H}_2\text{O}$ -2; Monosodium L-Glutamate (20 g/ℓ) was added as the primary nitrogen source. Sucrose (10 g/ℓ, autoclaved sepa-

rately) was used as the major carbon source. The above amino acid mixture is designed to simulate the composition of histidine-free casamino acids (casein hydrolysate). Hence, no unlabeled histidine was introduced into the medium. All media were made up in distilled water, and the final pH was adjusted to 7.1-7.2. The growth temperature was maintained at 27-29°C.

L-[2-<sup>13</sup>C]-histidine (100 mg/l) was added to each 100 ml culture initially. These cultures were grown for three days and then transferred to the 1l cultures of the same synthetic medium containing 50 mg/l of labeled histidine. 1 ml of a 2.5% (w/w) sterile solution of labeled histidine was added at 24-hour intervals to the 1l cultures for five days. After this time, the bacteria were harvested;  $\alpha$ -lytic protease activity was ~ 200 mg/l at this point. Activity was assayed versus the synthetic substrate N-ac-L-ala-L-pro-L-ala p-nitroanilide<sup>18</sup> in 0.1 M KCl, 0.05 M Tris-hydroxymethylaminomethane·HCl, pH 8.75, 25°C.

Isolation and purification of the enzyme was performed as per the method of Hunkapiller et al.,<sup>4</sup> with three minor modifications. 200 ml of Amberlite CG-50, pH 4.95, 0.1 M Na-acetate (settled bed volume) was added to the combined bacteria-free media, instead of 100 ml. Absorption of the enzyme onto this resin was continued for two days, rather than

one. Also, the final elution step required 0.50 M Na-citrate buffer, pH 6.40, rather than 0.27 M Na-citrate, pH 6.20. These changes were necessary due to some modification in the properties of the presently available CG-50 resin over that used in the previous isolations. The enzyme was chromatographed on CG-50 twice; fractions containing  $\alpha$ -lytic protease were dialyzed three times versus 0.1 M KCl and three times versus distilled water, and lyophilized. Yield was about 600 mg of enzyme from six liters of culture.

All materials were prepared by Robert Kaiser.

NMR Samples: NMR samples were made by dissolving the desired amount of protein in 2.0 ml of 0.2 M KCl (90% double-distilled water-10% D<sub>2</sub>O [v/v] and carefully adjusting the pH with 1 N KOH or 1 N HCl. The pH was measured using a combination electrode<sup>22</sup> before and after each run; agreement was  $\pm 0.05$  pH units. Protein concentration in each sample was checked by determining both the absorbance at 280 nm ( $[E] = 5.16 \times 10^{-5} \times A_{280}^{1\text{cm}}$ ,<sup>23</sup> and by monitoring the hydrolysis of N-ac-L-ala-L-pro-L-ala p-nitroanilide at 410 nm ( $5.0 \times 10^{-4}$  M in 0.1 M KCl, 0.05 M Tris·HCl, pH 8.75 25°C). These two methods agreed to within  $\pm 2\%$  and were  $\pm 5\%$  with respect to added mass of protein. Comparison of our nmr spectra with representative spectra done by Hunkapiller et al.<sup>4</sup> showed a <sup>13</sup>C-histidine enrichment of 65-75% and little nonspecific enrichment.

NMR Spectra:  $^{13}\text{C}$  nmr spectra were taken on three different spectrometers. Low field measurements were done on a Varian XL-100-15 operating at 25.14 MHz. 200 MHz data were performed on a Nicolet NT-200. The high field spectra were obtained on a Bruker WM-500 spectrometer. Sample tubes were 10, 12, and 20 mm in diameter, depending on the spectrometer used. The linewidths were determined by subtracting the line broadening applied to the FID (free induction decay) from the resulting transformed spectrum. Chemical shifts are reported relative to the arginine guanidinium carbons which resonate at 157.25 ppm downfield from tetramethylsilane and whose position did not change over the pH range investigated.

## RESULTS

Figure 1 shows the coupled and decoupled  $^{13}\text{C}$  nmr spectra for  $\alpha$ -lytic protease at pH 5.1. As can be seen, the resonances corresponding to the C-2 carbon of the histidine ring are clearly discernible above the unenriched protein carbon resonances. The observed coupling constant at this pH is 214 Hz, not 205 Hz as previously reported,<sup>4</sup> indicating that the imidazole ring is protonated at pH 5.1. However, if the coupling constant is measured using the method of Hunkapiller et al.<sup>4</sup> by taking twice the difference between the downfield resonance of the proton-coupled C-2 doublet and the decoupled C-2 resonance, a value of 206 Hz is obtained. This discrepancy between the observed coupling constant (from the coupled spectrum) and the calculated coupling constant will be discussed later.

Figure 2 shows the proton-coupled spectrum of  $\alpha$ -lytic protease at 125.76 MHz and pH 5.5. Two features appear at this frequency that are not seen at 25.14 MHz. First, a new doublet is seen centered at 135.54 ppm which has a coupling constant  $^1J_{\text{CH}} = 225$  Hz. Also, the intensities of the two peaks assigned to the C-2 resonance are noticeably different; this is also true at pH 8.1, and at pH 5.2 at 50.3 MHz.

As the pH is lowered from 5.5 to 4.8, a third doublet, slightly upfield of the other two doublets and centered at  $\delta = 134.34$  ppm, appears (Figure 3B). This

Figure 1

- a) 25.14 MHz proton-decoupled  $^{13}\text{C}$  nmr spectrum of  $\alpha$ -lytic protease in 10%  $\text{D}_2\text{O}$ : 7.5 mM enzyme, 0.2 M KCl,  $32^\circ\text{C}$ , pH = 5.1. 144,000 transients were taken with an acquisition time of 0.15 sec, 5 KHz spectral width, and a  $90^\circ$  pulse of 90  $\mu\text{sec}$ . A line broadening of 3 Hz was used. The FID was zero-filled to 8K data points.
- b) Proton-coupled spectrum of (a). Probe temperature was  $26^\circ\text{C}$ . 169,000 transients were taken using parameters in (a).



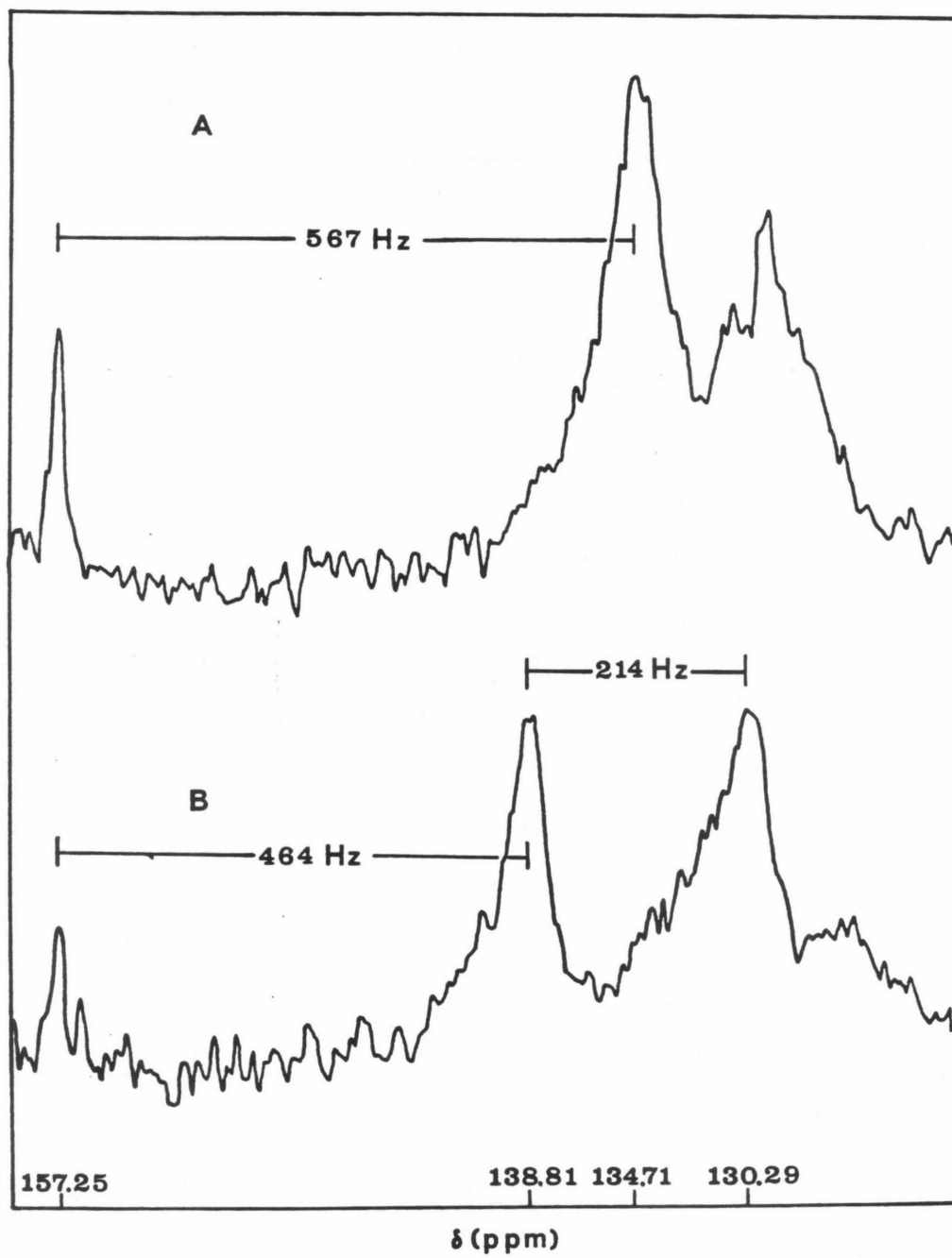
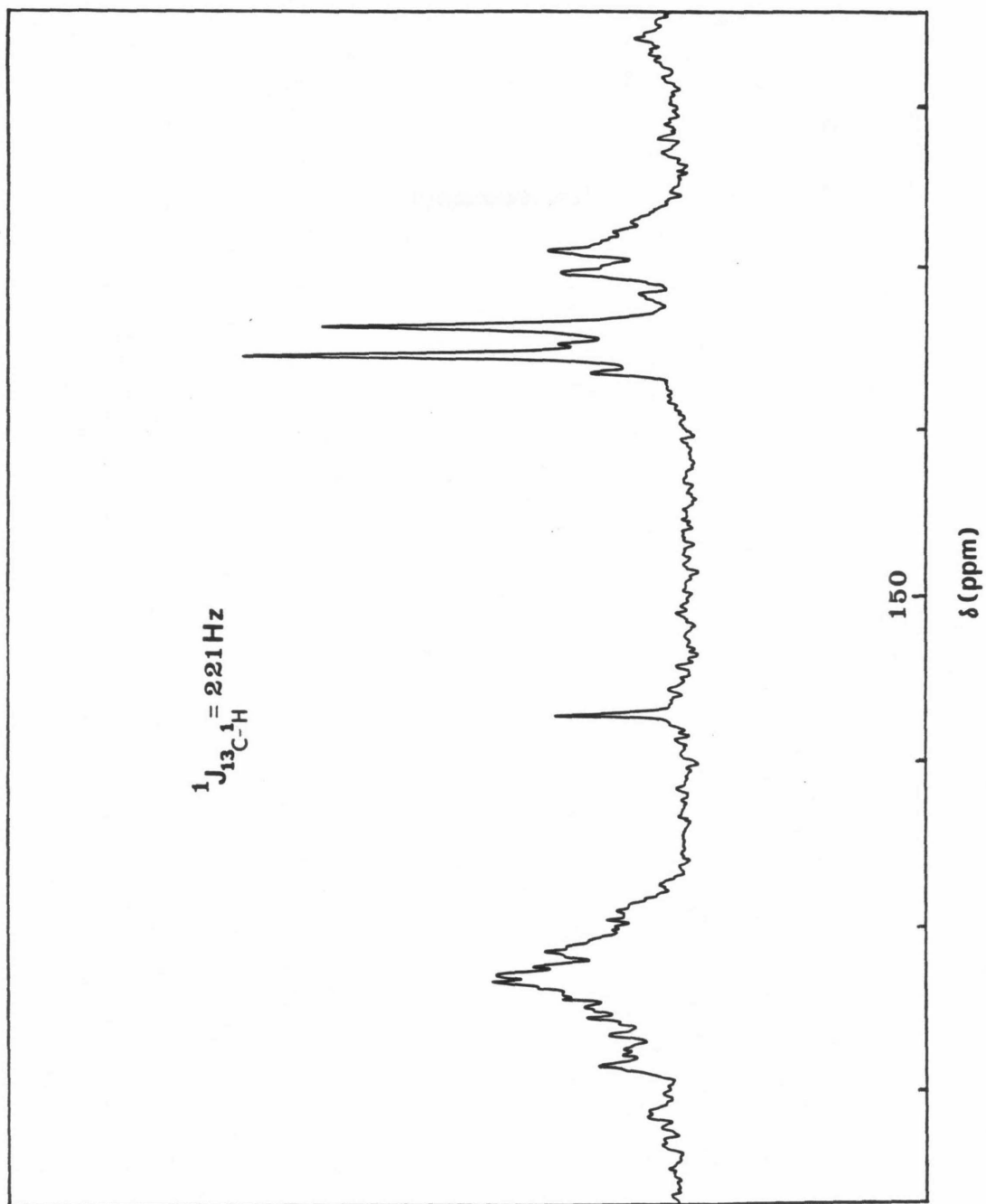


## Figure 2

125.76 MHz proton-coupled  $^{13}\text{C}$  nmr spectrum of  $\alpha$ -lytic protease in 10%  $\text{D}_2\text{O}$ : 3.2 mM enzyme, 0.2 M KCl,  $25^\circ\text{C}$  pH = 5.5. 37,660 transients were taken with an acquisition time of 0.52 sec, 31.25 KHz spectral width, and a  $23^\circ$  pulse of 30  $\mu\text{sec}$ . A line broadening of 5 Hz was used.



doublet disappears as the pH is raised to 5.5 (Figure 3C). The intensity of the downfield doublet does not change significantly at pH = 4.8 if the sample has not been at high pH first. When the sample is taken up to pH 8.1 (Figure 3D) and then brought down to pH 4.8, the spectrum E in Figure 3 is obtained. Raising the pH of this sample to 5.5 yields a spectrum similar to the previous 5.5 spectra, except that the intensity of the downfield doublet is greater (Figure 3F).

A summary of the titration data for the enzyme at 125.76 MHz is given in Figure 3. The nmr parameters for the spectra in Figures 1, 2, and 3 are summarized in Table I.

Figure 3

125.76 MHz proton-coupled  $^{13}\text{C}$  nmr spectra of  $\alpha$ -lytic protease in 10%  $\text{D}_2\text{O}$  at  $25.0^\circ$ .

- A) Sample from Figure 2, pH 5.5, 37,660 transients, 20 Hz line broadening.
- B) 2.0 mM protein in 0.2 M KCl. The pH was adjusted to 4.8 after initially having been at 5.5 during a prior spectrum. 7,600 transients, 20 Hz line broadening. Other parameters same as in Figure 2.
- C) Same sample as in (B). The pH was adjusted to 5.5 after having been at 4.8. 12,080 transients, 20 Hz line broadening.
- D) Same sample as in (A). pH 8.1, 8,630 transients, 20 Hz line broadening.
- E) Same sample as in (D), pH 4.8, 6,140 transients, 20 Hz line broadening.  
The lower trace is resolution-enhanced.
- F) Same sample as in (B). The pH was adjusted to 5.5 after having been at 8.1. 63,008 transients, 20 Hz line broadening.

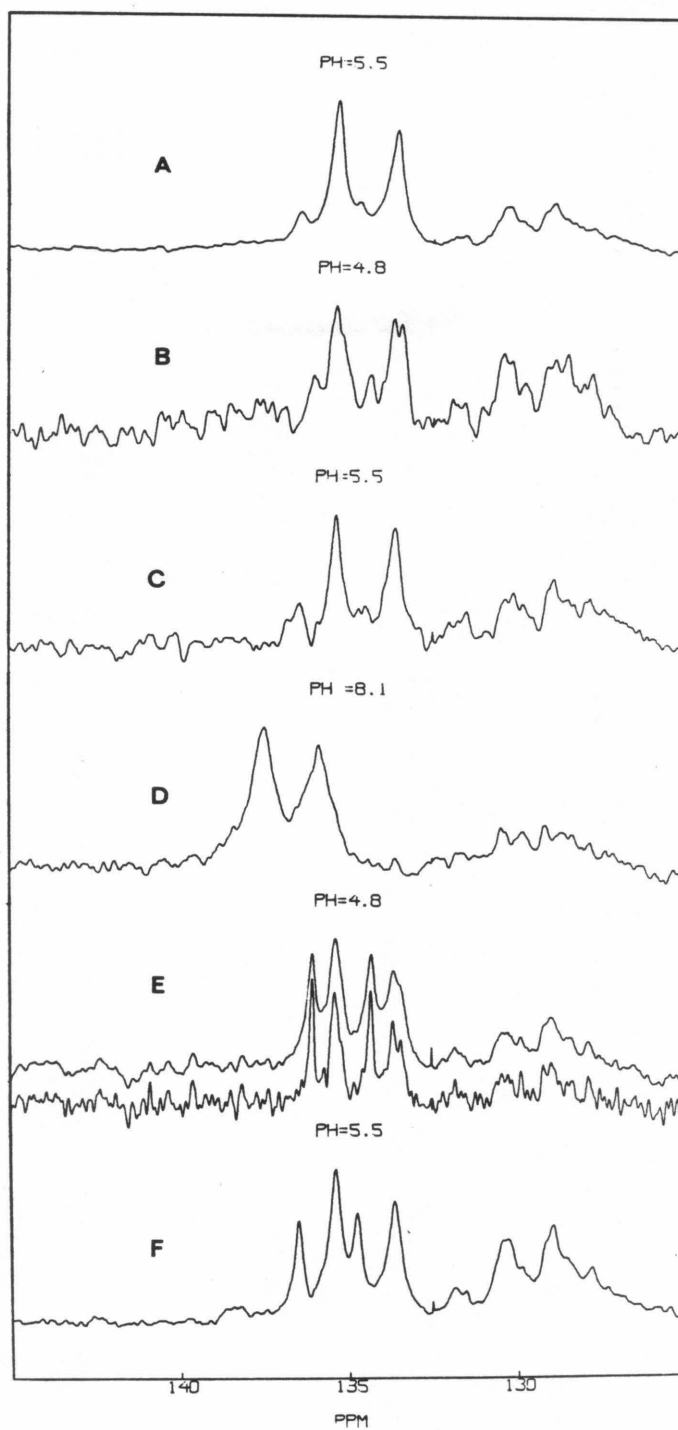


Table I

NMR Parameters for C-2 Carbon in Histidine Residue of  $\alpha$ -Lytic Protease.

Field (MHz)	pH	$\delta$ (ppm) <sup>a</sup>	$^1J_{CH}$ (Hz) <sup>b</sup>	$\nu_{1/2}$ (Hz) <sup>b</sup>
25.14	5.1	134.71 <sup>d</sup>	---	40
		134.55 <sup>e</sup>	214	40
50.3 <sup>f</sup>	5.2	134.52	218	40
125.76	8.1	136.68	204	50
	5.5	135.54	225	40
		134.47	221	40
	4.8	135.21	217	35
		134.55	214	35
		134.34	216	35

a) Chemical shifts are  $\pm 0.10$  ppm at 25.14 and 50.3 MHz, and  $\pm 0.05$  ppm at 125.76 MHz. The shifts are relative to TMS = 0.00 pm. b)  $^1J_{CH}$  values are  $\pm 3$  Hz. c)  $\nu_{1/2}$  values are  $\pm 10\%$ . d)  $^1H$  - decoupled. e)  $^1H$  - coupled. f) Sample in this case was 20 ml of 1.8 mM enzyme in 0.2 M KCl, 10%  $D_2O$ , due to the use of 20 mm nmr sample tube.

## DISCUSSION

For  $\alpha$ -lytic protease at pH 5.5, the coupling constant  $^1J_{CH}$  observed for C-2 of the imidazole ring of His<sup>57</sup> and its attached hydrogen are 218 Hz at 50.3 MHz and 221 Hz at 215.76 MHz; these values indicate a protonated imidazole<sup>4,26</sup> and agree with the  $^{15}N$  and  $^1H$  nmr observations<sup>10-15</sup> on  $\alpha$ -lytic protease and other serine proteases.

The  $^{13}C$  spectra of  $\alpha$ -lytic protease at 125.76 MHz at pH 5.5 show two  $^{13}C$  signals from the single histidine indicating two forms of the enzyme which are in slow exchange relative to the nmr time scale at this field. At lower fields these forms appear to be in fast to intermediate exchange. For both signals,  $^1J_{CH}$  is that characteristic of a protonated histidine<sup>24</sup> (at  $\delta = 134.47$  ppm,  $^1J_{CH} = 221$ ; at  $\delta = 135.54$  ppm,  $^1J_{CH} = 225$ ). Both signals appear to have about equal linewidths (30-40 Hz) which suggest that in neither case does the imidazole ring freely rotate in solution, as such a residue has a much narrower line ( $\sim 12$  Hz).<sup>4</sup> A reservation in this conclusion is that, if the exchange rate is on the borderline between slow and intermediate, the observed linewidth could reflect not only the mobility of the residue but could also be broadened by virtue of the exchange process itself. We cannot presently dissect the contributions of these two processes.



At pH 4.8, a third pair of resonances occurs at 134.34 ppm which likewise has a  $^1J_{CH}$  characteristic of a protonated imidazole. The overlap of these resonances with the resonances centered at  $\delta = 134.5$  ppm is what causes the difference in intensities observed for the upfield doublet at pH 5.5 and 8.1. The changes with pH in the nmr spectra are reversible if the sample has not been at high pH; by raising and then lowering the pH, the relative amount of the downfield species increases (Figures 3E and 3F), although the chemical shifts are the same as in spectra 3A through 3C. The resulting pH 8.1 spectra for all samples are identical to that of spectrum D in Figure 3. After nmr observation, the enzyme still retains  $96 \pm 5\%$  of its original catalytic activity.

The fact that different forms of His<sup>57</sup> are observed in the  $^{13}C$  nmr experiment at low pH is consistent with previous  $^1H$  nmr spectra of chymotrypsinogen and chymotrypsin.<sup>25</sup> The low pH spectrum of chymotrypsinogen showed two broad peaks at  $\delta = 18.06$  and  $13.06$  ppm which were assigned to the  $N^{\delta 1}$  proton of His<sup>57</sup>; the chymotrypsin spectrum exhibited only the resonance at  $\delta = 18.06$  ppm. In both cases, the  $\delta = 18.06$  ppm resonance possesses fractional intensity, i.e., the sum of the areas of the  $\delta = 18.06$  and  $13.06$  ppm peaks corresponds to one proton in the chymotrypsinogen spectrum, whereas the upfield peak

is exchange broadened in the chymotrypsin spectrum. These results were interpreted as representing the same proton in different, exchanging conformational states.<sup>25</sup> It was suggested that the two resonances might represent the different forms of His<sup>57</sup> in the protein as postulated by Matthews et al.<sup>26</sup> In their "flip-flop" model, the N<sup>δ1</sup> proton is bound alternatively to the O<sup>δ1</sup> and O<sup>δ2</sup> oxygens of Asp<sup>102</sup>.

We now know that there are multiple forms of His<sup>57</sup> at low pH whose C-2 resonances are in slow exchange at 125.76 MHz. However, at 25.14 MHz, most of the resonances are unobservable due to their being in intermediate to fast exchange. Furthermore, the exchange rate is a sensitive function of temperature. In the Hunkapiller et al.<sup>4</sup> experiment, the sample temperature was likely to be higher during the acquisition of decoupled spectra, a result of dielectric heating, than during the acquisition of coupled spectra, even though cooling air was used to maintain a nearly constant probe temperature. The result of this is depicted in Figure 1. Due to the higher temperature during decoupling, the decoupled resonance corresponding to C-2 has been shifted slightly downfield from the coupled chemical shift position because of the increase in the exchange rate. Thus, the measured difference between the coupled downfield peak and the decoupled resonance is less than the actual difference; this results in the calculation of an artifactually small coupling constant.

The low specific enrichment of the protein used in the previous work<sup>4</sup> precluded accurate direct measurement of the coupling constant. Use of a difference program to subtract out native, unenriched carbon resonances from the enriched resonances also led to substantial errors in measuring the coupling constant due to difficulties in the phasing of the resonances in the histidine region.

## CONCLUSION

The present study shows that His<sup>57</sup> of the catalytic triad of  $\alpha$ -lytic does become protonated with a pKa of 6.7 as measured by <sup>13</sup>C nmr. Moreover, it reveals the presence of multiple forms of the enzyme at acidic pH which may account for some of the reports regarding the low field <sup>1</sup>H resonance at 17-18 ppm in  $\alpha$ -lytic protease.<sup>4,14,16,25</sup>

Lastly, recent findings particularly using proton inventory techniques, reveal differences in catalytic behavior of serine proteases as a function of the substrate; larger, more physiological substrates manifest aspects of catalysis not observed with smaller substrates.<sup>18,20</sup> Accordingly, the nmr results on the ionization behavior of the catalytic residues of the free enzyme should, with appropriate caution, be extended to the behavior of these residues during catalysis.

REFERENCES

1. Blow, D. M. Accts. Chem. Res. 1976, 9, 145-152.
2. Stroud, R. M., Krieger, M., Loeppe, R. E., Kossiakoff, A. A. & Chambers, J. L. "Proteases and Biological Control," Reich, E., Rifkin, D. B. & Shaw, E., eds., Cold Spring Harbor, N.Y. pp. 13-32; 1021 (1975).
3. Kraut, J. Ann. Rev. Biochem. 1977, 46, 331-68.
4. Hunkapiller, M. W., Smallcombe, S. H., Whitaker, D. R. & Richards, J. H. Biochemistry 1973, 12, 4732-4743.
5. Koeppe, R. E. & Stroud, R. M. Biochemistry 1976, 15, 3450-3458.
6. Amidon, G. L. J. Theor. Biol. 1974, 46, 101-109.
7. Beppu, Y. & Yomosa, S. J. Phys. Soc. Jpn. 1977, 42, 1694-1700.
8. Kitayama, H. P. & Fukutome, H. J. Theor. Biol. 1976, 60, 1-18.
9. Scheiner, S., Klein, D. A. & Lipscomb, W. N. Proc. Natl. Acad. Sci. USA 1975, 72, 2606-2610.
10. Bachovchin, W. W. & Roberts, J. D. J. Am. Chem. Soc. 1978, 100, 8041-8047.
11. Markley, J. L. Accts. Chem. Res. 1975, 8, 70-80.
12. Markley, J. L. & Porubcan, M. A. J. Mol. Biol. 1976, 102, 487-509.

13. Markley, J. L. & Ibanez, I. B. Biochemistry 1978, 17, 4627-4640.
14. Markley, J. L. in "Biological Applications of Magnetic Resonance," Shulman, R. G. ed., Academic Press, Inc. N.Y., pp 397-461; 595 (1979)
15. Robillard, G. & Shulman, R. G. J. Mol. Biol. 1972, 71, 507-511.
16. Robillard, G. & Shulman, R. G. J. Mol. Biol. 1974, 86, 519-540.
17. Kossiakoff, A. A. & Spencer, S. A. Nature (London) 1980, 288, 414-416.
18. Hunkapiller, M. W., Forgacs, M. D. & Richards, J. H. Biochemistry 1976, 15, 5581-5588.
19. Elrod, J. P., Gandour, R. D., Hogg, J. L., Kise, M., Maggiora, G. M., Schowen, R. L. & Venkatasubban, K. S. Faraday Symp. Chem. Soc. 1975, 10, 145-153.
20. Elrod, J. P., Hogg, J. L., Quinn, D. M., Venkatasubban, K. S. & Schowen, R. L. J. Am. Chem. Soc. 1980, 102, 3917-3922.
21. Quinn, D. M., Elrod, J. P., Ardis, R., Friesen, P. & Schowen, R. L. J. Am. Chem. Soc. 1980, 102, 5338-5365.
22. The pH values reported are the meter readings of the 10% D<sub>2</sub>O solution using an electrode standardized versus 100% H<sub>2</sub>O buffer.

23. Whitaker, D. R. "Methods in Enzymology," Perlmann, G. E. & Lorand, L., eds., Volume XIX, Academic Press, Inc., N.Y. pp. 599-613; 1042. (1970)
24. Wasylishen, R. E. & Tomlinson, G. Biochem. J. 1975, 147, 605-607.
25. Markley, J. L. Biochemistry 1978, 17, 4648-4656.
26. Matthews, D. A., Alden, R. A., Birktoft, J. J., Freer, S. T. & Kraut, J. J. Biol. Chem. 1977, 252, 8875-8883.

PART V

A General Method for Performing  
Magnetization Transfer Experiments.



INTRODUCTION

One of the major contributions of nuclear magnetic resonance (nmr) spectroscopy has been to the study of dynamic molecular processes in solution. In the present chapter, the two site exchange case will be examined, i.e.



where  $k_A$  and  $k_B$  are rate constants for sites A and B. When such a system is close to the intermediate rate of exchange (on the nmr time scale), line shape analysis can be used to extract the rate constants.<sup>1</sup> For spectra that are undergoing slow exchange, magnetization transfer<sup>2</sup> and its pulse analog<sup>3,4,10</sup> have been used to determine rate constants for a variety of systems. However, in the case of magnetization transfer, all previous analyses have been performed assuming equal populations for the two sites because of the mathematical simplifications involved. A method will be presented which allows for the determination of rate constants for two unequally populated sites.

One problem associated with the pulse magnetization transfer experiment is in the application of the initial selective  $\pi$  pulse to one of the two resonances in exchange. Because of the way this pulse has been generated in the past, i.e., a long, low power pulse, the experiment has been limited

primarily to proton observation, with the decoupler providing the selective pulse; observation of other nuclei has involved extensive hardware modification. A scheme for circumventing this problem for other nuclei will be given, along with its application to the  $^{31}\text{P}$  spectrum of tri-(triphenylphosphine)-tetramethylene-nickel (II).

EXPERIMENTAL

Chemicals: Tris(triphenylphosphine)-tetramethylene-nickel (II)  $\left( (\text{PPh}_3)_3\text{Ni} \begin{array}{c} \diagup \\ \square \\ \diagdown \end{array} \right)$  was prepared by Ott as described previously.<sup>5</sup>

NMR measurements:  $^{31}\text{P}$  spectra were obtained with a JEOL FX-90Q spectrometer equipped with a PG-200 pulse programmer. Inversion recovery<sup>6</sup> was used for the determination of  $T_1$ .

Calculations: Analysis of eq. 11 to obtain rate constants from the nmr data was carried out on a Commodore PET microcomputer using a non-linear least squares program (see Appendix). Pulse simulations using eq. 13-15 were also done on the PET (see Appendix).

THEORY

Exchange: For the two site exchange system, the Bloch equations are<sup>7</sup>

$$\frac{dM_Z^A}{dt} = M_Z^B k_B - M_Z^A k_{1A} + M_\infty^A / T_{1A} \quad (2a)$$

$$\frac{dM_Z^B}{dt} = M_Z^A k_A - M_Z^B k_{1B} + M_\infty^B / T_{1B} \quad (2b)$$

where

$$k_{1i} = k_i + 1/T_{1i} \quad i = A \text{ or } B \quad (3)$$

Solving this system of linear differential equations yields<sup>2</sup>

$$M_Z^A = M_\infty^A + C_1 \exp(-\lambda_1 t) + C_2 \exp(-\lambda_2 t) \quad (4a)$$

$$M_Z^B = M_\infty^B + C_1 [(k_{1A} - \lambda_1)/k_B] \exp(-\lambda_1 t) \\ + C_2 [(k_{1A} - \lambda_2)/k_B] \exp(-\lambda_2 t) \quad (4b)$$

where  $C_1$  and  $C_2$  are constants of integration, and<sup>7</sup>

$$\lambda_1 = \frac{1}{2}(1/T_{1A} + 1/T_{1B} + k_B/P_A) + [\frac{1}{4}(k_{1A} - k_{1B})^2 + k_B^2 P_B/P_A]^{1/2} \quad (5a)$$

$$\lambda_2 = \frac{1}{2}(1/T_{1A} + 1/T_{1B} + k_B/P_A) - [\frac{1}{4}(k_{1A} - k_{1B})^2 + k_B^2 P_B/P_A]^{1/2} \quad (5b)$$

$P_i \equiv$  mole fraction of species  $i$  ( $P_A + P_B = 1$ )

If eq. 4b is subtracted from 4a, we obtain

$$\Delta M_Z = \Delta M_\infty + C_1 [1 - (k_{1A} - \lambda_1)/k_B] \exp(-\lambda_1 t) + \\ + C_2 [1 - (k_{1A} - \lambda_2)/k_B] \exp(-\lambda_2 t) \quad (6)$$

where

$$\Delta M_Z = M_Z^A - M_Z^B \quad (7)$$

$$\Delta M_\infty = M_\infty^A - M_\infty^B \quad (8)$$

At  $t = 0$ ,

$$\begin{aligned} \Delta M_Z &= \Delta M_0 \\ &= \Delta M_\infty + C_1[1 - (k_{1A} - \lambda_1)/k_B] + C_2[1 - (k_{1A} - \lambda_2)/k_B] \end{aligned} \quad (9)$$

Rearranging eq. 9,

$$C_1[1 - (k_{1A} - \lambda_1)/k_B] = \Delta M_0 - \Delta M_\infty - C_2[1 - (k_{1A} - \lambda_2)/k_B] \quad (10)$$

Substituting eq. 10 into eq. 6 yields the desired result:

$$\begin{aligned} \Delta M_Z &= \Delta M_\infty + [\Delta M_0 - \Delta M_\infty - C_2[1 - (k_{1A} - \lambda_2)/k_B]]\exp(-\lambda_1 t) \\ &\quad + C_2[1 - (k_{1A} - \lambda_2)/k_B]\exp(-\lambda_2 t) \end{aligned} \quad (11)$$

It should be noted that eq. 11 reduces to the formalism obtained by Dahlquist et al.<sup>3</sup> if  $P_A = P_B$  ( $k_A = k_B$ ) and

$$T_{1A} = T_{1B}:$$

$$\Delta M_Z = \Delta M_0 \exp(-(1/T_1 + 2k_B)t)$$

or

$$\ln|\Delta M_Z| = -(1/T_1 + 2k_B)t + \ln|\Delta M_0| \quad (12)$$

By collecting a series of magnetization transfer data for different values of  $t$  (the time between the selective and sampling pulses) and fitting the data to eq. 11, the rate of exchange may be obtained.

Selective Pulse: The transient solution of the Bloch equations following a short rf pulse is given by eqs.

13-15:<sup>8</sup>

$$M_z = M_z^- \cos \alpha - M_y^- \sin \alpha + M_\infty [1 - \exp(-t/T_1)] \quad (13)$$

$$M_x = (M_x^- \cos \Delta \omega t + M_y^- \cos \alpha \sin \Delta \omega t + M_z^- \sin \alpha \sin \Delta \omega t) \exp(-t/T_2) \quad (14)$$

$$M_y = (M_y^- \cos \alpha \cos \Delta \omega t + M_z^- \sin \alpha \cos \Delta \omega t - M_x^- \sin \Delta \omega t) \exp(-t/T_2) \quad (15)$$

where

$\alpha \equiv$  flip angle

$\Delta \omega \equiv$  frequency offset from the transmitter frequency

$M_i^- \equiv$  magnetization components preceding the rf pulse  
( $i = x, y, z$ )

As pointed out by Bodenhausen et al,<sup>9</sup> a series of short, small flips of the magnetization will yield a selective pulse with maxima at  $n/d$  where  $n$  is an integer and  $d$  is the interval between the short pulses. Figure 1 shows the effect of such a pulse train on the magnetization when a composite  $90^\circ$  pulse is applied.

The extension of this pulse sequence to magnetization transfer measurements is now obvious. By creating a composite  $180^\circ$  pulse, the desired selective perturbation is

obtained. However, it is important that the peak which should not be affected is not "hit" by a harmonic as is shown in Figure 2. To avoid this problem, the time between pulses can be reduced, thus increasing the frequency difference between harmonics. This, in conjunction with the placement of the carrier on the peak to be flipped, will give the desired result. This is depicted in Figure 3.

Figure 1

Plot of  $M_y$  and  $M_z$  vs frequency offset for a selective  $90^\circ$  pulse calculated using eqs. 13-15 and the following conditions: 19 pulses,  $\alpha = 4.7^\circ$ ,  $t_{\text{on}} = 1 \mu\text{sec}$ ,  $t_{\text{off}} = 2 \text{ msec}$ ,  $T_1 = T_2 = 1 \text{ sec}$ .



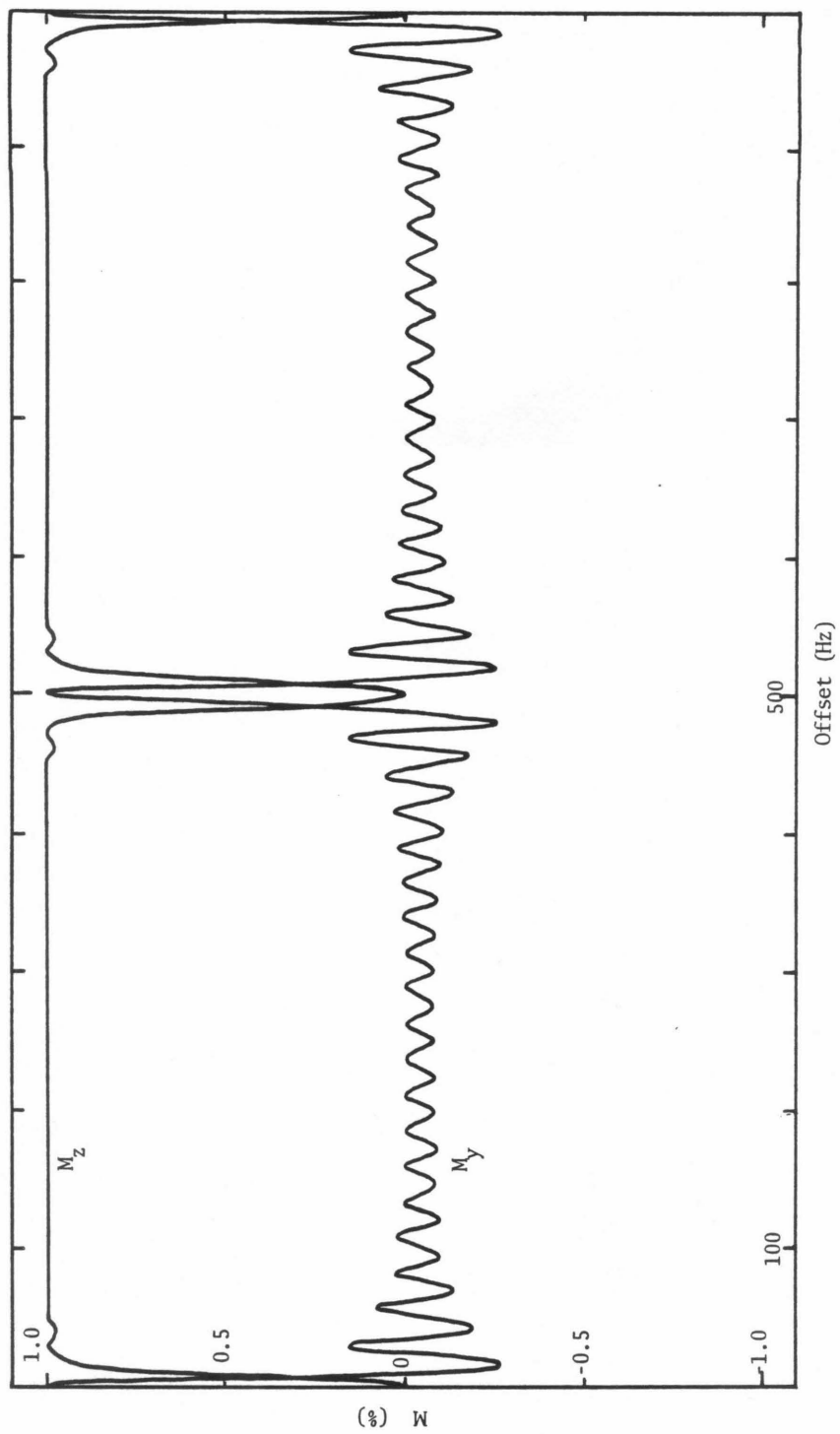


Figure 2

Plot of  $M_y$  and  $M_z$  vs frequency offset for a selective  $180^\circ$  pulse calculated using eqs. 13-15 and the following conditions:  
39 pulses,  $\alpha = 4.6^\circ$ ,  $t_{\text{on}} = 1 \mu\text{sec}$ ,  
 $t_{\text{off}} = 2 \text{ msec}$ ,  $T_1 = T_2 = 1 \text{ sec}$ .

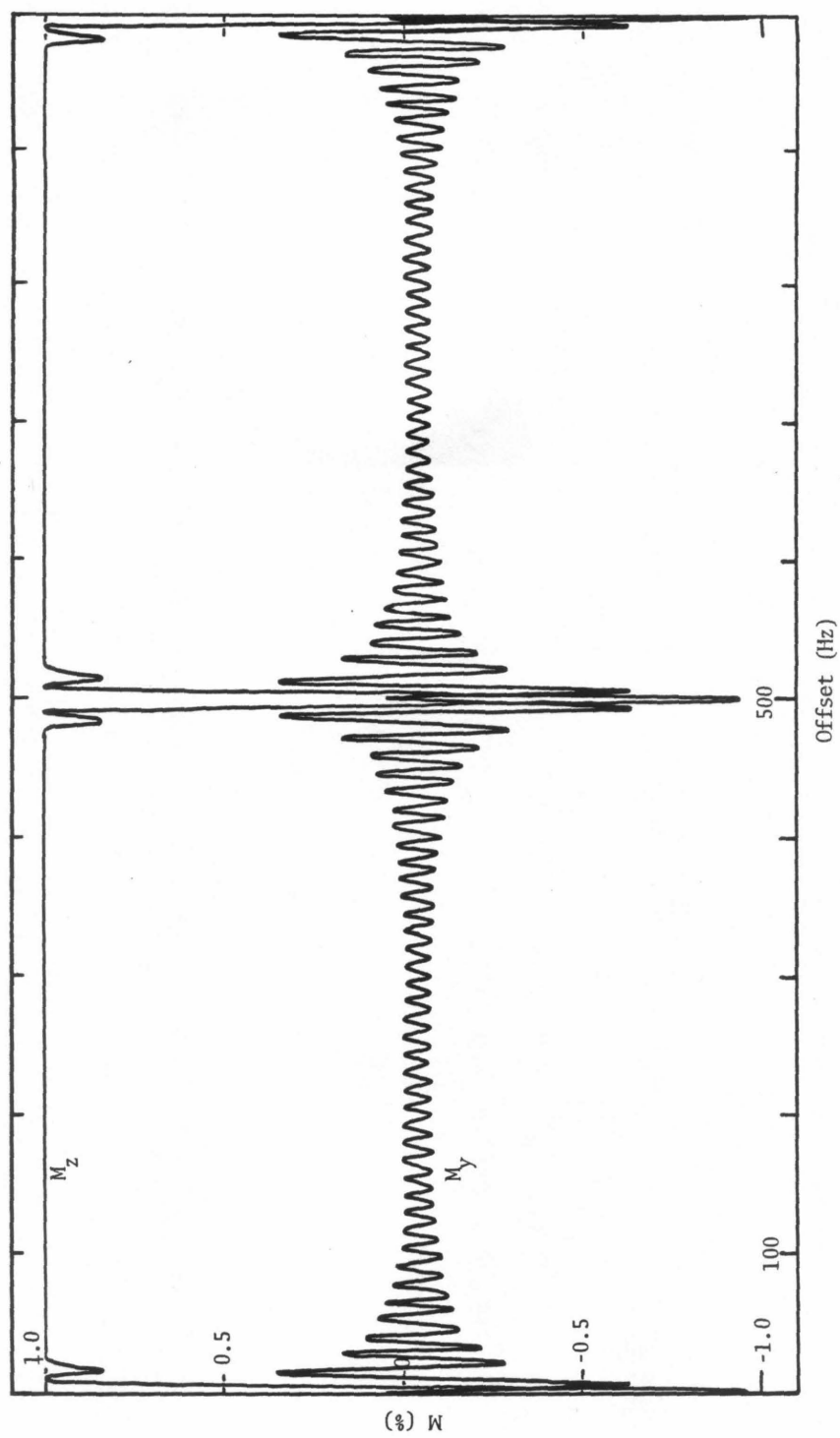
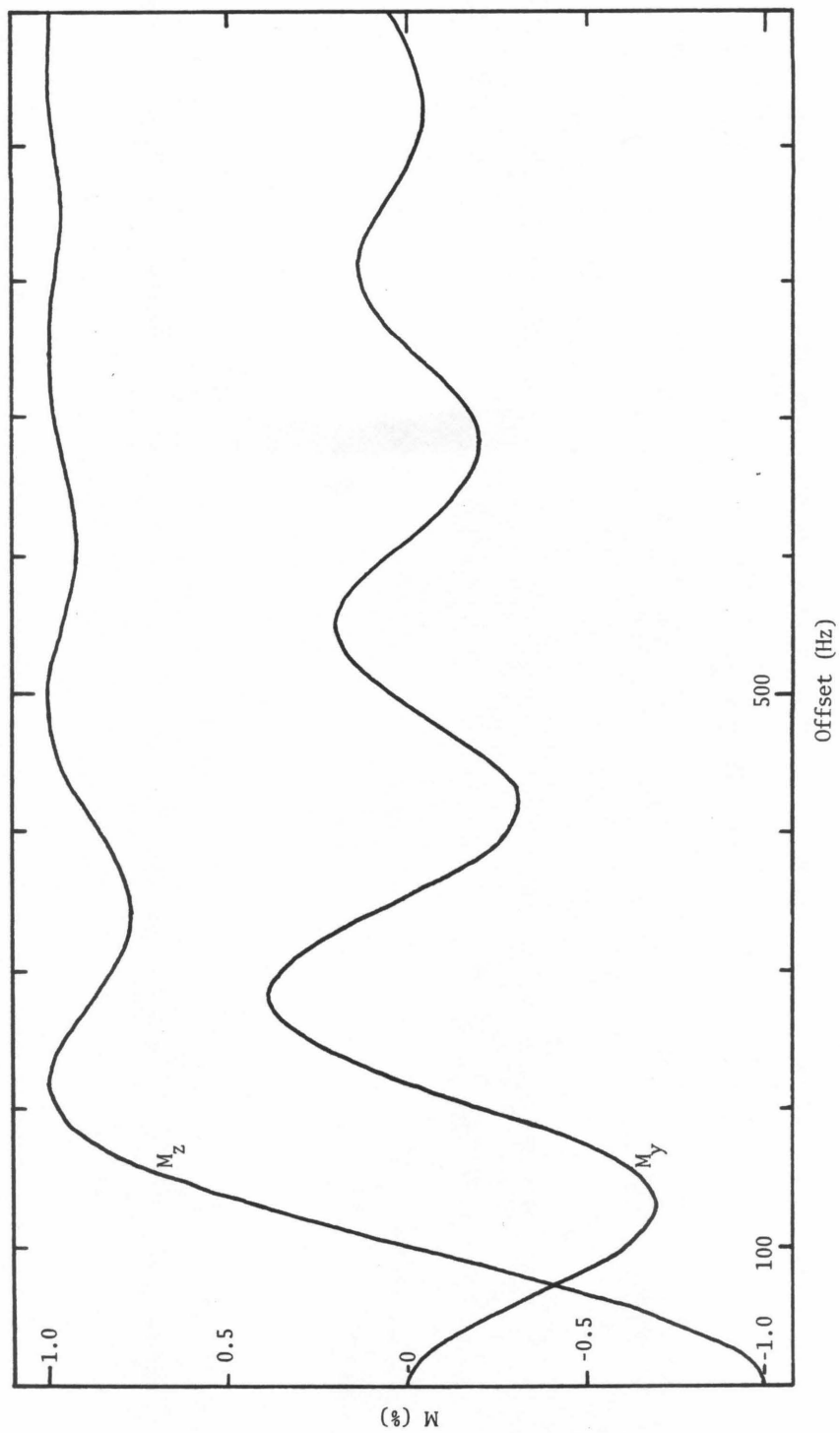


Figure 3

Plot of  $M_y$  and  $M_z$  vs frequency offset for a selective  $180^\circ$  pulse calculated using eqs. 13-15 and the following conditions: 78 pulses,  $\alpha = 2.3^\circ$ ,  $t_{\text{on}} = 1 \text{ } \mu\text{sec}$ ,  $t_{\text{off}} = 50 \text{ } \mu\text{sec}$ ,  $T_1 = T_2 = 1 \text{ sec}$ .



## RESULTS AND DISCUSSION

The exchange process first studied using the general magnetization transfer equation (eq. 11) and a composite selective  $180^\circ$  pulse was the following:

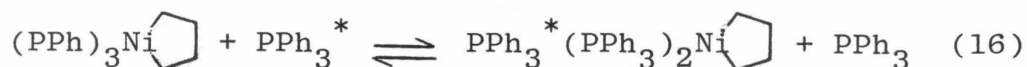


Figure 4 shows the  $^{31}\text{P}$  spectra of this system at  $-90^\circ\text{C}$  after a selective  $180^\circ$  pulse has been applied to free  $\text{PPh}_3$ . As can be seen, inversion is complete for the free  $\text{PPh}_3$  and, as  $\tau$  increases, magnetization is transferred between the two sites. Table I summarizes the exchange rates obtained for this system using magnetization transfer at two temperatures. Also given in the table are the results from lineshape analysis. As can be seen, the two methods are in good agreement at  $-80^\circ\text{C}$ , but only in moderate agreement at  $-90^\circ\text{C}$ . This is because the spectrum at  $-90^\circ\text{C}$  is in very slow exchange on the nmr time scale ( $\Delta\nu = 1195 \text{ Hz}$ ), so large errors are introduced when  $k$  is determined via lineshape analysis; the magnetization transfer experiment does not suffer from this problem.

The general nature of this method makes it possible to look at exchanging systems with unequal populations for the two sites. One example would be the study of hapten binding dynamics with antibodies. Previous work carried out by Kooistra et al<sup>4</sup> used eq. 12 to study the interactions of  $^{19}\text{F}$  labelled nitrophenyl haptens with the mouse

Figure 4

$^{31}\text{P}$  magnetization transfer spectra of triphenyl phosphine (B) and tris(triphenylphosphine)tetramethylene-nickel (II) (A) at  $-90^\circ\text{C}$ . The selective pulse sequence used was  $[(2.3^\circ \text{ pulse} - 50 \mu\text{sec delay})_{78} - \tau - 90^\circ \text{ pulse-acquisition-pulse delay}]_n$ . Peak B was positioned in the middle of the spectrum so that it was inverted selectively.  $T_{1A} = 1.34 \text{ sec}$ ,  $T_{1B} = 1.32 \text{ sec}$ ,  $P_A = 0.46$ ,  $P_B = 0.54$ . Peak C is bis(triphenylphosphine)-tetramethylene-nickel (II).

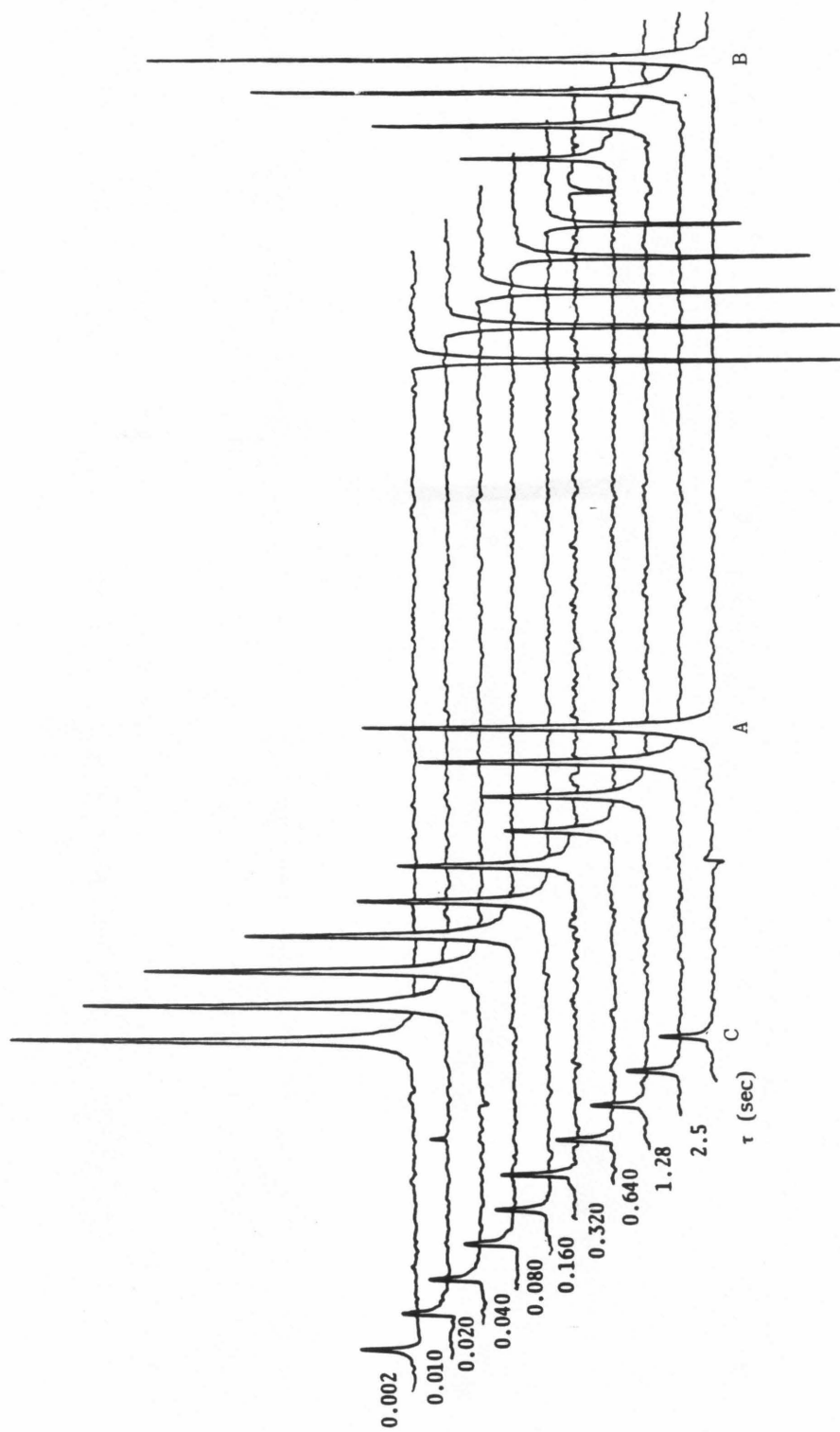




Table I

Summary of Exchange Data for Tris(triphenylphosphine)tetramethylene-nickel (II)

<u>Temp (°C)</u>	From Magnetization Transfer			From Lineshape Analysis <sup>c</sup>		
	<u>k<sub>A</sub></u>	<u>k<sub>B</sub><sup>a</sup></u>	<u>k<sup>b</sup></u>	<u>k<sub>A</sub></u>	<u>k<sub>B</sub></u>	<u>k<sup>b</sup></u>
-80	51 ± 4	44 ± 3	95 ± 7	59	51	110
-90	5.5 ± 0.5	4.7 ± 0.4	10 ± 1	3.8	3.3	7.1

---

a) obtained using eq. 11.  $P_A = 0.46$ ;  $P_B = 0.54$ ;  $A \equiv (\text{PPh}_3)\text{Ni} \begin{array}{c} \diagup \\ \diagdown \end{array}$   $B \equiv \text{PPh}_3$

b)  $k = k_A k_B (1/k_A + 1/k_B)$ .

c) analysis done with a NIC BNC-12 data system (WH-180).

plasmacytoma antibody MOPC-315. Because of the constricting nature of eq. 12, they were limited to working with solutions which had 50% bound and 50% free hapten. By using eq. 11, the rates of exchange for the haptens could be obtained for a variety of protein:hapten population ratios. Such an experiment might yield further information into the binding dynamics of haptens, especially in the realm of slow exchange where lineshape analysis is not reliable.

The method described here is very general and could be applied to any nmr-observable system undergoing chemical exchange. The only requirements are access to a pulse programmer and a computer to perform the data analysis.

REFERENCES

1. Pople, J. A., Schneider, W. G. & Bernstein, H. J.  
"High-Resolution Nuclear Magnetic Resonance,"  
McGraw Hill, N.Y., Chapter 10 and references within  
(1959).
2. Forsen, S. & Hoffman, R. A. J. Chem. Phys. 1963,  
39, 2892.
3. Dahlquist, F. W., Longmuir, K. J. & DuVernet, R. B.  
J. Magn. Reson. 1975, 17, 406.
4. Kooistra, D. A., Richards, J. H. & Smallcombe, S. H.  
Org. Magn. Reson. 1980, 13, 1.
5. Ott, Kevin, private communication (1980).
6. Farrar, T. C. & Becker, E. D. "Pulse and Fourier  
Transform NMR," Academic Press, Inc., N.Y., p. 21  
(1971).
7. Leigh, J. S., Jr. J. Magn. Reson. 1971, 4, 308.
8. Freeman, R. & Morris, G. A. J. Magn. Reson. 1978,  
29, 433.
9. Bodenhausen, G., Freeman, R. & Morris, G. A. J.  
Magn. Reson. 1976, 23, 171.
10. Brown, T. R. & Ogawa, S. Proc. Natl. Acad. Sci. USA,  
1977, 74, 3627-3631.

PART VI

500.13 MHz  $^1\text{H}$  Nuclear Magnetic Resonance  
Investigation of Substrate Binding  
to Horse Liver Alcohol Dehydrogenase.

INTRODUCTION

Alcohol dehydrogenases constitute a family of enzymes which catalyze an oxidation-reduction reaction involving an alcohol which undergoes a two electron oxidation to an aldehyde, and nicotinamide adenine dinucleotide ( $\text{NAD}^+$ ) which is concomitantly reduced by two electrons to  $\text{NADH}$ .<sup>1</sup> In this process a hydrogen atom is transferred from the alcohol to the  $\text{NAD}^+$ ;<sup>2</sup> the hydrogen acquired by  $\text{NAD}^+$  in its conversion to  $\text{NADH}$  is the same hydrogen as that removed from carbon-1 of the alcohol in its oxidation to aldehyde.



One of the most widely studied enzymes of this family is horse liver alcohol dehydrogenase (EC 1.1.1.1<sup>3</sup> (LADH)). Loewus et al<sup>2</sup> showed that the reaction is stereospecific; subsequent research has revealed the structural characteristics of the enzyme<sup>4-11</sup> and of the ways the substrates, alcohol and  $\text{NAD}^+$ , interact with the enzyme and each other during catalysis.<sup>12-18</sup>

Stereospecific studies have dealt with either crystal<sup>12,13</sup> or solution<sup>14,15</sup> complexes of LADH with substrate analogs, as well as with metal-substituted LADH<sup>16-18</sup> (the two identical subunits of LADH each contain two Zn atoms<sup>1</sup>). These studies have yielded conflicting results concerning the nature of the binding of alcohol to the protein and thus its probable orientation relative to  $\text{NAD}^+$  within the

active site. The crystal structure of the native protein<sup>12,13</sup> and the nuclear magnetic resonance (nmr) work of Boccalon et al.<sup>17</sup> with the Co(II) substituted enzyme indicate that the alcohol is bound directly to the active site Zn through the hydroxyl oxygen of the substrate. However, Sloan et al.<sup>16</sup> and Drysdale et al.,<sup>18</sup> also working with the Co(II) enzyme, have concluded that the substrate is bound to the Zn through a bridging water molecule. In either case the chiral nature of the interaction of substrate with  $\text{NAD}^+$  has not been observed directly. The present investigation is an attempt to examine this problem.

Proton nmr spectra have been obtained at 500.13 MHz of the interactions of the R,S mixture of  $\text{CD}_3\text{CHDOD}$  with LADH in the presence and absence of excess NADH at various enzyme/substrate concentrations. The results yield information not only about the binding constant for the ethanol-(NADH-LADH) complex, but also about the local environmental differences for the R and S protons when the alcohol is bound to the protein.

EXPERIMENTAL

Chemicals: NADH and ethanol free LADH from Sigma were used without further purification. All samples were prepared in 0.1 M phosphate buffer in D<sub>2</sub>O (pD = 7.0) containing 1.0 mM sodium 2,2-dimethyl-2-silapentane-5-sulfonate (DSS) as both a chemical shift and concentration reference. Ethanol was added to the 5 mm nmr sample tubes using a 10  $\mu$ l Hamilton syringe.

CD<sub>3</sub>CHDO Synthesis: Dry diglyme (50 ml, dried over CaH<sub>2</sub> and distilled) was cooled to -5°C in an ice/methanol bath and 2.20g of NaBH<sub>4</sub> were then added. The system was purged with N<sub>2</sub> gas, and kept dry by means of a drying tube containing Drierite. Five g of CD<sub>3</sub>CDO (Merck, 99 atom% D) in 10 ml of cold diglyme were added dropwise to the NaBH<sub>4</sub>-diglyme suspension while maintaining the temperature at less than 10°C. When the addition was complete, the solution was allowed to warm to room temperature overnight. Ten ml of D<sub>2</sub>O were then added slowly, after which the mixture was stirred for half an hour at which time another 10 ml of D<sub>2</sub>O were added. The mixture was then stirred for two hours, during which time a white gelatinous precipitate formed. The solution was filtered, and the filtrate was distilled below 90°C. The distillate was extracted several times with CDCl<sub>3</sub> to remove diglyme. <sup>1</sup>H nmr analysis in D<sub>2</sub>O: broad ( $\nu_{\frac{1}{2}}$  = 7 Hz) multiplet at  $\delta = 3.610 \pm 0.001$  ppm downfield from DSS. The concentration of the resulting ethanol/D<sub>2</sub>O solution

was 2.24 M as determined by integration of an nmr sample containing a known amount of DSS.

NMR Measurements: Proton nmr spectra were acquired with the Southern California Regional NMR Facility's Bruker WM-500 nmr spectrometer operating at a proton frequency of 500.13 MHz. For most of the spectra no line broadening was used as the signal to noise ratio was excellent. Gaussian-Lorentzian resolution enhancement was used when needed.

Calculations: In order to obtain both the binding constant  $K_I$  and the chemical shift,  $\delta_{\text{bound}}$ , for  $\text{CD}_3\text{CHDOD}$  bound to LADH, the method of Gammon et al.<sup>19</sup> was used with some modification. For LADH, there are two identical, non-cooperative subunits that make up the protein. Consequently, the concentration of binding sites is twice that of the actual enzyme concentration. The system can be described by eq. 2:



where

$$K_I = \frac{[\text{E}][\text{I}]}{[\text{EI}]}$$

and  $[\text{E}] = 2 \times [\text{LADH}]$

Since the ethanol is in fast exchange with the active site,<sup>4,20</sup> the observed chemical shift is given by<sup>19</sup>



$$\delta_{\text{obs}} = \delta_{\text{free}} + \frac{(\delta_{\text{bound}} - \delta_{\text{free}})}{[\text{I}]_t}$$

$$\times \left\{ \frac{[\text{E}]_t + [\text{I}]_t + K_I - \sqrt{([\text{E}]_t + [\text{I}]_t + K_I)^2 - 4[\text{E}]_t[\text{I}]_t}}{2} \right\} \quad (4)$$

where

$$[\text{I}]_t = [\text{I}] + [\text{EI}] \quad (5)$$

$$[\text{E}]_t = [\text{E}] + [\text{EI}] \quad (6)$$

Rather than use the iterative procedure of Gammon et al.<sup>19</sup> to obtain  $K_I$  and  $(\delta_{\text{bound}} - \delta_{\text{free}})$ , we decided to fit the enzyme/substrate concentration data to eq. 4 using non-linear least squares methods. The program used for this is listed in the Appendix. The parameters which were fit were  $\delta_{\text{free}}$ ,  $\delta_{\text{bound}}$ , and  $K_I$ . This procedure was found to be significantly faster than the method of Gammon et al.

THEORY

The observed chemical shift is given by eq. 7, as the exchange of ethanol with LADH is very fast on the nmr time-scale:<sup>4,20,21</sup>

$$\delta_{\text{obs}} = p_{\text{free}} \delta_{\text{free}} + p_{\text{bound}} \delta_{\text{bound}} \quad (7)$$

where  $p_{\text{free}}$  and  $p_{\text{bound}}$  are the mole fractions of the ethanol free and bound. If one assumes that the R and S protons of  $\text{CD}_3\text{CHDOD}$  have different chemical shifts when bound to the protein, eq. 7 becomes

$$\delta_{\text{R}} = p_{\text{free}} \delta_{\text{free}} + p_{\text{bound}} \delta_{\text{bound}_{\text{R}}} \quad (8a)$$

$$\delta_{\text{S}} = p_{\text{free}} \delta_{\text{free}} + p_{\text{bound}} \delta_{\text{bound}_{\text{S}}} \quad (8b)$$

Thus, the observed chemical shifts for the R and S protons at C-1 can differ if  $\delta_{\text{bound}_{\text{R}}}$  and  $\delta_{\text{bound}_{\text{S}}}$  are different and if  $p_{\text{bound}}$  is sufficiently large.

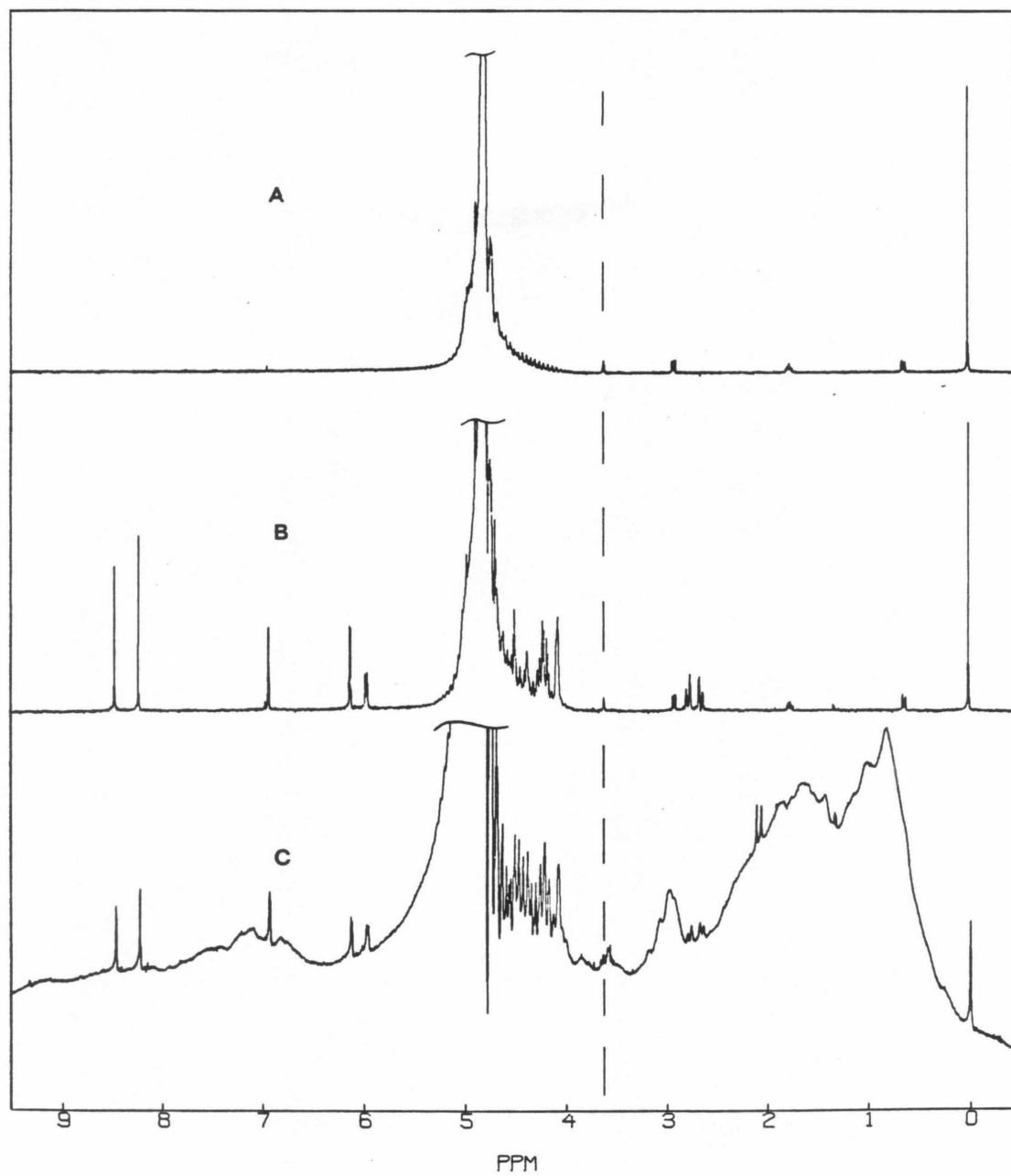
## RESULTS AND DISCUSSION

Figure 1a is the 500.13 MHz proton nmr spectrum of  $\text{CD}_3\text{CHDOD}$  in  $\text{D}_2\text{O}$ . The singlet at  $\delta = 3.610$  ppm downfield from DSS is a septet of triplets, the splittings being a result of two and three bond H-D couplings within the molecule. In the presence of two-fold excess NADH the chemical shift of the ethanol C-1 proton did not change (Figure 1b). However, addition of LADH to this sample resulted in an upfield shift and splitting of the alcohol resonance into two peaks of equal area at 3.572 and 3.588 ppm (Figure 1c). No change in chemical shift was observed in a NADH-free solution ( $\delta_{\text{CD}_3\text{CHDOD}} = 3.611$  ppm). Both of these observations can be compared with previous results obtained by Hollis while monitoring the  $\text{CH}_3$  triplet of  $\text{CH}_3\text{CH}_2\text{OH}$ .<sup>4</sup> In a solution of LADH- $\text{CH}_3\text{CH}_2\text{OH}$  he observed no change in chemical shift or linewidth, while in a yeast ADH (YADH)- $\text{NAD}^+$ - $\text{CH}_3\text{CH}_2\text{OH}$  solution he observed a slight change in linewidth for the methyl group. He did not report the chemical shift of a LADH-NADH- $\text{CH}_3\text{CH}_2\text{OH}$  solution.

The two resonances in the LADH-NADH solution could represent the R and S protons of the  $\text{CD}_3\text{CHDOD}$  experiencing different chemical shift environments when bound to the protein, but addition of more  $\text{CD}_3\text{CHDOD}$  to the sample led to both peaks moving downfield in such a way that the sepa-

Figure 1

500.13 MHz proton nmr spectra. A) 2 mM  $\text{CD}_3\text{CHDOD}$  and 1.0 mM DSS in 0.1 M phosphate in  $\text{D}_2\text{O}$  (pD = 7.0). B) Sample (A) plus two-fold excess NADH. c) Sample (B) plus LADH. [LADH] = 0.9 mM.



ration between them remained constant which was not consistent with eq. 8. Spin-lattice ( $T_1$ ) relaxation measurements showed that the  $T_1$  for the downfield peak was shorter than that for the upfield peak; this is consistent with the downfield resonance representing the species  $CD_3CH_2OD$  which was presumably produced catalytically by the LADH and trace quantities of oxidized NADH ( $NAD^+$ ). In order to confirm this interpretation, Gaussian-Lorentzian resolution enhancement was applied to the spectrum. The result of this, Figure 2, clearly shows that the downfield peak exhibits the correct splitting pattern for the C-1 protons of  $CD_3CH_2OD$ .

Table I summarizes the results of the ethanol-LADH and ethanol-LADH-NADH proton spectra. Also given are the binding constants,  $K_I$ , and the bound chemical shifts obtained for the substrates using eq. 4. The values for  $K_I$  calculated from the nmr data are in excellent agreement with  $K_I$  obtained from kinetics measurements.<sup>9</sup>

The chemical shifts of the R and S protons of  $CD_3CHDOD$  could not be resolved in the presence of LADH and NADH. These observations set an upper limit on the maximum possible chemical shift difference for the two protons when the substrate is bound to the protein. From the data analysis using eq. 4, a value of  $2.79 \pm 0.08$  ppm was obtained for the bound chemical shift of the R and S methylene protons of

Figure 2

500.13 MHz proton nmr spectrum of  $\text{CD}_3\text{CHDOD}$  with  $\text{CD}_3\text{CH}_2\text{OD}$  produced catalytically by LADH.  $^2J_{\text{HD}} = 1.6 \text{ Hz}$ ,  $^3J_{\text{HD}} = 1.0 \text{ Hz}$ . Gaussian-Lorentzian resolution enhancement was used to resolve the multiplets.

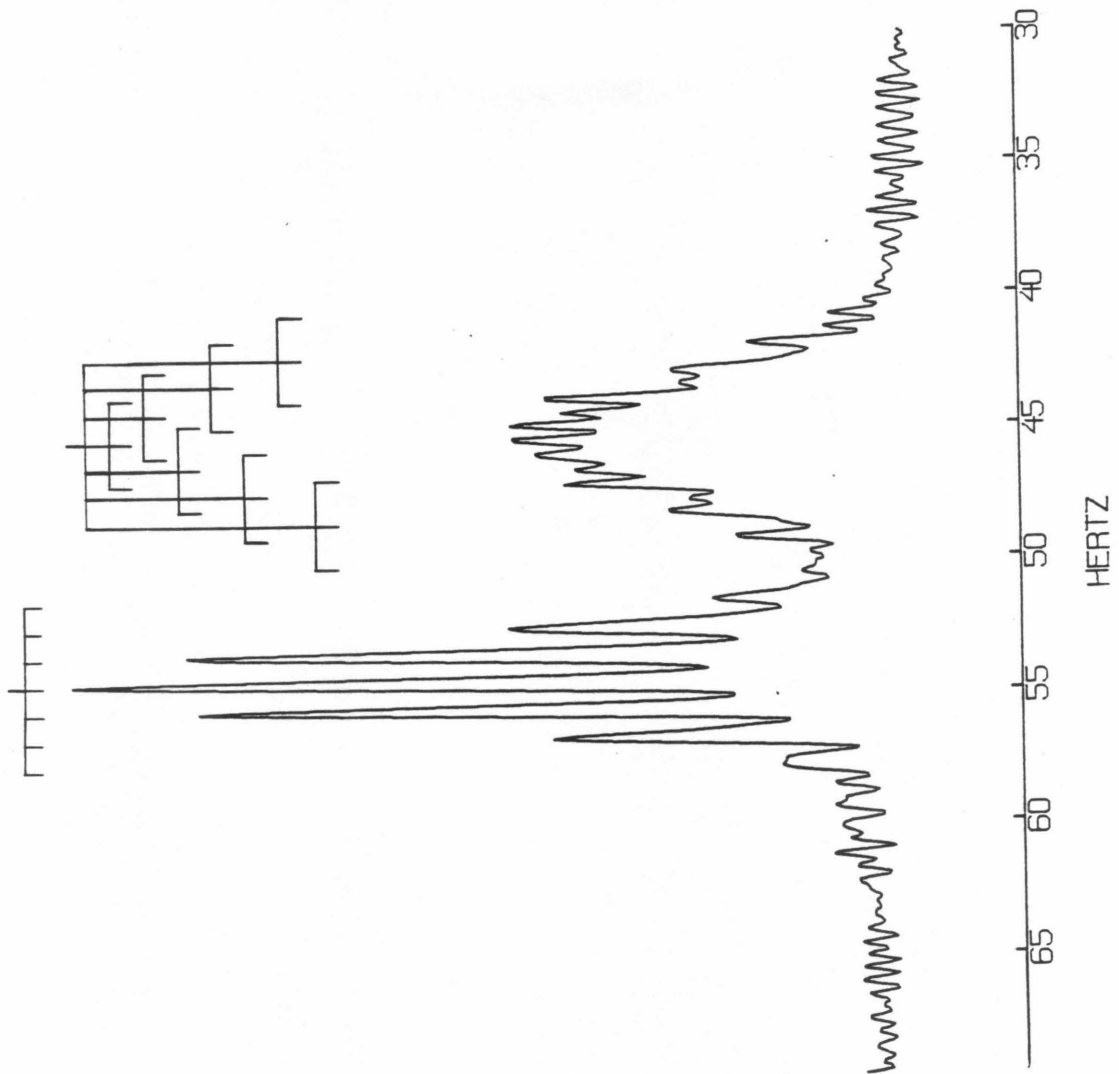




Table I

Summary of ethanol-LADH-NADH NMR Parameters<sup>a</sup>

<u>Species</u>	<u><math>\delta_{\text{free}}</math> (ppm)<sup>b</sup></u>	<u><math>\delta_{\text{bound}}</math> (ppm)<sup>b</sup></u>	<u><math>K_I</math> (mM)<sup>b</sup> (40<sup>e</sup>)</u>	<u><math>\delta_{\text{LADH}}</math><sup>c</sup></u>	<u><math>K_I</math> (mM)<sup>d</sup></u>
CD <sub>3</sub> CHDOD	3.612 $\pm$ 0.001	2.79 $\pm$ 0.08	34 $\pm$ 4	3.611	4.6
CD <sub>3</sub> CH <sub>2</sub> OD	3.629 $\pm$ 0.001	2.80 $\pm$ 0.05	33 $\pm$ 2	--	-

- 
- a) All chemical shifts relative to internal 1.0 mM DSS in 0.1 M phosphate, pD = 7.0; observed shifts are  $\pm$  0.001 ppm.  
b) Obtained using non-linear least squares analysis of eq. 4.  
c) Chemical shift of 1.5 mM CD<sub>3</sub>CHDOD and 0.4 mM LADH (0.8 mM in binding sites).  
d)  $K_I$  for LADH-CH<sub>3</sub>CH<sub>2</sub>OH complex (from ref. 9).  
e)  $K_I$  for LADH-NADH-CH<sub>3</sub>CH<sub>2</sub>OH complex (from ref. 9).

$\text{CD}_3\text{CHDOD}$  and  $2.80 \pm 0.05$  ppm for  $\text{CD}_3\text{CH}_2\text{OD}$ . If one uses the errors associated with these values as a measure of the difference in chemical shift between the R and S protons when the ethanol is bound, the bound chemical shifts could differ by 0.16 ppm in the case of  $\text{CD}_3\text{CHDOD}$  and 0.10 ppm for  $\text{CD}_3\text{CH}_2\text{OD}$ .

The difference in bound chemical shifts for the R and S protons can be estimated in another way. The value for  $K_I$  obtained from the non-linear analysis of eq. 4 and the minimum nmr-observable concentration of  $\text{CD}_3\text{CHDOD}$  relative to the LADH concentration can be used together with eq. 8 to obtain a value for  $|\delta_{\text{bound}_R} - \delta_{\text{bound}_S}|$ . For  $[\text{ethanol}] = 2 \text{ mM}$  and  $[\text{LADH}] = 0.9 \text{ mM}$ , eq. 4 yields

$$\begin{aligned}\delta_R &= 0.95 \times \delta_{\text{free}} + 0.05 \times \delta_{\text{bound}_R} \\ \delta_S &= 0.95 \times \delta_{\text{free}} + 0.05 \times \delta_{\text{bound}_S}\end{aligned}$$

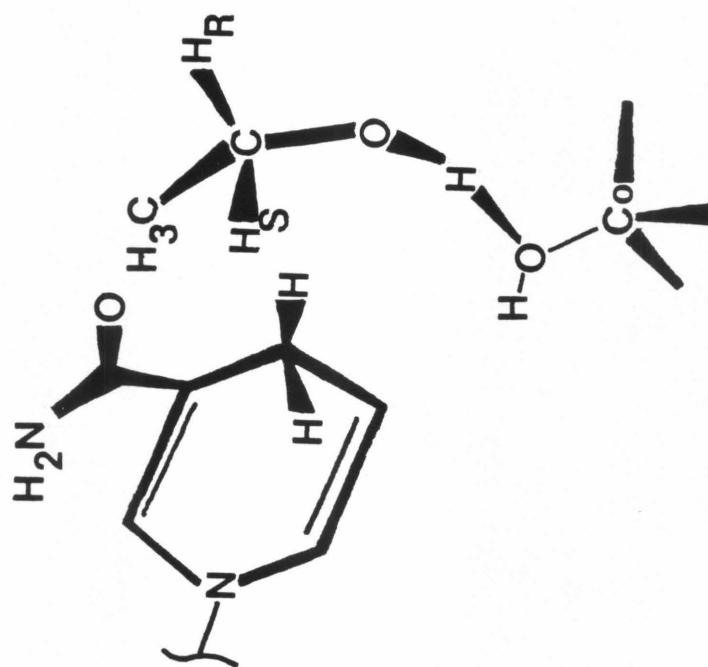
The smallest observable chemical shift difference which could be observed for the C-1 proton resonance at 500.13 MHz should be greater than 1 Hz (0.002 ppm). Setting  $|\delta_R - \delta_S| = 0.002$  ppm and solving for  $|\delta_{\text{bound}_R} - \delta_{\text{bound}_S}|$ ,

$$|\delta_{\text{bound}_R} - \delta_{\text{bound}_S}| \leq 0.04 \text{ ppm.}$$

This chemical shift difference is in agreement with the error limit analysis described above; both analyses are consistent with the proposed orientation for ethanol within the LADH binding site.<sup>16,22</sup> The ethanol binding in the presence of NADH is depicted in Figure 3.

## Figure 3

Proposed orientation of ethanol when bound to LADH in the presence of NADH. The structure is for the Co(II) enzyme.<sup>16</sup> The R and S labels are given for the appropriate stereo isomer of  $\text{CD}_3\text{CHDOD}$ .



Future experiments which might allow for the spectral resolution of the chemical shift difference of the R and S protons should be directed towards using NADH analogs to lower the binding constant of the ethanol. This would increase the amount of ethanol bound to LADH and thus enable detection of separate resonances for the R and S C-1 protons if this difference is on the order of 0.005 ppm and the lines have not become excessively broad.

REFERENCES

1. Brändén, C.-I., Jörnvall, H., Eklund, H. & Furugren, B. in "The Enzymes" 3rd ed., Vol. II, Chapter 3, Academic Press, New York (1975).
2. Loewus, F. A., Westheimer, F. H. & Vennesland, B. J. Am. Chem. Soc. 1953, 75, 5018-5023.
3. Worthington Enzyme Manual, p. 1 (1972).
4. Hollis, D. P. Biochemistry 1967, 6, 2080-2087.
5. Drakenberg, T. J. Magn. Reson. 1974, 15, 354-358.
6. Czeisler, J. L. & Hollis, D. P. Biochemistry 1973, 12, 1683-1689.
7. Bobsein, B. R. & Myers, R. J. J. Am. Chem. Soc. 1980, 102, 2454-2455.
8. Hayes, J. E., Jr. & Velick, S. F. J. Biol. Chem. 1954, 207, 225-244.
9. Theorell, H. & McKinley-McKee, J. S. Acta Chem. Scand. 1961, 15, 1811-1833.
10. McKinley-McKee, J. S. Acta Chem. Scand. 1963, 17, 5339.
11. Eklund, H., Nordström, B., Zeppezauer, E., Söderlund, G., Ohlson, I., Boiwe, T., Söderberg, B.-Ö., Tapia, O., Brändén, C.-I. & Åkeson, Å. J. Mol. Biol. 1976, 102, 27-59.
12. Plapp, B. V., Eklund, H. & Brändén, C.-I. J. Mol. Biol. 1978, 122, 23-32.

13. Eklund, H. & Brändén, C.-I. J. Biol. Chem. 1979, 254, 3458-3461.
14. Sloan, D. L. & Mildvan, A. S. Biochemistry 1974, 13, 1711-1718.
15. Dunn, M. F. & Hutchison, J. S. Biochemistry 1973, 12, 4882-4892.
16. Sloan, D. L., Young, J. M. & Mildvan, A. S. Biochemistry 1975, 14, 1998-2008.
17. Boccalon, G., Grillo, G., Baroncelli, V., Renzi, P. & Parretta, A. J. Mol. Catal. 1978, 4, 307-312.
18. Drysdale, B.-E. & Hollis, D. P. Arch. Biochem. Biophys. 1980, 205, 267-279.
19. Gammon, K. L., Smallcombe, S. H. & Richards, J. H. J. Am. Chem. Soc., 1972, 94, 4573-4580.
20. Gilleland, M. J. & Shore, J. D., Biochem. Biophys. Res. Commun. 1970, 40, 230.
21. Becker, E. D. "High Resolution NMR" Chapter 10, Academic Press, New York (1969).
22. Mildvan, A. S. & Weiner, H. J. Biol. Chem. 1969, 244, 2465.

PART VII

Elucidation of the Structure of Crosslinked

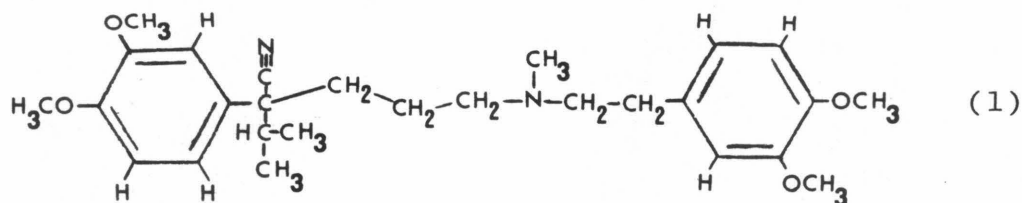
Verapamil using 500.13 MHz  $^1\text{H}$

Nuclear Magnetic Resonance Spectroscopy.



## INTRODUCTION

The chemical verapamil (1) has been shown to be a member of a class of drugs known as calcium channel



blockers.<sup>1,2</sup> As such, it inhibits transmembrane  $\text{Ca}^{2+}$  influx in smooth and cardiac muscle causing immediate positive effects on cardiac arrhythmias,<sup>3</sup> as well as being extremely effective in the treatment of acute and chronic hypertension.<sup>4</sup> Recently, Herndier,<sup>5</sup> in studies with isolated rat peritoneal mast cells, observed that verapamil at low doses (20  $\mu\text{g}/\text{ml}$ ) behaved as a calcium ion antagonist while at doses approximately ten times greater mediated the release of vasoactive amines, histamine, and serotonin, consistent with calcium ion mobilizing activity. This latter discovery suggests that the regulation of  $\text{Ca}^{2+}$  metabolism by verapamil is more complex than originally proposed. In his study he found that formaldehyde crosslinked verapamil (a putative dimer as determined by molecular weight sizing) was 30-fold more effective in releasing serotonin than the monomer. In order to elucidate the possible interactions of vera-

pamil and polymerized verapamil with mast cells and determine the structural parameters of calcium ion antagonism and mobilization, structural and conformational studies of the monomer and putative dimer were performed.

The proton nuclear magnetic resonance (nmr) spectra for both verapamil and crosslinked verapamil have been obtained at 500.13 MHz. These spectra have been used to define a structure for the predominant crosslinked species. In addition, these data, as well as high temperature, 200 MHz nmr spectra, reveal that the monomeric verapamil exists in a preferred, rigid conformation.

## EXPERIMENTAL

Chemicals: Verapamil was a gift from the Knoll Pharmaceutical Company, Whippany, New Jersey. The cross-linked verapamil was prepared by Herndier.<sup>5</sup> The nmr samples were prepared by adding either verapamil or crosslinked verapamil to 0.6 ml of either D<sub>2</sub>O or d<sub>6</sub>-DMSO in a 5 mm nmr tube. 2,2-Dimethyl-2-silapentane-5-sulfonate (DSS) was added to the monomer sample as a chemical shift reference.

NMR Measurements: Proton nmr spectra were acquired with the Southern California Regional NMR Facility's Bruker WM-500 nmr spectrometer which has a proton resonant frequency of 500.13 MHz. High temperature spectra were obtained on a Varian XL-200. No line broadening or resolution enhancement of the free induction decay (FID) was done unless otherwise indicated. Inversion recovery<sup>7</sup> was used to obtain the relative spin-lattice ( $T_1$ ) relaxation times for the crosslinked verapamil.

## RESULTS AND DISCUSSION

### Verapamil

The 500.13 MHz proton nmr spectrum and peak assignments for verapamil in D<sub>2</sub>O are shown in Figure 1. Table I summarizes the results from homonuclear decoupling experiments, as well as the integrals for each resonance. The magnetic nonequivalence observed for the two protons on each of the three methylene groups b, c, and g must be due to conformational rather than configurational differences, as decoupling one of the protons has an effect on the other (i.e., decoupling b affects b'). This would not be the case if the sets of peaks represented two different configurational isomers in solution.

Spectral observation at 200 MHz and 90°C revealed that the b, c, and g protons do not coalesce. This result indicates that the aliphatic chain which these protons are associated with is extremely rigid, whereas, as revealed at lower temperature and higher field, the 3,4-dimethoxybenzyl group attached to the nitrogen seems to be mobile. Such a result is not surprising, as the isopropyl, 3,4-dimethoxyphenyl, and cyano groups create a tremendous steric barrier to rotation for not only the aliphatic chain but also for the isopropyl methyl groups. In all cases, the magnetic nonequivalence observed is primarily a result of the ring current associated with the 3,4-dimethoxyphenyl group.

Figure 1

500.13 MHz proton magnetic resonance spectrum  
and peak assignments of verapamil in D<sub>2</sub>O.

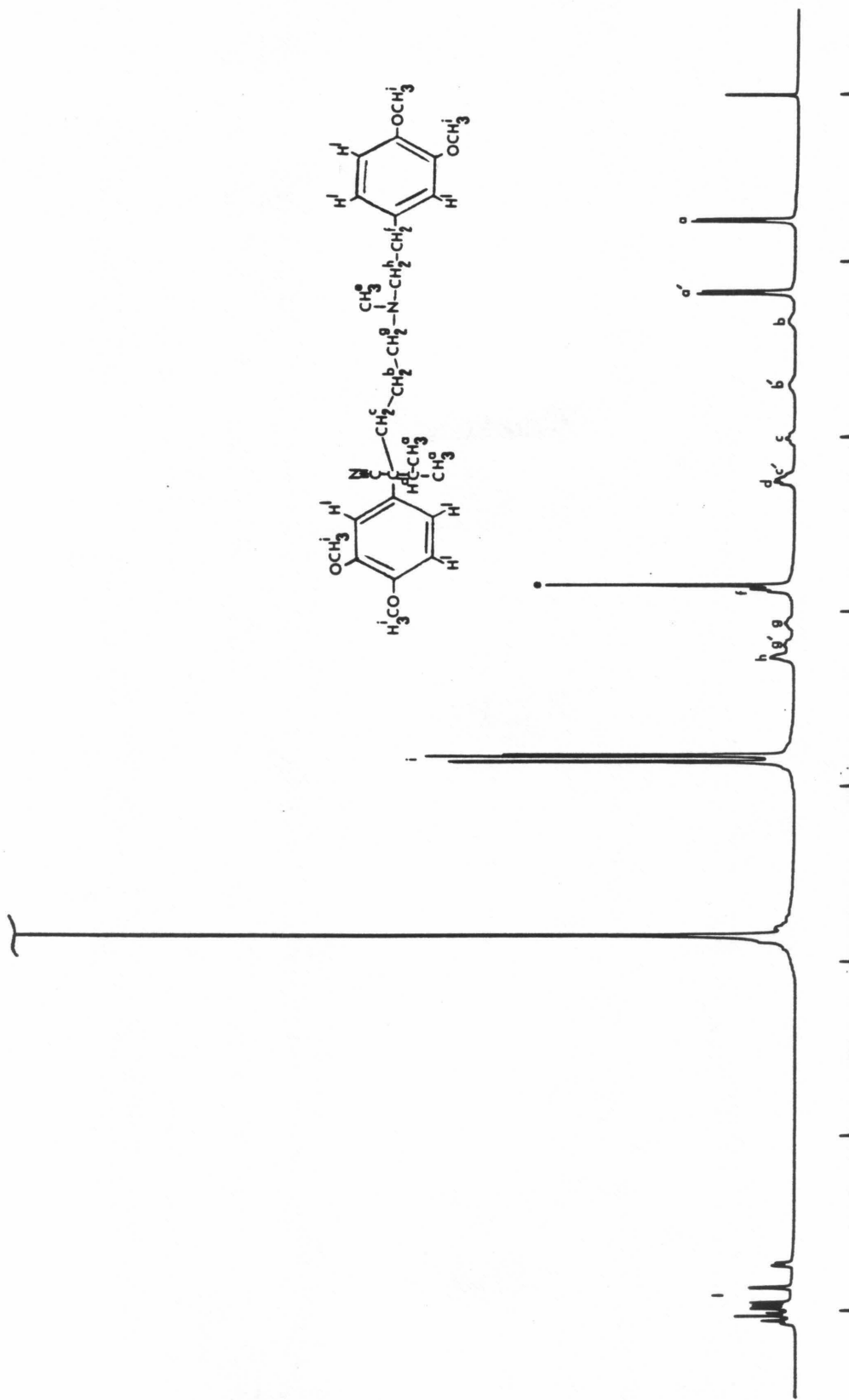


Table I

## NMR Data for Verapamil

<u>Resonance</u>	<u>Decoupling<sup>a</sup></u>	<u>Integration<sup>b</sup></u>	<u>Reference for Assignment</u>
a	d	3	8
a'	d	3	8
b	b', c, c', g, g'	1	-
b'	b, c, c', g, g'	1	-
c	b, b', c'	1	8
c'	b, b', c	1	8
d	a, a'	1	8
e	-	3	9
f	h	2	10, 11
g	b, b', g'	1	9
g'	b, b', g	1	9
h	f	2	11
i	-	12	12
l	-	6	-

167

a) the resonances listed are those that are affected by decoupling the resonance in the first column. b) normalized.

### Crosslinked Verapamil

Figure 2 shows the 500.13 MHz proton nmr spectrum of crosslinked verapamil in  $D_2O$ . Also given is the proposed structure which is consistent with homonuclear decoupling,  $T_1$ , and integration measurements. The decoupling and integration data are summarized in Table II.

Finding the methylene bridge resonance was considered to be the most important peak assignment, as it would reveal not only whether or not more than one species of dimer existed, but also the presence of any dimer species in solution (molecular sizing data<sup>5</sup> was used to infer the existence of a dimer species). However, the resonance was believed to be under the  $-OCH_3$  envelope. In order to find this methylene, a  $T_1$  measurement was carried out at 500.13 MHz. The inversion recovery spectrum for  $\tau = 0.5$  sec is shown in Figure 3. The positive resonance is due to the methylene bridge protons, while the negative peaks are due to the o-methoxy groups. This clearly shows that the bridging methylene protons have a shorter  $T_1$  than the methoxy protons which is consistent with the presence of an immobilized  $-CH_2-$  and freely rotating  $-CH_3$  groups.<sup>14</sup> The fact that the methylene peak is a singlet and, from the fully relaxed spectrum has an integration value corresponding to two protons, indicates that the major polymerized species is a dimer, thus supporting the previous molecular sizing data.<sup>5</sup>



## Figure 2

500.13 MHz proton magnetic resonance spectrum  
and peak assignments of crosslinked verapamil  
in D<sub>2</sub>O.

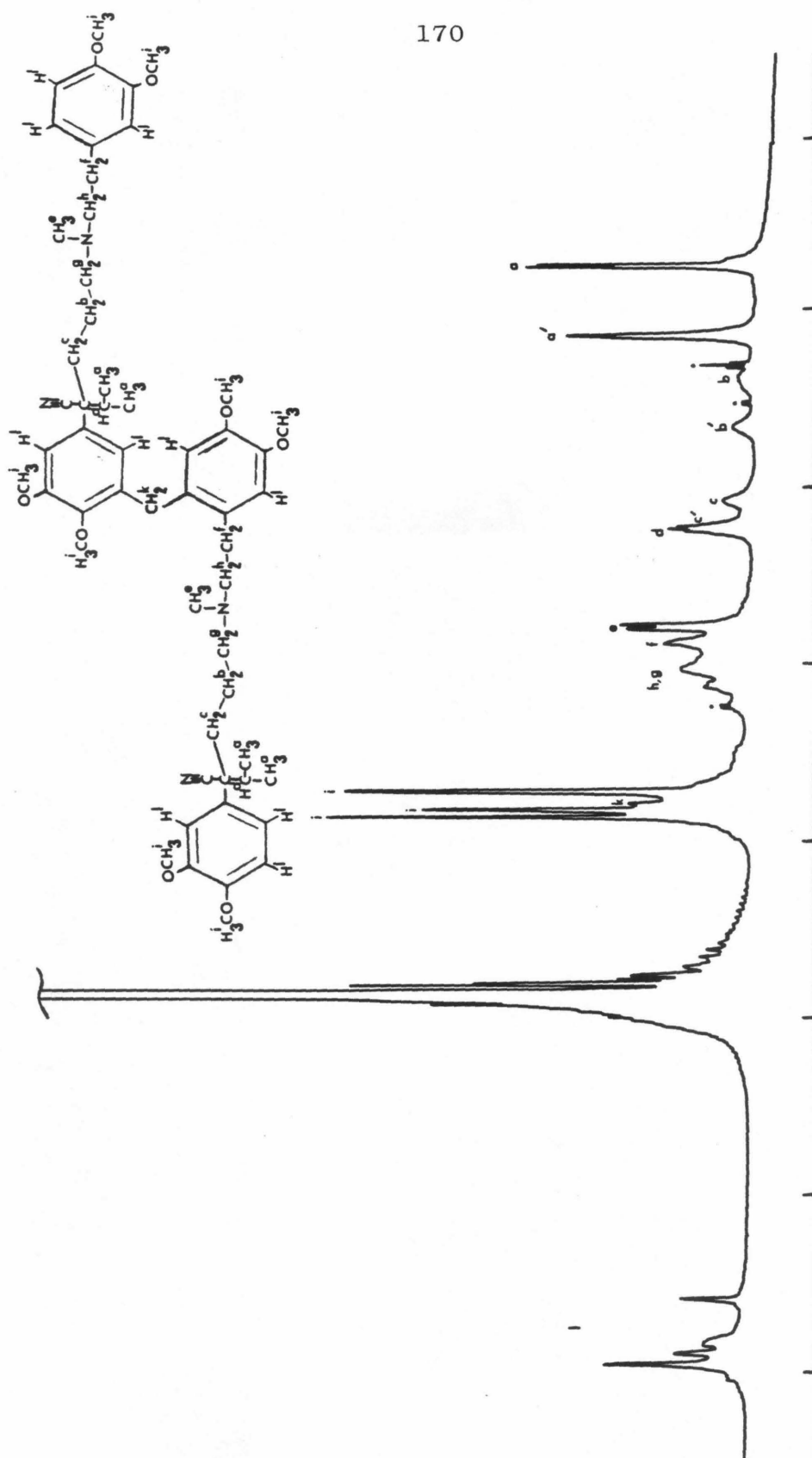


Table II

## NMR Data for Crosslinked Verapamil

<u>Resonance</u>	<u>Decoupling</u> <sup>a</sup>	<u>Integration</u>	<u>Reference for Assignment</u>
a	d	6	8
a'	d	6	8
b	b',c,c',g	2	-
b'	b,c,c',g	2	-
c	b,b',c'	2	8
c'	b,b',c	2	8
d	a,a'	2	8
e,e'	-	6	9
f	g,h	4	10,11
g,h	b,b',f	8	9,11
i	-	24	12
k	-	2	13
l	-	10	-

171

a) the resonances listed are those that are affected by decoupling the resonance in the first column.

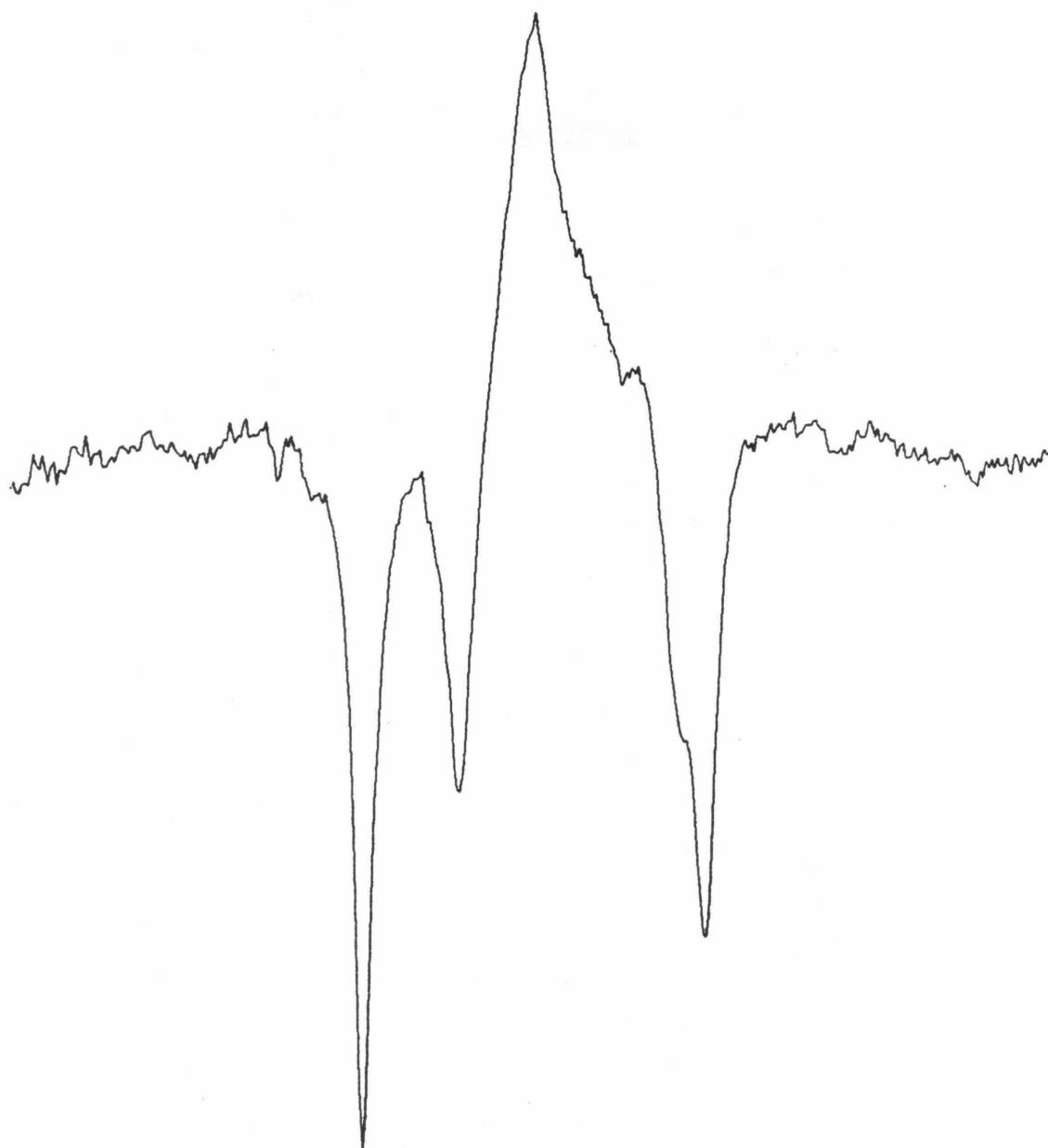
## Figure 3

Expansion of the inversion recovery proton  
nmr spectrum of crosslinked verapamil.

The positive peak is the methylene bridge  
resonance while the negative peaks are the  
methoxy resonances.

173

TAU=0.5 SEC



4.05 4.00 3.95 3.90 3.85 3.80 3.75 3.70 3.65

PPM

The asymmetric nature of the dimer is inferred from the loss of symmetry for the downfield isopropyl methyl groups. Figure 4 shows the coupled and decoupled spectra for these resonances. If the dimer were symmetric, then the downfield methyl resonance would be a clean doublet; in fact it is two overlapping doublets which yield an apparent triplet. Irradiation of the CH isopropyl resonance leaves one peak for the upfield methyls and two for the downfield methyls (Figure 4B) thus confirming the assignment of the downfield resonances. These observations, in conjunction with the detection of two N-CH<sub>3</sub> resonances (e) and a loss of symmetry for resonances b, support the existence of an asymmetric structure for the crosslinked verapamil.

The relative order of reactivity of o-dimethoxybenzene to electrophilic substitution (para > ortho) and steric effects due to the bulky isopropyl and cyano groups (ortho > para)<sup>15</sup> were considered in the determination of the position of the methylene bridge.

In order to detect the amount of terminal benzyl alcohol groups (a result of incomplete reaction with formaldehyde) the nmr spectrum of the crosslinked verapamil was obtained in d<sub>6</sub>-DMSO. As shown in Figure 5, two resonances are visible at  $\delta \sim 4.4$  and  $\delta \sim 4.7$  ppm. These correspond to the methylene benzyl protons for the para<sup>12</sup>

Figure 4

Expansion of the isopropyl methyl region of the proton nmr spectrum of crosslinked verapamil: (a) coupled; (b) decoupled from the isopropyl C-H proton.

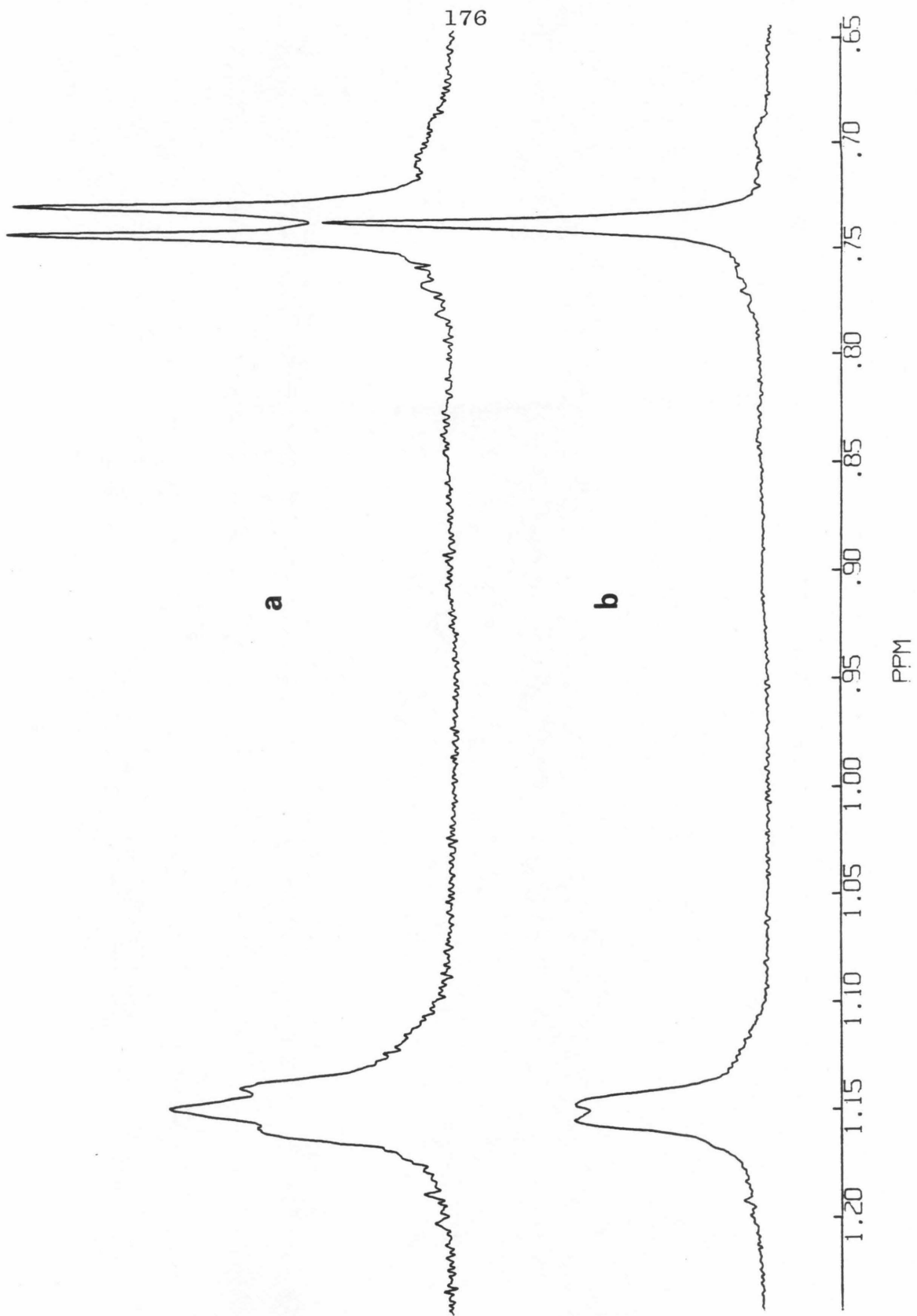
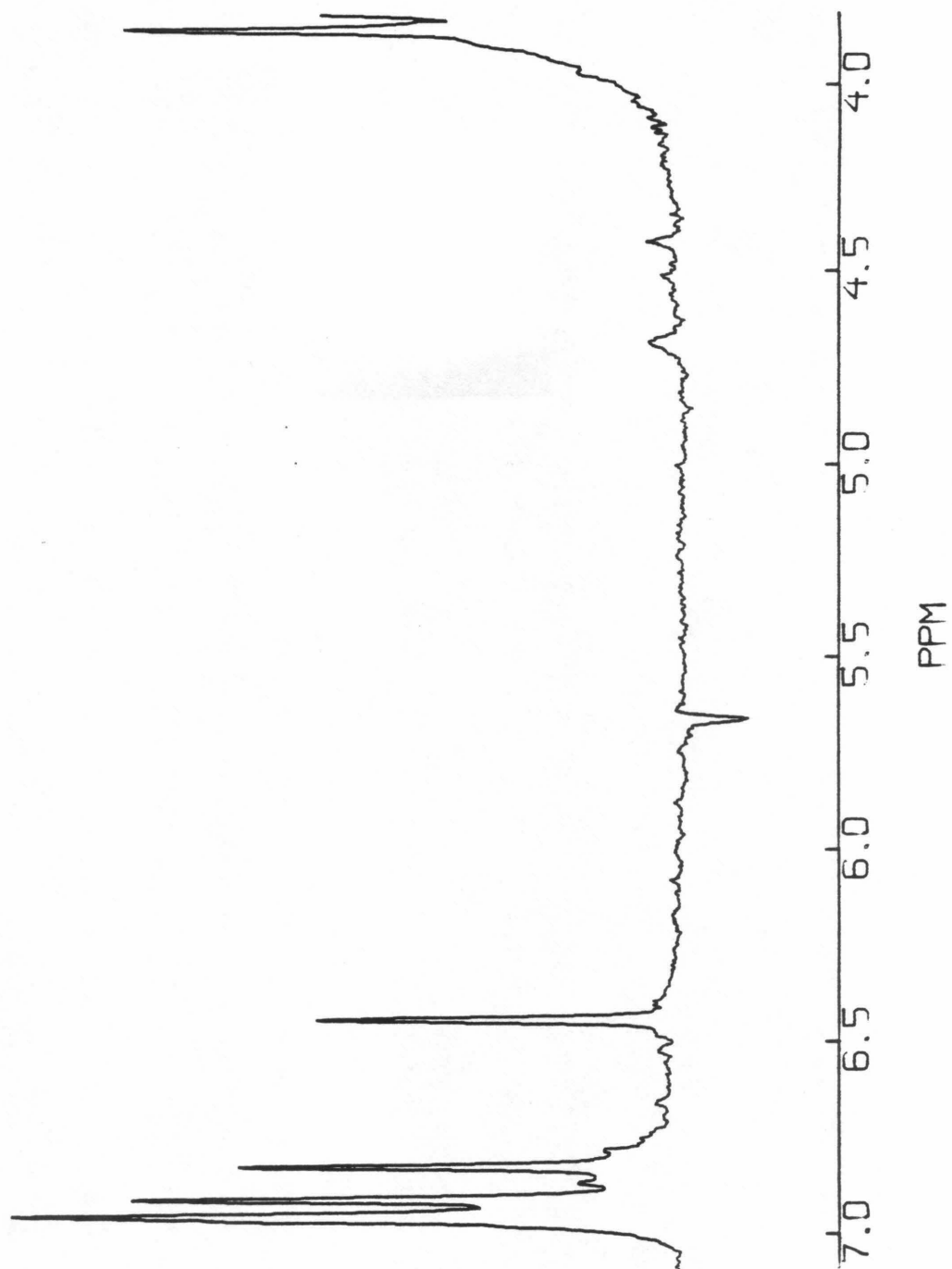




Figure 5

Expansion of the downfield region of the proton nmr spectrum of crosslinked verapamil in  $d_6$ -DMSO. The methylene bridge resonance is at the right end of the spectrum. The inverted peak at  $\delta \sim 5.7$  is an image of the solvent resonance.

178



and ortho<sup>16</sup> resonances, respectively. Their total concentration in the sample is estimated to be less than 10% as determined from the integrals of the two peaks. Thus, the predominant species has the structure shown in Figure 2.

The spectrum of the crosslinked species was obtained at 90°C on an XL-200. As with verapamil, the resonances of the crosslinked species also showed little change with temperature, indicating a similar, rigid conformation for the molecule.

In conclusion, it has been shown that the predominant crosslinked verapamil species is an asymmetric dimer and, like verapamil, exists in a rigid conformation. To further characterize the actions of these drugs on living systems, a future effort should include the study of the conformation of these drugs as they interact with cellular systems.

REFERENCES

- 1) Clark, M. & Shapiro, D. Newsweek 1981, 97:13, 86.
- 2) Fleckenstein, A. Ann. Rev. Pharmacol. Toxicol. 1977, 17, 149.
- 3) Shamroth, L., Krikler, D. M. & Garrett, G. Brit. Med. J. 1972, 1, 660.
- 4) Zsoter, T. T. Amer. Heart J. 1980, 99, 806.
- 5) Herndier, B. Ph.D. Thesis, California Institute of Technology (1981).
- 6) Morrison, R. T. & Boyd, R. N. "Organic Chemistry," Allyn and Bacon, Boston, p. 1042 (1973).
- 7) Farrar, T. C. & Becker, E. D. "Pulse and Fourier Transform NMR," Academic Press, Inc. NY p. 20 (1971).
- 8) Pouchert, C. J. & Campbell, J. R. "The Aldrich Library of NMR Spectra," Aldrich Chemical Co., Milwaukee Vol. IV, p. 5 (1974).
- 9) ibid, Vol. II, p. 13.
- 10) ibid, Vol. IV, p. 1.
- 11) ibid, Vol. V, p. 118.
- 12) ibid, Vol. V, p. 16.
- 13) ibid, Vol. IV, p. 7.
- 14) Becker, E. D. "High Resolution NMR," Academic Press, NY p. 202 (1969).
- 15) Herndier, B., private communication (1981).
- 16) Pouchert, C. J. & Campbell, J. R. "The Aldrich Library of NMR Spectra," Aldrich Chemical Co., Milwaukee, Vol. V, p. 14. (1974).

APPENDIX

Listings of Computer Programs.

The following programs are written in  
Microsoft BASIC for a Commodore PET microcomputer.

```

10 REM NON-LINEAR LEAST SQUARES PROGRAM FOR FITTING RELAXATION DATA
15 PRINT "J":POKE59468,12:C$=" "
20 V1=4.01040576:V2=0.45239076:V3=11.20776484
25 DEFFNF(Q)=1/(CSA+DD)
30 DEFFNE(Q)=S*SQR(ABS(Q))
35 E1=0.02:E2=E1+1:E3=1
40 INPUT "DO YOU HAVE POINTS TO ADD TO STORED DATA";A$
45 IFA$<>"YES"THEN55
50 INPUT "HOW MANY POINTS ARE TO BE ADDED";AP:GOTO60
55 INPUT "DO YOU HAVE STORED DATA";A$:IFA$<>"YES"GOTO85
60 OPEN1:INPUT#1,N0:INPUT#1,M0:INPUT#1,N
65 DIMA(N0),B(N0,N0),O(N0,N0),X(M0,N+AP),Y(N+AP),S(N+AP),C(N0),TB(15),DIMD(N0)
70 FORI=1TON:FORK=1TOM0
75 INPUT#1,X(K,I):NEXTK:INPUT#1,Y(I):INPUT#1,S(I):NEXTI
80 CLOSE1:GOTO480
85 INPUT "NUMBER OF PARAMETERS";N0
90 INPUT "NUMBER OF VARIABLES";M0
95 DIMA(N0)
100 FORI=1TON0
105 PRINT "GUESS FOR PARAMETER";I;
110 INPUTA(I):NEXTI
115 INPUT "NUMBER OF MEASUREMENTS";N
120 DIMX(M0,N),Y(N),S(N),O(N0,N0),B(N0,N0),C(N0),D(N0),TB(15)
125 FORJ=1TOM0:FORK=1TON
130 PRINT "X(";J;",";I;")";:INPUTX(J,I)
135 NEXTI:NEXTJ
140 FORI=1TON
145 PRINT "Y(";I;"), S(";I;")";:INPUTY(I),S(I):S(I)=1/(S(I)*S(I)):NEXTI
150 INPUT "DO YOU WANT TO STORE THESE DATA";B$:IFB$<>"YES"THEN185
155 OPEN1,1,1
160 PRINT#1,N0:PRINT#1,M0:PRINT#1,N
165 FORI=1TON:FORK=1TOM0
170 PRINT#1,X(K,I):NEXTK:PRINT#1,Y(I):PRINT#1,S(I):NEXTI
175 CLOSE1
180 FORK1=.1T0π/2STEP.02:A4=K1:FORL1=.1T0π/2STEP.02:A5=L1
185 PRINT:PRINT:S1=0
190 S=0
195 GOSUB615
200 GOSUB580
205 FORI=1TON
210 GOSUB830
215 F1=FNF(I)
220 V=F1-Y(I)
225 S=S+V*V*S(I)
230 FORJ=1TOM0
235 A(J)=A(J)*E2
240 GOSUB580
245 GOSUB830
250 F2=FNF(I)
255 A(J)=A(J)/E2
260 GOSUB580
265 D(J)=(F2-F1)/(E1*A(J))
270 C(J)=C(J)+V*D(J)*S(I)
275 FORK=1TOJ
280 B(J,K)=B(J,K)+D(J)*D(K)*S(I)
285 B(K,J)=B(J,K)
290 NEXTK
295 NEXTJ
300 NEXTI
305 S=SQR(S/(N-N0))
310 PRINTABS((S1-S)/S);A1:A2:A3:A4:A5
315 IFABS(S1-S)<.00001*SGOTO345
320 S1=S
325 GOSUB650
330 FORI=1TON0:FORK=1TOM0
335 A(I)=A(I)-C(J)*O(I,J)*E3:NEXTJ:NEXTI
340 GOTO190
345 OPEN5,4:CMD5:PRINT:PRINT
350 PRINT "FINAL PARA. STD.DEV.":PRINT

```

```

355 FORI=1TON0
360 PRINTA(I);C$;C$;FNE(O(I,I)):NEXTI
365 PRINT:PRINT"STD.DEV.="S
370 PRINT:PRINT:PRINT" I      X0BS      FIELD      Y0BS      YC9LC      RESIDUAL"
375 PRINT
380 B9=0
385 FORI=1TON
390 GOSUB830
395 F=.001*INT(1000*FNF(I) -.5)
400 R1=.001*INT(1000*(F-Y(I))+.5)
405 B9=B9+R1*R1
410 PRINTI;SPC(6-LEN(STR$(I)))X(1,I)SPC(8-LEN(STR$(X(1,I))))X(2,I)SPC(8-LEN(STR
$(X(2,I))))
415 PRINTY(I)SPC(9-LEN(STR$(Y(I))))F;SPC(11-LEN(STR$(F)))R1
420 NEXTI
425 PRINT:PRINT"R.M.S. DEV.=";SQR(B9/(N-N0))
430 PRINT:PRINT"CORRELATION OF PARAMETERS":PRINT
435 FORI=2TON0:K=I-1:FORJ=1TOK:PRINTI;J;C$;S*S*O(I,J)/(FNE(O(I,I))*FNE(O(J,J)))
440 NEXTJ:NEXTI
445 PRINT:PRINT#5:CLOSE5
450 NEXTL1,K1
455 PRINT"DO YOU WANT TO PLOT THESE DATA";:INPUTA$:IFA$<>"YES"THEN470
460 GOSUB875
465 GETA$:IFA$=""THEN465
470 INPUT"DO YOU WANT TO RUN WITH THIS DATA AGAIN":A$:A$=LEFT$(A$,2)
475 IFA$="NO"THENSTOP
480 PRINT"DO YOU WANT TO DELETE POINTS";:INPUTA$:IFA$<>"YES"THEN540
485 INPUT"HOW MANY POINTS DO YOU WANT TO      DELETE";D3
490 PRINT"WHICH";D3;"POINTS ARE TO BE DELETED--LAST FIRST AND FIRST LAST";
495 FORI=1TOD3
500 INPUTD1
505 IFD1=NGOTO535
510 FORJ=D1+1TON
515 Y(J-1)=Y(J):S(J-1)=S(J)
520 FORK=1TOM0
525 X(K,J-1)=X(K,J)
530 NEXTK:NEXTJ
535 N=N-1:NEXTI
540 INPUT"DO YOU WANT TO ADD POINTS":A$:A$=LEFT$(A$,3):IFA$<>"YES"THEN565
545 INPUT"HOW MANY POINTS DO YOU WANT TO ADD";D5
550 FORI=N+1TON+D5:FORK=1TOM0:PRINT"X(";K;",";I;")";:INPUTX(K,I):NEXTK
555 PRINT"Y(";I;"), S(";I;")";:INPUTY(I),S(I):S(I)=1/(S(I)*S(I)):NEXTI
560 N=N+D5
565 FORI=1TON0:PRINT"GUESS FOR PARAMETER";I;
570 INPUTA(I):NEXTI
575 GOTO150
580 ONN0GOTO605,600,595,590,585
585 A5=A(5)
590 A4=A(4)
595 A3=A(3)
600 A2=A(2)
605 A1=A(1)
610 RETURN
615 FORI=1TON0
620 FORJ=1TON0
625 B(I,J)=0
630 NEXTJ
635 C(I)=0
640 NEXTI
645 RETURN
650 FORI=1TON0
655 FORJ=1TON0
660 O(I,J)=0
665 NEXTJ
670 O(I,I)=1
675 NEXTI
680 FORJ=1TON0
685 FORI=JTON0
690 IFB(I,J)<>0GOTO710

```

1010 DATA 32,123,126,97,108,98,127,252,124,255,226,236,225,254,251,160



```

100 REM BLOCH EQUATIONS: TRANSIENT SOLN.
110 DIMTB(15):C$=" ":FORI=0TO15:READTB(I)
120 DATA32,123,126,97,108,98,127,252,124,255,226,236,225,254,251,160
130 NEXTI:DIMX(80),Y(80),Z(80):DEFFNI(Q)=.001*INT(1000*Q+.5)
140 PRINT"DO YOU HAVE STORED DATA?":INPUTA$:IFA$="NO"THEN240
150 OPEN1
160 INPUT#1,H1:INPUT#1,N:INPUT#1,T0:INPUT#1,T1:INPUT#1,T2:INPUT#1,A1:FORI=0TO80
170 INPUT#1,X(I):NEXTI:FORI=0TO80:INPUT#1,Y(I):NEXTI:FORI=0TO80:INPUT#1,Z(I)
180 NEXTI:CLOSE1
190 PRINT"OFFSET MAXIMUM ="H1/(PI*2):"HZ"
200 PRINT"NUMBER OF PULSES ="N:PRINT"EVOLUTION PERIOD ="T0/1E-3:"MSEC"
210 PRINT"TOTAL PULSE ANGLE ="FNI(A1*N*180/PI):"DEGREES"
220 PRINT"T1 ="T1:"SEC":PRINT"T2 ="T2:"SEC":PRINT:PRINT:IFQ1=1THENRETURN
230 GOTO480
240 PRINT"INPUT DESIRED PULSE ANGLE (DEGREES), 90 * PULSE (USEC), TOTAL NUMBER "
250 PRINT"OF PULSES, EVOLUTION PERIOD BETWEEN PULSES (MSEC), MAXIMUM OFFSET (
HZ)":
260 PRINT", AND T1 AND T2 (SEC)":INPUTA1,P2,N,T0,H1,T1,T2:A1=A1*PI/(N*180)
270 P2=P2*1E-6:TP=2*A1*P2/PI:C1=COS(A1):S1=SIN(A1):H1=2*PI*H1:K=0:T0=T0*1E-3
280 PRINT"OFFSET (HZ)"TAB(15)"MX"TAB(24)"MY"TAB(33)"MZ"
290 PRINT"TAB(15)"TAB(24)"TAB(33)"
300 FORD1=0TOH1+1STEPH1/80
310 X0=0:Y0=0:Z0=1:C2=COS(D1*TP):C3=COS(T0*D1):S2=SIN(D1*TP):S3=SIN(D1*T0)
320 IFB$<"YE"THEN340
330 X0=X(K):Y0=Y(K):Z0=Z(K)
340 FORI=1TON:IFB$="YE"THEN400
350 X(K)=(X0*C2+Y0*C1*S2+Z0*S1*S2)*EXP(-TP/T2)
360 Y(K)=(Y0*C1*C2-X0*S2+Z0*S1*C2)*EXP(-TP/T2)
370 Z(K)=Z0*C1-Y0*S1+1-EXP(-TP/T1)
380 X0=X(K):Y0=Y(K):Z0=Z(K)
390 IFB$="YE"THEN440
400 X(K)=(X0*C3+Y0*S3)*EXP(-T0/T2)
410 Y(K)=(Y0*C3-X0*S3)*EXP(-T0/T2)
420 Z(K)=Z0+1-EXP(-T0/T1)
430 X0=X(K):Y0=Y(K):Z0=Z(K):NEXTI:IFB$="YE"THEN350
440 PRINT:FNI(D1/(PI*2)):TAB(13):FNI(X(K)):TAB(22):FNI(Y(K)):TAB(31):FNI(Z(K))
450 K=K+1:NEXTD1
460 PRINT"DO YOU WANT TO PLOT THE FREQUENCY DOMAIN OF THE EXCITATION?":INPUTA$
470 A$=LEFT$(A$,2):IFA$="NO"THEN550
480 PRINT"WHICH ONE WOULD YOU LIKE TO PLOT: X, Y, Γ- Z":INPUTA$
490 A$=LEFT$(A$,1):IFA$<"X"OR A$<"Y"THENB1=3
500 IFA$="X"THENB1=1
510 IFA$="Y"THENB1=2
520 GOSUB780
530 PRINT"WOULD YOU LIKE TO PLOT ANOTHER VECTOR?":INPUTA$:A$=LEFT$(A$,2)
540 IFA$<"NO"THEN480
550 PRINT"WOULD YOU LIKE TO STORE THESE DATA?":INPUTA$:A$=LEFT$(A$,2):IFA$="NO"
THEN610
560 OPEN1,1,1:PRINT#1,H1
570 PRINT#1,N:PRINT#1,T0:PRINT#1,T1
580 PRINT#1,T2:PRINT#1,A1:FORI=0TO80
590 PRINT#1,X(I):NEXTI:FORI=0TO80:PRINT#1,Y(I):NEXTI
600 FORI=0TO80:PRINT#1,Z(I):NEXTI:CLOSE1
610 PRINT"WOULD YOU LIKE A LISTING OF THE DATA?":INPUTA$:A$=LEFT$(A$,2)
620 IFA$="NO"THEN710
630 PRINT"Q1=1:OPEN2,4:CMD2:GOSUB190
640 PRINT"OFFSET MX MY MZ":PRINT
650 FORI=0TO80:H$="":I$="":J$=""
660 L$=STR$(FNI(H1*I/(160*PI))):H=LEN(L$):H=10-H:FORJ=1TOH:H$=H$+C$:NEXTJ
670 M$=STR$(FNI(X(I))):H=LEN(M$):H=10-H:FORJ=1TOH:I$=I$+C$:NEXTJ
680 N$=STR$(FNI(Y(I))):H=LEN(N$):H=10-H:FORJ=1TOH:J$=J$+C$:NEXTJ
690 O$=STR$(FNI(Z(I)))
700 PRINTL$;H$;M$;I$;N$;J$;O$:NEXTI:PRINT#2,C$:CLOSE2:Q1=0
710 PRINT"WOULD YOU LIKE TO APPLY A NON-SELECTIVE 90 * PULSE TO THESE DATA?":
720 PRINT"#####":INPUTB$:B$=LEFT$(B$,2):IFB$="NO"THEN770
730 N=1:TP=P2:PRINT"INPUT THE DELAY TIME BETWEEN THE SELEC- TIVE PULSE AND THE
";
740 PRINT" 90 * PULSE (MSEC)":INPUTA$:T0=VAL(A$)*1E-3:C1=0:S1=1:K=0:A1=PI/2

```

```

750 PRINT"OFFSET (HZ)"TAB(15)"MX"TAB(24)"MY"TAB(33)"MZ"
760 PRINT"TAB(15)"TAB(24)"TAB(33)"J":GOTO300
770 END
780 PRINT"J":FORI=32808TO33697STEP40:POKEI,93:POKEI+39,93:NEXTI
790 FORI=32769TO32806:POKEI,64:POKEI+480,64:POKEI+960,64:NEXTI
800 POKE33248,107:POKE33287,115:POKE32768,112:POKE32807,110:POKE33767,125:POKE3
3728,109
810 XL=-H1*.0375:XB=H1*1.025:YL=-1.1:YB=1.1
820 FORI=0TO80:ONB1GOSUB990,1000,1010
830 X=H1*(I/80):GOSUB870
840 NEXTI
850 GETA$:IFA$=""THEN850
860 RETURN
870 XS%=79*((X-XL)/(XB-XL)):YS%=49*((YB-Y)/(YB-YL))
880 XC%=XS%/2:YL%=YS%/2:Q=YL%*40+XC%+32768
890 IX=XS%AND1
900 JX=(YS%+1)AND1
910 KX=(JX+1)*(IX*3+1)
920 L=PEEK(Q)
930 FOR J=0 TO 15:IFL=TB(J)THEN960
940 NEXT J
950 J=0
960 KX=KXORJ
970 PTX=TB(KX)
980 POKE Q,PTX:RETURN
990 Y=X(I):RETURN
1000 Y=Y(I):RETURN
1010 Y=Z(I):RETURN

```

```

100 DIMTB(15),X(1,50),Y(50),X1(1,50),Y1(50)
105 FORI=0TO15:READTB(I):NEXTI
110 DATA32,123,126,97,108,98,127,252,124,255,226,236,225,254,251,160
115 DEFFNE(Q)=S*SQR(ABS(Q))
120 E1=0.02:E2=E1+1:E3=1
125 INPUT"RATE OR TIME";A$:IFA$="R"ORA$="RATE"THENB8=1
130 IFB8=1THENINPUT"T1A VALUE=";A8
135 IFB8=1THENINPUT"T1B VALUE=";A9
140 IFB8=1THENINPUT"MOLE FRACTION (PA)=";PA:PB=1-PA:PC=PB-PA
145 IFA9<>0THENA9=1/A9
150 IFA8<>0THENA8=1/A8
155 ONB8+1GOSUB875,880
160 INPUT"DO YOU HAVE STORED DATA";A$:IFA$<>"YES"GOTO180
165 OPEN1
170 INPUT#1,N0:INPUT#1,M0:INPUT#1,N:DIMA(N0)
175 FORI=1TON:INPUT#1,X(1,I):INPUT#1,Y(I):NEXTI:CLOSE1:GOTO490
180 PRINT"NUMBER OF PARAMETERS";:INPUTN0:DIMA(N0)
185 PRINT"NUMBER OF VARIABLES";:INPUTM0
190 FORI=1TON0
195 PRINT"GUESS FOR PARAMETER";I;:INPUTA(I):NEXTI
200 PRINT"NUMBER OF MEASUREMENTS";:INPUTN
205 FORJ=1TOM0:FORI=1TON
210 PRINT"MEASUREMENT";TAB(12);I;"FOR VARIABLE";TAB(30);J;
215 INPUT X(J,I):NEXTI:NEXTJ
220 FORI=1TON:PRINT"Y(";I;")";:INPUTY(I):NEXTI
225 PRINT"DO YOU WANT TO STORE THESE DATA";:INPUTB$:IFB$<>"YES"GOTO240
230 OPEN1,1,1:PRINT#1,N0:PRINT#1,M0:PRINT#1,N
235 FORI=1TON:PRINT#1,X(1,I):PRINT#1,Y(I):NEXTI:CLOSE1
240 PRINT:PRINT:S1=0
245 S=0
250 GOSUB585
255 GOSUB555
260 FORI=1TON
265 IFB8=1THENGOSUB900
270 F1=FNFI
275 V=F1-Y(I)
280 S=S+V*V
285 FORJ=1TOM0
290 A(J)=A(J)*E2
295 GOSUB555
300 IFB8=1THENGOSUB900
305 F2=FNFI
310 A(J)=A(J)/E2
315 GOSUB555
320 D(J)=(F2-F1)/(E1*A(J))
325 C(J)=C(J)+V*D(J)
330 FORK=1TOJ
335 B(J,K)=B(J,K)+D(J)*D(K)
340 B(K,J)=B(J,K)
345 NEXTK:NEXTJ:NEXTI
350 S=SQR(S/(N-N0))
355 PRINTABS((S1-S)/S);
360 IFABS(S1-S)<0.00001*SGOTO385
365 S1=S:GOSUB 590
370 FORI=1TON0:FORJ=1TON0
375 A(I)=A(I)-0(I,J)*C(J)*E3
380 NEXTJ:NEXTI:GOTO245
385 OPEN5,4:CMD5:PRINT:PRINT
390 PRINT"FINAL PARA.      STD. DEV.":PRINT
395 FORI=1TON0:PRINTA(I)SPC(15-LEN(STR$(A(I))))FNE(0(I,I)):NEXTI
400 PRINT:PRINT"STD. DEV.="S:PRINT
405 PRINT:PRINT"I      XOBS      YOBS      YCALC      RESIDUAL":PRINT
410 FORI=1TON:F=.001*INT(1000*FNFI+.5)
415 R1=.001*INT(1000*(F-Y(I))+.5)
420 PRINTI:SPC(6-LEN(STR$(I)))X(M0,I)SPC(8-LEN(STR$(X(M0,I))))Y(I)SPC(8-LEN(STR$(Y(I))))
425 PRINTF:SPC(11-LEN(STR$(F)))R1:NEXTI
430 PRINT:PRINT"CORRELATION OF PARAMETERS":PRINT
435 FORI=2TON0:K=I-1:FORJ=1TOK

```

```

440 PRINT I; J; S*0(I, J)/(FNE(0(I, I))*FNE(0(J, J))):NEXT J:NEXT I
445 PRINT:PRINT#5:CLOSE5
450 IFB8=1THENB9=1/A3
455 IFB8=0THENB9=A3
460 PRINT:PRINT"DO YOU WANT TO PLOT THESE DATA";
465 INPUTA$:A$=LEFT$(A$,3):IFA$<>"YES"THEN480
470 GOSUB725
475 GETA$:IFA$=""THEN475
480 PRINT"DO YOU WANT TO RUN WITH THESE DATA AGAIN";
485 INPUTA$:A$=LEFT$(A$,2):IFA$="NO"THEN910
490 PRINT"DO YOU WANT TO DELETE POINTS";
495 INPUTA$:A$=LEFT$(A$,2):IFA$="NO"GOTO525
500 PRINT"HOW MANY POINTS DO YOU WANT TO DELETE":INPUTD$:D3=VAL(D$)
505 PRINT"WHICH";D3;"POINTS ARE TO BE DELETED--LAST FIRST AND FIRST LAST";
510 FORI=1TOD3:INPUTD$:D1=VAL(D$):IFD1=NGOTO520
515 FORJ=D1+1TON:Y(J-1)=Y(J):X(1, J-1)=X(1, J):NEXT J
520 N=N-1:NEXT I
525 PRINT"DO YOU WANT TO ADD POINTS";
530 INPUTA$:A$=LEFT$(A$,2):IFA$="NO"GOTO550
535 PRINT"HOW MANY POINTS DO YOU WANT TO ADD":INPUTD$:D5=VAL(D$)
540 PRINT"FIRST X, THEN Y";
545 FORI=N+1TON+D5:INPUTX(1, I),Y(I):NEXT I:N=N+D5
550 FORI=1TON:PRINT"GUESS FOR PARAMETER";I:INPUTA(I):NEXT I:PRINT"J":GOTO240
555 ONN0GOTO575,570,565,560
560 A4=A(4)
565 A3=A(3)
570 A2=A(2)
575 A1=A(1)
580 RETURN
585 FORI=1TON0:FORJ=1TON0:B(I, J)=0:NEXT J:C(I)=0:NEXT I:RETURN
590 FORI=1TON0:FORJ=1TON0:O(I, J)=0:NEXT J:O(I, I)=1:NEXT I
595 FORJ=1TON0:FORI=1TON0
600 IFB(I, J)>0GOTO620
605 NEXT I
610 PRINT"SINGULAR MATRIX"
615 STOP
620 FORK=1TON0
625 S5=B(J, K)
630 B(J, K)=B(I, K)
635 B(I, K)=S5
640 S5=O(J, K)
645 O(J, K)=O(I, K)
650 O(I, K)=S5
655 NEXT K
660 T=1/B(J, J)
665 FORK=1TON0
670 B(J, K)=T*B(J, K)
675 O(J, K)=T*O(J, K)
680 NEXT K
685 FORL=1TON0
690 IFL=JGOTO720
695 T=-B(L, J)
700 FORK=1TON0
705 B(L, K)=B(L, K)+T*B(J, K)
710 O(L, K)=O(L, K)+T*O(J, K)
715 NEXT K
720 NEXT L:NEXT J:RETURN
725 PRINT"J":G9=0
730 IFA1<0THENB7=.8*A1-1.2*A2
735 IFA1<0THENB6=.8*A1
740 IFA1>0THENB7=1.2*(A1-A2)
745 IFA1>0THENB6=1.2*A1
750 FORI=1TON:IFX(1, I)>B9*5THEN760
755 GOSUB790
760 X1(1, I)=X(1, I):Y1(I)=Y(I):NEXT I
765 G9=1
770 FORI=0TOB9*5STEPB9/16:X(1, I)=I:Y(I)=FNF(X(1, I)):GOSUB790:NEXT I
775 FORI=1TON:X(1, I)=X1(1, I):Y(I)=Y1(I):NEXT I
780 PRINT"#####MAXIMUM T=";B9*5;"SEC"

```

```

785 RETURN
790 XS%=15.8*X(1,I)/B9
795 YS%=49*(B6-Y(I))/B7
800 XC%=XS%/2:YL%=YS%/2
805 Q=YL%*40+XC%+32768
810 IZ%=XS%AND1
815 JZ%=(YS%+1) AND 1
820 KZ%=(JZ%+1)*(IZ%*3+1)
825 K=PEEK(Q)
830 FORJ=0TO15
835 IFK=TB(J)THEN845
840 NEXTJ:J=0
845 KZ%=KXORJ
850 PTZ%=TB(KZ%)
855 IFG9<0THEN865
860 POKEQ,87:RETURN
865 G6=PEEK(Q):IFG6=87THENRETURN
870 POKEQ,PTZ%:RETURN
875 DEFNF(Q)=A1+(A2-A1)*EXP(-X(1,Q)/A3):RETURN:REM T1 FUNCTION
880 DEF FNC(Q)=A4*(1-(A8+A3*PB/PA-(A8+A9+A3/PA)/2+B1)/A3)
885 DEF FND(Q)=A1+(A2-A1-FNC(Q))*EXP(-X(1,Q)*((A8+A9+A3/PA)/2+B1))
890 DEF FNF(Q)=FND(Q)+FNC(Q)*EXP(-X(1,Q)*((A8+A9+A3/PA)/2-B1))
895 RETURN:REM MAG. TRANS. FUNCTION
900 B1=SQRT(((A3*PC/PA+A8-A9)*2)/4+A3*A3*PB/PA)
905 RETURN
910 END

```

## ABSTRACTS OF PROPOSITIONS

## Proposition I

The measurement of the anisotropy of the chemical shift tensor for  $^{13}\text{CO}$  bound to solid human hemoglobin using sideband analysis of the cross polarization/magic angle spinning carbon-13 nmr spectrum is proposed.

## Proposition II

A study of the complexation of vanadium(III) within the vanadocytes of the ascidian Ascidacea ceratodes using Resonance Raman spectroscopy is proposed.

## Proposition III

The development of a combined gas chromatograph/Fourier transform mass spectrometer/Fourier transform nmr spectrometer which uses an array processor to automate the identification of each gc fraction using pattern recognition is proposed.

## Proposition IV

The application of mercury-199 nmr to the study of the binding of the methylmercuric ion to nucleotides and fragments of DNA is proposed.

## Proposition V

The synthesis of a hemoglobin binding pocket model which contains a nitrogen nucleophile and is based structurally on the "pocket" porphyrin of Collman et al is proposed.

## PROPOSITION I

In the past few years advances in solid state nuclear magnetic resonance (nmr) spectroscopy, primarily the combination of cross polarization (CP)<sup>1</sup> and magic angle spinning (MAS),<sup>2</sup> have enabled researchers to obtain high resolution <sup>13</sup>C nmr spectra of solid samples.<sup>3</sup> CP/MAS has been applied to a variety of solid systems, and, in recent years, to both powdered<sup>4</sup> and crystalline<sup>5</sup> proteins. Using various numerical analyses of the CP/MAS spectrum,<sup>6-9</sup> it is possible to obtain information about the anisotropy of the chemical shift tensor for each resonance. This becomes important for a complicated spectrum, as the overlap of the powder patterns for each resonance in the non-rotating sample would make the spectrum uninterpretable. For this reason, it is proposed that the chemical shift anisotropy (CSA) of <sup>13</sup>CO bound to crystallized hemoglobin A be measured via analysis of the CP/MAS spectrum. Such data should yield valuable information regarding the similarities and/or differences between the solid and solution forms of carbonmonoxyhemoglobins.

When a solid nmr sample is spun at the magic angle (54.7°), rotational sidebands are observed as a frequency  $\nu_{\text{res}} \pm N\nu_r$  when  $\nu_r$  (the rotational frequency) is less than  $\Delta\sigma \times \nu_{\text{res}}$ , where  $\Delta\sigma$  is the anisotropy of the chemical shift tensor and  $\nu_{\text{res}}$  is the resonance frequency. As proposed by Maricq and Waugh,<sup>8</sup> moment analysis may be

used to extract the anisotropy from the amplitude of the sidebands. They noted that for the  $\ell^{\text{th}}$  moment of species  $n$ ,

$$M_{\ell n} = \omega_r^{\ell} \frac{\sum_{N=N^-}^{N^+} N^{\ell} A_N}{\sum_N A_N} \quad (1)$$

where

$A_N$  = amplitude of the  $N^{\text{th}}$  sideband

$$\omega_r = 2\pi\nu_{\text{rot}}$$

Knowing the expressions for the  $\ell^{\text{th}}$  moment as a function of the anisotropy ( $\Delta\sigma$ ) and the asymmetry ( $\eta$ ), it is possible to obtain  $\Delta\sigma$ . However, this also requires measuring the amplitudes for all of the sidebands -- a formidable task in the case of a complicated protein spectrum.

In recent months, Herzfeld and Berger<sup>9</sup> have overcome this problem. The intensity of the  $N^{\text{th}}$  sideband is given by

$$I_N = \frac{1}{4\pi} \int_0^{\pi} \int_0^{2\pi} |F|^2 d\alpha \sin\beta d\beta \quad (2)$$

where

$$F = \frac{1}{2\pi} \int_0^{2\pi} \exp[i(-N\theta + \Delta_- \tau_-(\alpha, \beta, \theta) + \Delta_+ \tau_+(\beta, \theta))] d\theta$$

$\alpha, \beta$  are the Euler angles

$$\Delta_- = -(\omega_o/\omega_r)(\sigma_{xx} - \sigma_{yy})$$

$$\Delta_+ = -(\omega_o/\omega_r)3(\sigma_{av} - \sigma_{zz})$$



$$\begin{aligned}
\tau_{-}(\alpha, \beta, \theta) = & \left(\frac{1}{24}\right) \cos(2\alpha) [3 + \cos(2\beta)] \sin(2\theta) \\
& - \left(\frac{1}{6}\right) \sin(2\alpha) \cos\beta \cos(2\theta) \\
& + \frac{\sqrt{2}}{6} \cos(2\alpha) \sin(2\beta) \sin\theta \\
& - \frac{\sqrt{2}}{3} \sin(2\alpha) \sin\beta \cos\theta
\end{aligned}$$

$$\tau_{+}(\beta, \theta) = \left(\frac{1}{24}\right) [\cos(2\beta) - 1] \sin(2\theta) + \left(\frac{\sqrt{2}}{6}\right) \sin(2\beta) \sin\theta$$

Using eq. 2 and letting

$$\mu = \omega_o / \omega_r (\sigma_{33} - \sigma_{11}) \quad (3)$$

and

$$\rho = \frac{(\sigma_{11} + \sigma_{33} - 2\sigma_{22})}{(\sigma_{33} - \sigma_{11})} \quad (4)$$

where

$$\sigma_{33} > \sigma_{22} > \sigma_{11}$$

plots of  $\mu$  vs.  $\rho$  vs.  $I_N/I_O$  have been created.<sup>9</sup> Thus, by measuring the ratio  $I_N/I_O$  for a few sidebands, values for  $\rho$  and  $\mu$  can be determined for a given resonance. In conjunction with eq. 5,

$$\sigma_{AV} = \frac{1}{3}(\sigma_{11} + \sigma_{22} + \sigma_{33}) \quad (5)$$

values for  $\sigma_{11}$ ,  $\sigma_{22}$ , and  $\sigma_{33}$ , and thus  $\Delta\sigma$ , may be obtained.

Creating a solid sample of  $^{13}\text{CO}$  HbA should be relatively straight forward, as methods of crystallization are well documented.<sup>10</sup> The availability of a CP/MAS nmr

spectrometer at Caltech is imminent because of the arrival of a 4.7 T widebore magnet which will become a part of the Southern California Regional NMR Facility. Thus, this experiment could be done within the next year.

Comparison of the solid state  $\Delta\sigma$  for  $^{13}\text{CO}$  bound to hemoglobin A with  $\Delta\sigma$  obtained in solution<sup>11</sup> would help answer some important questions concerning the effects of crystal packing forces on the structure of crystallized proteins. The work of Maciel et al.<sup>5</sup> shows that the  $^{13}\text{C}$  CP/MAS nmr spectrum of  $^{13}\text{CO}\cdot\text{HbA}$  looks much like the solution spectrum, implying that there is no difference between the protein in the solution and crystalline forms. However, large changes in  $\Delta\sigma$  would not necessarily manifest themselves in the isotropic solid spectrum. This is evident from the fact that  $\Delta\sigma$  for  $^{13}\text{CO}$  bound to the monomeric hemoglobin of the marine annelid, Glycera dibranchiata, is twice as large as that for  $^{13}\text{CO}\cdot\text{HbA}$ , yet the isotropic chemical shifts differ by less than 1%.<sup>11</sup>

REFERENCES

1. Pines, A., Gibby, M. G. & Waugh, J. S. J. Chem. Phys. 1973, 59, 569-590.
2. Schaefer, J. & Stejskal, E. O. J. Am. Chem. Soc. 1976, 98, 1031-1032.
3. Schaefer, J. & Stejskal, E. O. Top. Carbon-13 NMR Spectrosc. 1979, 3, 283-324.
4. Opella, S. J., Frey, M. H. & Cross, T. A. J. Am. Chem. Soc. 1979, 101, 5856-5857.
5. Maciel, G. E., Shatlock, M. P., Houtchens, R. A. & Caughey, W. S. J. Am. Chem. Soc. 1980, 102, 6884-6885.
6. Lippma, E., Alla, M. & Turherm, T. Proceedings of the 19th Congress Ampère, Heidelberg 1976, 113-118.
7. Waugh, J. S., Maricq, M. M. & Cantor, R. J. Magn. Reson. 1978, 29, 183-190.
8. Maricq, M. M. & Waugh, J. S. J. Chem. Phys. 1979, 70, 3300-3316.
9. Herzfeld, J. & Berger, A. E. J. Chem. Phys. 1980, 73, 6021-6030.
10. Perutz, M. F. J. Cryst. Growth 1968, 2, 54-56.
11. Perkins, T., Ph.D. Thesis, California Institute of Technology (1981).

## PROPOSITION II

In most parts of the world's oceans, there exists a group of small creatures known as tunicates. They vary in size from being microscopic to several centimeters long.<sup>1</sup> This does not sound very interesting until one looks at a particular class, that of Ascidiacea, more commonly known as sea squirts. Sea squirts are found to concentrate vanadium in very large amounts relative to dry body weight. This has prompted numerous studies of sea squirts over the past 60 years.<sup>2-5</sup> Most of this work has not been done on the living system, specifically, the vanadium-containing vacuoles, known as vanadopores, which are housed in the blood cells (vanadocytes). Rather, the cells have been lysed, and various components isolated for study.

Not working with the intact, living cells has created numerous artifacts because of the unusual nature of the vanadium-vanadocyte system.<sup>3</sup> Inside the vanadopores vanadium exists in the atmospherically unstable (III) state. The vanadopores contain sulfuric acid at a concentration of 3.66 M,<sup>2</sup> along with an organic ligand of some kind (empirical formula  $C_{16}H_{17}N_3O_{11}$ )<sup>1</sup> and a large ( $\sim 55,000$  MW)<sup>2</sup> protein, commonly known as hemovanadin, although it does not contain a porphyrin of any kind.<sup>3</sup> The relationship between these observations and the function of the vanadium

still remains a mystery, although it is generally accepted that it is not used in the transport of dioxygen.<sup>3</sup>

Recently, two studies on living vanadocytes were carried out. Swinehart et al.<sup>5</sup> looked at the uv-visible spectrum of both intact cells and chromatographed fractions of lysed cells from A. ceratodes. They found that the vanadium (III) is primarily coordinated by  $\text{SO}_4^{-2}$  and  $\text{H}_2\text{O}$ . This conclusion was also reached by Carlson,<sup>4</sup> who found that the vanadium is at least penta-coordinated with these inorganic ligands, leaving one coordination site available for binding an organic ligand or protein. But what is this remaining ligand? Does it exist, or is the vanadium coordinated to just  $\text{H}_2\text{O}$  and  $\text{SO}_4^{-2}$ ? With the hope of answering these questions, it is proposed that resonance Raman spectroscopy be used to observe vanadium-ligand stretching frequencies within the intact vanadocytes of the ascidian A. ceratodes.

Resonance Raman spectroscopy has been used in recent years to study chromophores in various biochemical systems.<sup>6,7</sup> The advantages of resonance Raman in its applications to biological chromophores are that water does not interfere with the detection of the desired frequencies (as with infrared studies), and its tremendous sensitivity compared to normal Raman spectroscopy. The latter can be seen if one examines the contributions to the intensity of

the observed Raman line. For randomly reorienting molecules, the Raman line intensity is given by eq. 1.<sup>6</sup> The

$$I = \frac{128 \cdot \pi^5}{9 \cdot c^4} I_0 \nu_s \sum_{ij} |\alpha_{ij}|^2 \quad (1)$$

where

$I_0$  = intensity of the incident light

$\nu_s$  = frequency of the scattered light

$\alpha_{ij}$  = element of the molecular polarizability matrix,  $\hat{\alpha}$  element of the molecular polarizability matrix,  $\alpha_{ij}$ , is obtained using second-order perturbation theory:<sup>6</sup>

$$(\alpha_{ij})_{mn} = \frac{1}{h} \sum_e \frac{(M_j)_{me} (M_i)_{en}}{(\nu_e - \nu_0)} + \frac{(M_i)_{me} (M_j)_{en}}{(\nu_e + \nu_s)} \quad (2)$$

where

$m, n$  = initial, final states of the molecule

$e$  = excited state

$\left. \begin{matrix} (M_j)_{me} \\ (M_i)_{en} \end{matrix} \right\} =$  electric dipole transition moments along directions  $i$  and  $j$ , from  $me$  to  $e$  and from  $e$  to  $n$

$\nu_e$  = frequency of transition from  $m$  to  $e$

$\nu_0$  = frequency of incident light.

From this equation it can be seen that as  $\nu_0$  approaches  $\nu_e$ ,  $\alpha_{ij}$  becomes very large. So, if coherent radiation from a laser is used as the incident light, and, if  $\nu_0$  is close to a particular electronic transition  $\nu_e$ , the Raman intensities of the observed lines will be greatly enhanced.

The proposed experiment will be carried out as follows. Resonance Raman spectra of whole vanadocytes from the ascidian A. ceratodes will be obtained using laser wavelengths of 260 nm (Chromatix CMX-4 tunable dye laser),<sup>8</sup> 325 nm (He-Cd laser), and 351 nm (Ar-ion laser). These wavelengths are directed towards the main absorptions of the cells and their chromatographed fractions (240 nm, 300-320 nm, and 335 nm).<sup>5</sup> Three stretching frequency regions are of interest: 2)  $> 400 \text{ cm}^{-1}$  (V-O stretch); b)  $250\text{--}400 \text{ cm}^{-1}$  (V-N stretch); c)  $< 270 \text{ cm}^{-1}$  (V-S stretch). Each of these regions is of interest because they contain the three most likely metal-ligand interactions within the cells. Region (a) should show activity due to coordinated  $\text{SO}_4^{2-}$  and  $\text{H}_2\text{O}$ .<sup>9,10</sup> Region (b) should have metal-amine stretching frequencies if either the organic ligand found in the hemolysate or the hemovanadin (which contains 48 residues with amino groups)<sup>2</sup> coordinates to the vanadium.<sup>9</sup> If any vibrations are observed below  $270 \text{ cm}^{-1}$ , then it could be concluded that there is some protein-vanadium interaction (hemovanadin contains 24 cysteine residues).<sup>2</sup> Such observations have been made on iron-sulfur proteins.<sup>11</sup>

The results obtained from this experiment will give information as to whether or not there is a protein-metal or ligand-metal interaction within the vanadopore, or that

the vanadium is acting as some sort of redox sink, oscillating between vanadium (III) and vanadium (IV) with the production of acid for some still unspecified reason.<sup>3</sup>

Although modest in the amount of information obtained, this experiment should help clarify what ligands vanadium interacts with inside of the vanadocytes of sea squirts.



REFERENCES

1. Senozan, N. M. J. Chem. Ed. 1974, 51, 503-505.
2. Bielig, H. J., Bayer, E., Dell, H. D., Rohns, G., Möllinger, H. & Rudiger, W. "Protides of the Biological Fluids" H. Peeters, ed., Elsevier Publishing Co., Amsterdam, pp. 197-204, (1965).
3. Biggs, W. R. & Swinehart, J. H. "Metal Ions in Biological Systems" H. Sigel, ed. Vol. 6, Marcel Dekker, Inc., N.Y. pp. 141-196 (1976).
4. Carlson, R. M. K. Proc. Natl. Acad. Sci. USA 1975, 72, 2217-2221.
5. Swinehart, J. H., Biggs, W. R., Halko, D. J. & Schroeder, N. C. Biol. Bull. 1974, 146, 302-312.
6. Spiro, T. G. Acc. Chem. Res. 1974, 7, 339-344.
7. Adar, F. & Erecinska, M. Biochemistry 1978, 17, 5484-5488.
8. Birge, R. R. 1979, private communication.
9. Nakamoto, K. "Infrared and Raman Spectra of Inorganic and Coordination Compounds" 3rd ed., John Wiley and Sons, Inc. N.Y. (1978).
10. Ferraro, J. R. "Low Frequency Vibrations of Inorganic and Coordination Compounds" Plenum Press, N.Y. (1971).
11. Tang, S. P. W., Spiro, T. G., Mukai, K. & Kimura, T. Biochem. Biophys. Res. Comm. 1973, 53, 869-874.

## PROPOSITION III

In recent years technological advances in chemical instrumentation have enhanced the productivity of analytical laboratories. Developments in the spectroscopies (infrared (ir) and uv-vis, for example) and the spectrometries (nuclear magnetic resonance (nmr) and mass spectrometry (ms)) have contributed at an accelerating rate. The coupling of some of these to gas chromatography (gc) has helped to automate many routine analyses. gc/ms<sup>1,2</sup> is probably the best known and most widely used, as it has proved to be both a valuable tool and time-saver for the analysis of organic mixtures. With the recent arrival of Fourier transform (FT)<sub>ms</sub><sup>3</sup> also known as FT/icr, the amount of sample required for MS analysis has been drastically reduced; this means that only a small portion of a given gc fraction would be needed for ms analysis if an FT<sub>ms</sub> were interfaced to a gc. The question becomes what can be done with the rest of the gc fraction? It is proposed that nmr micro-probe<sup>4</sup> technology be used to enable nmr analysis of the gc fractions. In addition to this, it is proposed that an array processor<sup>5</sup> be used to facilitate complete on-site pattern recognition<sup>6</sup> analysis of the gc/FT<sub>ms</sub>/FT<sub>nmr</sub> data which will result in the structural identification of each fraction.

The schematic for the proposed gc/FTms/FTnmr is shown in Figure 1. The first splitter value (A) will remain open throughout the experiment. The choice of a flame ionization detector (fid) was made because of the fact that it should require less than 1% of the total effluent, yet be more sensitive than using a non-destructive detector in a series configuration.<sup>1</sup> Splitter value (B) will be opened by the computer only when the gc fraction is detected, thus minimizing sample loss. While the FTms is collecting data on the fraction, the remainder of the gc sample will be collected and flowed through an <sup>1</sup>H nmr probe similar in design to that used in liquid chromatography nmr analysis,<sup>7,8</sup> although the receiver coil and sample volume will be scaled down to micro-probe dimensions.<sup>4</sup> Total FTms and nmr acquisition times should be less than one minute per gc fraction. After the collection of each ms and nmr spectrum, the data will be shipped over to the array processor for transformation and then stored on disk.

Once all of the fractions have been sampled, the array processor will be used to perform two variable pattern recognition on each fraction. For the first experiments, the linear pattern classifier<sup>9</sup> will be used. This classifier uses the dot product of the sample pattern vector,  $\hat{y}$ , and the trained weight vector,  $\hat{w}$ , to yield the classifier output  $s$ :

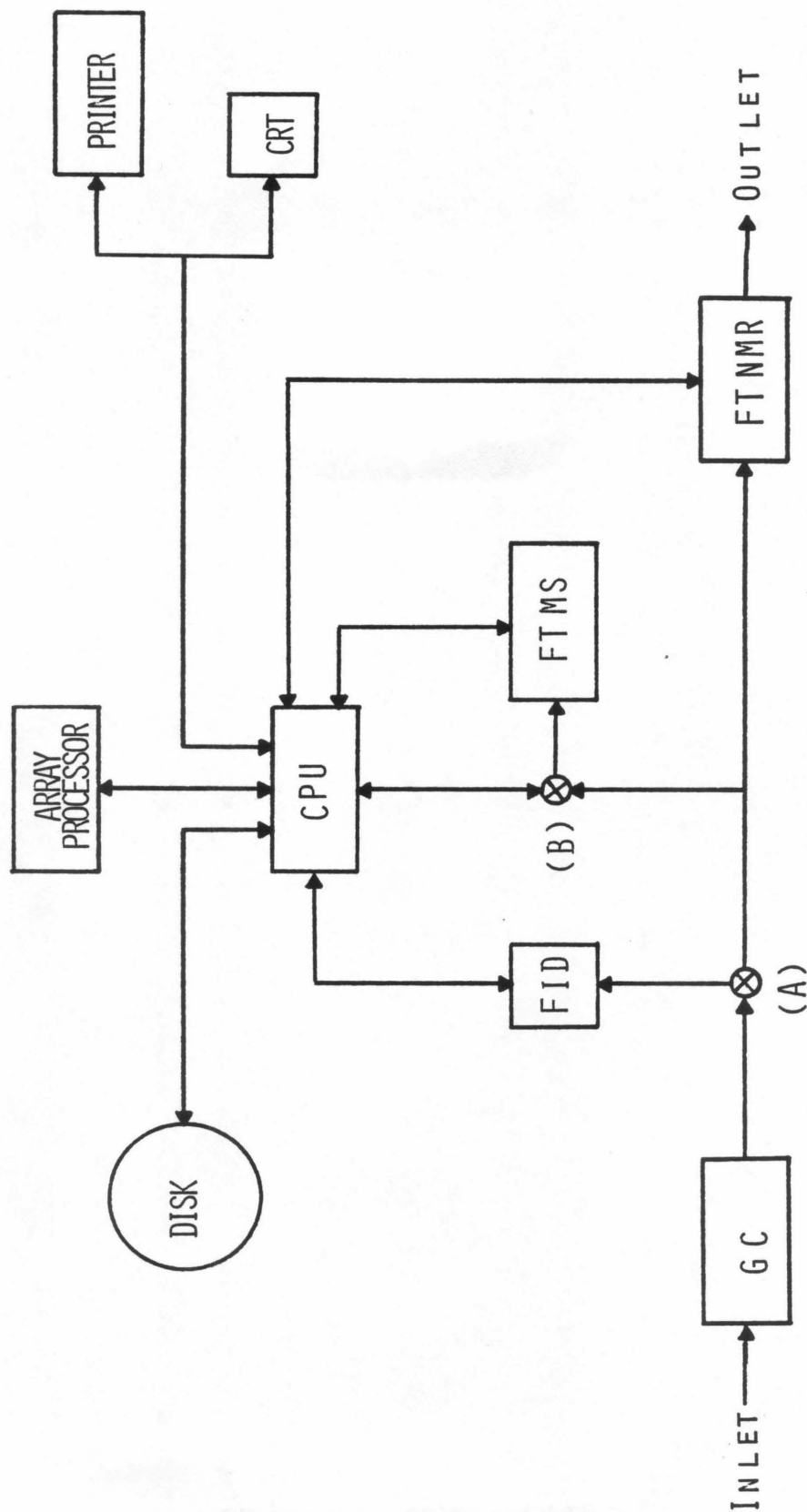


FIGURE 1.

$$s = \hat{w}_{ms} \cdot \hat{y}_{ms} + \hat{w}_{nmr} \cdot \hat{y}_{nmr} + C \quad (1)$$

where  $\hat{w}_{ms}$ ,  $\hat{w}_{nmr}$ , and  $c$  are determined from the training data set.

The pattern vectors for the ms data will be derived directly from the mass spectrum. In the case of the nmr data, autocorrelation will be carried out.<sup>9,10</sup> For the function  $F(f)$ , the autocorrelation function is defined as

$$A(s) = \int_f F(f)F(f + x)df \quad (2)$$

This removes the chemical shift information from the spectrum, but retains the patterns associated with the spectrum (for example, the basic pattern for the  $^1\text{H}$  spectrum of the  $\text{CH}_3\text{CH}_2$ -group).

After the pattern recognition operation is completed, the structure obtained for each GC fraction will be output on the printer and, if a high resolution CRT is used, on the CRT.

Initial start-up costs for this instrument should be high, primarily because of the software development and the FTms, although the latter should become less expensive as more are produced commercially. However, the long-term benefits of such an instrument in terms of the efficient analysis of unknown mixtures far outweigh the initial costs.

APPENDIX I

Some notes on array processors:

The choice of using an array processor for the Fourier transformations and pattern recognition instead of a mini-computer or data transfer to a large mainframe computer arises from the analysis of both the speed and cost per operation. Table I summarizes the results obtained on five different data systems including the FPS AP-120B array processor. As can be seen, the array processor is 65.6 times as fast as a PDP 11/70 (minicomputer) and 6.8 times as fast as an IBM 370-168 (mainframe computer). In addition, the array processor is also the cheapest computer to use per floating point operation per second.

Table I

Representative Computation Times for Vector Operations on  
Various Systems.<sup>5</sup>

<u>Computer</u>	<u>MFLOPS</u> <sup>a</sup>	<u>Relative Operating Speed</u>	<u>\$/FLOPS</u> <sup>b</sup>
Cray I	38.4	426.7	0.21
FPS AP-120B	5.9	65.6	0.03
IBM 370-168	0.87	9.7	2.30
VAX	0.26	2.9	0.77
PDP 11/70	0.09	1.0	1.67

a) Million floating point operations per second. These include data transfer overhead.

b) Includes front end costs.

REFERENCES

1. Junk, G. A. Int. J. Mass Spectrom. Ion Phys. 1972, 9, 1-71.
2. McFadden, W. "Techniques of Combined Gas Chromatography/Mass Spectrometry: Applications in Organic Analysis", John Wiley and Sons, N.Y. (1973).
3. McIver, R. T., Jr. Am. Lab. 1980, 12, 18-30.
4. JEOL Ltd. Technical Bulletin no. 2301B030 (1980).
5. Bucy, R. S. & Senne, K. D. Comp. and Maths. with Appls. 1980, 6, 317-338.
6. Stuper, A. J., Brügger, W. E. & Jurs, P. C. "Computer Assisted Studies of Chemical Structure and Biological Function", John Wiley and Sons, N.Y. (1979).
7. Haw, J. F., Glass, T. E., Hausler, D. W., Motell, E. & Dorn, H. C. Anal. Chem. 1980, 52, 1135-1140.
8. Haw, J. F., Glass, T. E. & Dorn, H. C., presented at the 22nd Experimental NMR Conference, Asilomar, California, 6-9 April, 1981.
9. Kowalski, B. R. & Reilly, C. A. J. Phys. Chem. 1971, 75, 1402-1411.
10. Kowalski, B. R. & Bender, C. F. Anal. Chem. 1972, 44, 1405-1411.



## PROPOSITION IV

The toxic and mutagenic properties of the methylmercuric ion ( $\text{CH}_3\text{Hg(II)}$ ) and related species are well documented.<sup>1,2</sup> The binding of mercuric ions to the sulfhydryl groups of proteins is considered to be the major reason for the toxic nature of these ions, whereas the mutagenic property is believed to involve binding of methylmercuric ions to DNA nucleotides, causing the separation of base pairs within DNA strands.<sup>3</sup> In recent years, nuclear magnetic resonance (nmr) spectroscopy has been used to investigate various methylmercuric species in solution.  $^1\text{H}$ ,<sup>4</sup>  $^{13}\text{C}$ ,<sup>5</sup> and  $^{199}\text{Hg}$ <sup>6</sup> nmr have yielded information about the solution chemistry of  $\text{CH}_3\text{HgOH}$  and related ionic species as well as the interactions of the ionic species with sulfhydryl-containing peptides. Resonance Raman<sup>7-9</sup> and  $^1\text{H}$  nmr<sup>9,10</sup> spectroscopies have been used to investigate the binding of methylmercuric ions to various nucleosides and nucleotides. The extension of these latter studies to the investigation of  $\text{CH}_3\text{Hg(II)}$  binding to polymeric nucleotides and native DNA is not straightforward, as the Resonance Raman and nmr spectra become very complex. Also, in the case of the  $^1\text{H}$  nmr data, chemical exchange can complicate spectra even further. With this in mind, it is proposed that the binding of  $\text{CH}_3\text{Hg(II)}$  to nucleotides and, ultimately, strands of DNA be examined

with  $^{199}\text{Hg}$  nmr.

The advantages of using  $^{199}\text{Hg}$  nmr as a probe of  $\text{CH}_3\text{Hg(II)}$  complexation with nucleotides arise primarily from the fact that the  $^{199}\text{Hg}$  nmr spectrum will be much less complex than the  $^1\text{H}$  spectrum as there are less spins to be observed. The known chemical shift range for  $^{199}\text{Hg}$  is large ( $> 2600$  ppm);<sup>10</sup> this could mean that subtle differences in binding of  $\text{CH}_3\text{Hg(II)}$  to different nucleotide bases will be manifested in the  $^{199}\text{Hg}$  nmr spectrum. In terms of obtaining dynamic (i.e., chemical exchange) information, the large chemical shift range might allow for the measurement of exchange rates between the methylmercuric ions in different sites through the use of magnetization transfer techniques.<sup>12</sup> Although lineshape analysis has been used to examine the binding dynamics of  $\text{CH}_3\text{Hg(II)}$  with 2',3'-cAMP,<sup>10</sup> such methods will be impractical when larger systems are examined, as the spectra will become exceedingly complex.

Preliminary experiments should involve the collection of  $^{199}\text{Hg}$  nmr spectra of  $\text{CH}_3\text{Hg(II)}$  bound to purine and pyrimidine nucleotides within the pH range of 1 to 13. This will help to characterize the  $^{199}\text{Hg}$  chemical shifts for the various methylmercuric (II)-base species. In addition, the kinetic parameters of the  $\text{CH}_3\text{Hg(II)}$  binding should also be measured, presumably using magnetization transfer, as the various species in solution are expected to be in slow exchange with each other.

Once the small systems have been well characterized, the complexation of  $\text{CH}_3\text{Hg}(\text{II})$  to fragments and large strands of native DNA may be studied with  $^{199}\text{Hg}$  nmr. These experiments should help define the nature of the structural and dynamic interactions of the methylmercuric ion with nucleic acids.

REFERENCES

1. Mulvihill, J. J. Science 1972, 176, 132.
2. Fridberg, L. & Vostal, J. "Mercury in the Environment: An Epidemiological and Toxicological Appraisal," CRC Press, Cleveland (1972).
3. Gruenwedel, D. W. & Davidson, N. Biopolymers 1967, 6, 847-861.
4. Libich, A. & Rabenstein, D. L. Anal. Chem. 1973, 45, 118.
5. Rabenstein, D. L. & Fairhurst, M. T. J. Am. Chem. Soc. 1975, 97, 2086.
6. Sudmeier, J. L., Birge, R. R. & Perkins, T. G. J. Magn. Reson. 1978, 30, 491-496.
7. Mansy, S., Wood, T. E., Sprowles, J. C. & Tobias, R. S. J. Am. Chem. Soc. 1974, 96, 1762-1770.
8. Mansy, S. & Tobias, R. S. J. Am. Chem. Soc. 1974, 96, 6874-6885.
9. Mansy, S. & Tobias, R. S. Biochemistry 1975, 14, 2952-2961.
10. Hoc, D.-L. & McConnell, B. J. Am. Chem. Soc. 1979, 101, 7470-7477.
11. Sens, M. A., Wilson, N. K., Ellis, P. D. & Odom, J. D. J. Magn. Reson. 1975, 19, 232.
12. Perkins, T. G. Ph.D. Thesis, California Institute of Technology (1981).

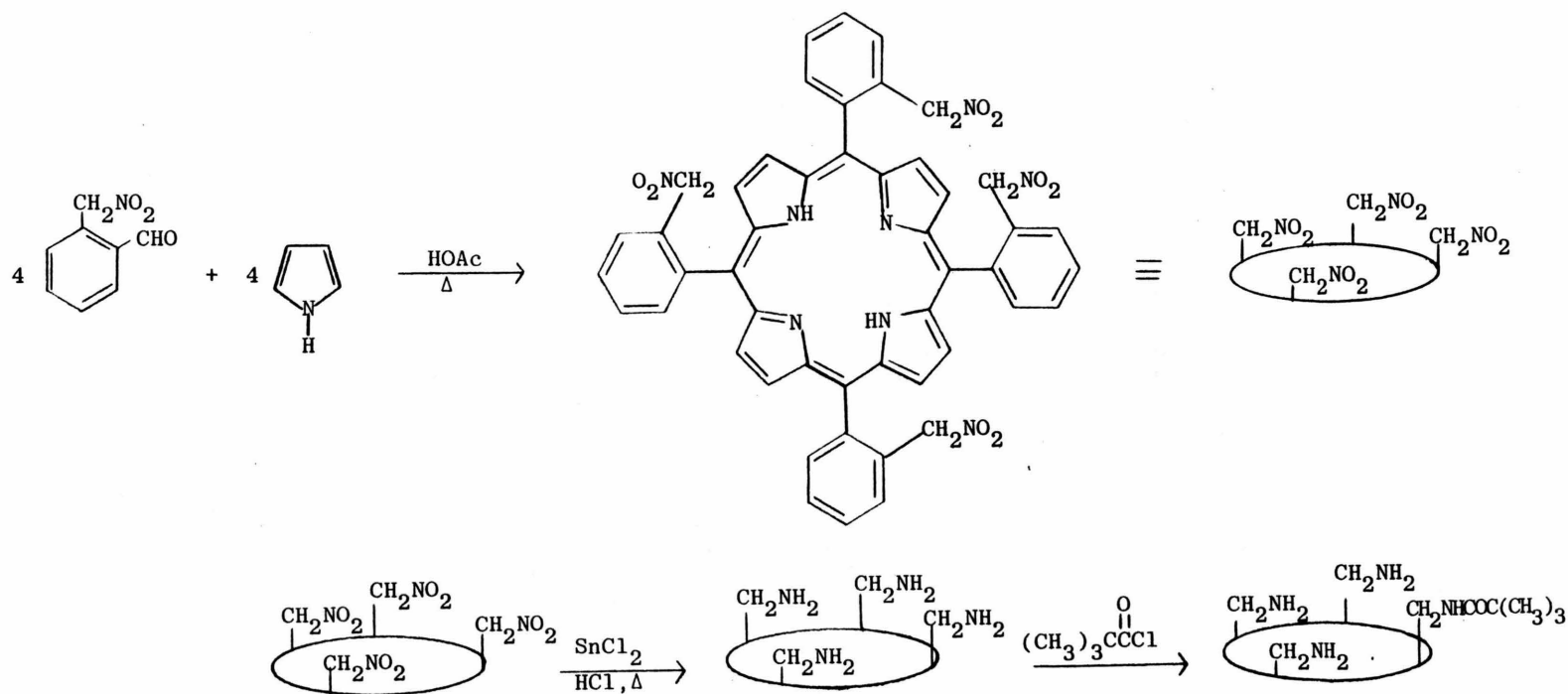
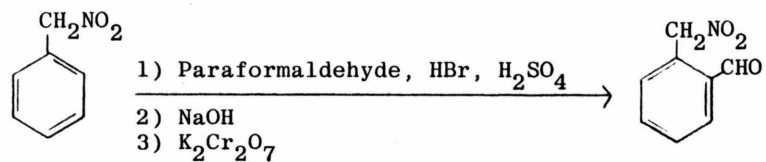
## PROPOSITION V

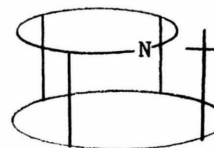
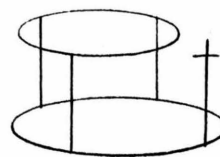
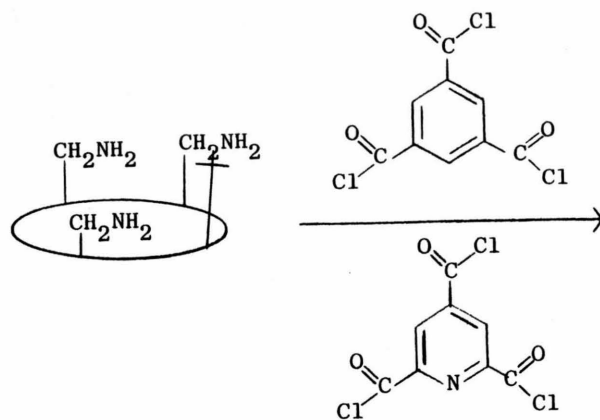
Much work has been carried out in recent years directed towards creating model complexes which mimic the O<sub>2</sub> binding sites in hemoglobins and myoglobins. Chang and Traylor<sup>1</sup> synthesized a derivative of protoheme IX which had an attached imidazole ring; the ring nitrogen could coordinate to the heme iron, thus simulating the proximal histidine within the protein. Collman et al.<sup>2</sup> mimicked the hydrophobic pocket that envelops the ligand binding site within the proteins by creating a molecule known as the "picket fence" porphyrin. This was one of the first model heme systems that bound oxygen reversibly and, as determined from the x-ray structure, showed that O<sub>2</sub> binds to the iron off-axis through one oxygen as first proposed by Pauling.<sup>3</sup> Most recently Collman et al.<sup>4</sup> synthesized a "pocket" porphyrin which, by creating a sterically hindered ligand binding site to simulate the proposed distal steric effect within the proteins, appeared to have a reduced carbon monoxide binding affinity similar to that of hemoglobins and myoglobins. However, this result is in conflict with the recent work of Traylor and Berzini<sup>4</sup> which found that reduced CO affinity could be obtained for a model system without any steric hindrance.

As first proposed by Maxwell and Caughey<sup>6</sup> and demonstrated by Satterlee et al.<sup>7</sup> and Perkins,<sup>8</sup> a nucleophilic interaction

exists between the distal histidine nitrogen and heme coordinated CO within hemoglobins. It has been postulated that this interaction helps to reduce the CO affinity. However, no model system has been synthesized which would examine this particular CO affinity reduction mechanism. With this in mind, it is proposed that a modified "pocket" porphyrin be synthesized which will provide both steric hindrance as well as a nitrogen nucleophile which can interact with bound CO.

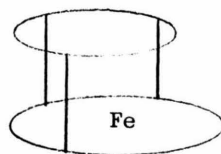
The synthesis of the proposed "nucleophilic pocket" porphyrin is outlined in Figure 1. The pyridine nitrogen will serve as the nucleophile rather than an imidazole nitrogen as in the proteins. Because of the unavailability and, most likely, instability of the pyridine analog of benzene triacetic acid, the 2,4,6-tricarboxylic acid of pyridine has been chosen as the "cap" for the porphyrin. This means that the chain which connects the porphyrin cap to the porphyrin itself must be lengthened by using O-nitro-methyl benzaldehyde rather than O-nitro benzaldehyde for the synthesis of the porphyrin. To produce this substrate, the reaction of Buehler et al<sup>9</sup> is used to make O-nitro-methyl benzylbromide from  $\alpha$ -nitrotoluene, which is then converted by standard methods to the benzaldehyde. From this point on, the synthesis is relatively straightforward. The non-nucleophilic derivative of this "pocket" porphyrin will also be synthesized in this fashion. The ligand trans



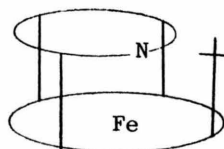


and two other  
isomers

$\text{FeBr}_2$ ,  
 2,6-lutidine,  
 1:1 THF/ $\text{C}_6\text{H}_6$



or





to the pocket coordinate site will be either 1-methylimidazole or 1,2-dimethylimidazole.

Once the two "pocket" porphyrins have been isolated, the binding affinities for both  $O_2$  and CO may be obtained using standard spectrophotometric techniques. Also, the measurement of the  $C\equiv O$  infrared stretching frequency should prove useful in determining how the presence of the pyridine nitrogen affects the CO environment.

The primary advantage of this experiment is that two virtually identical systems may be compared, the only difference between the two being the presence or absence of a nucleophile, the pyridine nitrogen. Such a direct comparison has not been done in the past, thus explaining the controversy about the affinity reduction mechanism for CO binding in hemoglobins and myoglobins. It is hoped that this experiment will help to clarify the exact role of the distal residues within the protein ligand binding site.

REFERENCES

1. Chang, C. K. & Traylor, T. G. Proc. Nat. Acad. Sci. USA 1973, 70, 2647-2650.
2. Collman, J. P. Gagne, R. R., Reed, C. A., Halbert, T. R., Lang, G. & Robinson, W. T. J. Am. Chem. Soc. 1975, 97, 1427-1439.
3. Pauling, L. Stanford Med. Bull. 1948, 6, 215.
4. Collman, J. P., Brauman, J. I., Collins, T. J., Iverson, B. & Sessler, J. L. J. Am. Chem. Soc. 103, 2450-2452.
5. Traylor, T. G. & Berzinis, A. P. Proc. Natl. Acad. Sci. USA 1980, 77, 3171-3175.
6. Maxwell, J. C. & Caughey, W. S. Biochemistry 1976, 15, 383-396.
7. Satterlee, J. D., Teintze, M. & Richards, J. H. Biochemistry 1978, 17, 1456-1462.
8. Perkins, T. G., Ph.D. Thesis, California Institute of Technology (1981).
9. Buehler, C. A., Kirchner, F. K. & Deebel, G. F. Org. Syn. Coll. Vol. 1967, 3, 468.